4-26-2024

Determining the Role of DDR2 in Acquired Chemo-Resistance in Ovarian Cancer

Alyssa Oplt
Washington University in St. Louis

WASHINGTON UNIVERSITY IN ST. LOUIS

Division of Biology and Biomedical Sciences
Molecular Genetics and Genomics

Dissertation Examination Committee:
Gregory Longmore, Chair
John Edwards, Co-Chair
Christopher Maher
Jessica Silva-Fischer
Jason Weber

Determining the Role of DDR2 in Acquired Chemo-Resistance in Ovarian Cancer

by
Alyssa Oplt

A dissertation presented to
Washington University in St. Louis
in partial fulfillment of the
requirements for the degree
of Doctor of Philosophy

May 2024
St. Louis, Missouri

Table of Contents

List of Figures

List of Tables

Acknowledgments

First, I would like to thank my mentor Gregory Longmore for taking me in when I needed help and providing excellent mentorship and scientific guidance. Special thanks to John Edwards for being an amazing mentor and always being there for support. I would also like to thank my previous lab mentors Hollie Noia, Danny Wilke, and Elena Lomonosova for providing mentorship, guidance, support, and encouragement. Additionally, thank you to the Center for Reproductive Health Sciences leaders and administrators, Sarah England, Dineo Khabele, Magdelena Nelson, Kirsten Biggs, and Audry Johnson. They all provided support and created an excellent work environment focused on female sciences. Additionally, this degree would not have been possible without the support of my fellow students in the lab Emilee Kotnik, Angela Schab, Isabelle Seppa, and Judith Sokai. Thank you for your continued support and friendship.

Thank you to the Markey Pathway and Laura Scheuttpelz for the introduction to bench-to-bedside science and furthering my interest in translational research. Thank you to Jim Skeath, Kristine Wylie, and Lauren Johnson for allowing me the opportunity to mentor high school students and watch them grow into young scientists.

Lastly thank you to my family: Mom, Dad, Natalie, Joe, Jeff, Nora, Phil, and Ishtar for your unconditional love and support throughout this entire process. Thank you to all my friends especially Alissa Cullen, Emilee Kotnik, Jasmen O'Hara, Colton Lewis, and Laura Fischer for emotional support and advice throughout my thesis work. I could not have done it without your support, and I am so lucky to have you all in my life.

Alyssa Oplt

Washington University in St. Louis

May 2024

Dedicated to my grandparents Donald and Sheila Ary

ABSTRACT OF THE DISSERTATION

Determining the Role of DDR2 in Acquired Chemo-resistance in Ovarian Cancer by

Alyssa Oplt

Doctor of Philosophy in Biology and Biomedical Sciences

Molecular Genetics and Genomics

Washington University in St. Louis, 2024

Dr. Gregory Longmore, Chair

Dr. John Edwards, Co-Chair

Ovarian cancer is the 5th leading cause of cancer death in women with a 5-year survival rate around 30%. Up to 80% of ovarian cancer patients experience disease recurrence and the majority of those cases are resistant to treatment. Therefore, there is a need to understand the mechanisms of chemo-resistance in order to create new therapies and increase patient survival. To accomplish this, I first developed novel, chemo-resistant, syngeneic mouse ovarian cancer cell lines by serial passaging ovarian cancer cells through mice and treating with increasing doses of chemotherapy. These cell lines fill a need in the field for matched chemo-sensitive (CNAS) and chemo-resistant (CHRP5) ovarian cancer cell lines that can be used in immunocompetent mice. After developing these cell lines, I then performed whole exome RNA sequencing comparing CNAS to CHRP5 gene expression. Differential expression analysis revealed many genes that are differentially regulated in acquired resistance such as ABCG2, a chemo efflux protein, and GMPNB, a glycoprotein. We confirmed differential expression of these genes but did not experiment further.

We identified DDR2 as a potentially important part of acquired chemo-resistance using patient data correlating high DDR2 expression and reduced response to chemotherapy. We then used both *in vitro* and *in vivo* models to determine if DDR2 depletion can re-sensitize tumor cells to chemotherapy using CNAS and CHRP5 cells I developed, in addition to other human immortalized cell line models. We found that neither genetic nor pharmacological inhibition of DDR2 changed tumor response to chemotherapy.

In tandem, we also investigated the effectiveness of novel small molecule inhibitor (AVB-500) of the receptor tyrosine kinase, AXL. We found that treatment with AVB-500 in addition to chemotherapy or bevacizumab treatment for mice injected with multiple cancer cell models reduced tumor burden *in vivo.*

Overall, we filled a need for a new tool in acquired chemo-resistance experiments and determined that DDR2 is not necessary or sufficient to create resistance to chemotherapy.

Chapter 1: Introduction

1.1 Ovarian Cancer Overview

Ovarian cancer is the 5th leading cause of cancer-related death in women in the United States and the 13th most common cause of cancer death overall (American Cancer Society). Approximately 1% of women will develop ovarian cancer in their lifetimes. This reflects upwards of 20,000 new diagnoses per year (Pokhriyal et al 2019, American Cancer Society). As such, it remains important to increase our understanding of ovarian cancer biology to identify newer strategies to improve patient survival.

1.1.1 Ovarian cancer treatments and survival

At diagnosis, cancer is classified by clinical stage, which dictates the approach to therapy, and prognosticates for clinical outcomes. Stage I ovarian cancer is a tumor localized to the ovary. Patients with stage I disease have higher 5-year survival rates comparatively as the tumor can be fully resected during surgery. In stage II disease the cancer has spread to other parts of the pelvic area such as the uterus or colon but has not spread further. Stage III disease has spread from the ovary and pelvis to the surface of organs within the abdominal cavity, such as the omentum. Stage IV disease has spread from the abdominal cavity to other organs or the plural space (National Cancer Institute). Unfortunately, most women are diagnosed with ovarian cancer at stages III or IV. In part, this is because there are no screening tests for early detection and early-stage ovarian cancer is usually asymptomatic or exhibits vague, unspecific symptoms making early detection extremely difficult. Patients with late-stage ovarian cancer do not respond well to treatments and do not have durable responses to treatment leading to frequent relapse. When they

do relapse, frequently their tumors are now resistant to standard therapies. The 5-year survival rates for Stage III/IV patients is less than 30%.

The standard treatment for ovarian cancer is surgical debulking of visible tumor followed by platinum/taxane combination adjuvant chemotherapy. Chemotherapy can also be given before surgery (neo-adjuvant). Currently paclitaxel and carboplatin are the best tolerated, and most responsive chemotherapeutic combination, as up to 80% of patients clinically respond to platinum. Despite this, the mean progression free survival time is only 13.6 to 19.3 months (Pokhriyal et al 2019). When, after initial treatment, cancer recurs, it is prone to be chemo-resistant to the prior drugs. Up to 80% of high-stage ovarian cancer and about 25% of low stage ovarian cancer will develop recurrent disease (Pokhriyal et al 2019). Patients that develop recurrent disease within 6 months of initial chemo regiment are labeled resistant to chemotherapy. Given the high frequency advanced stage at diagnosis and high rates of and early time to recurrence, with acquired chemo-resistance, it is imperative that new methods of treatment are developed to combat metastasis as well as recurrent and chemo-resistant disease.

Unlike other solid tumors that spread or metastasize via lymphatics and blood vessels, ovarian cancer mostly disseminates into the peritoneal cavity where it is carried by ascitic fluid flow to adhere to and invade through the exterior surface or covering (peritoneum) of various organs within the abdomen. Organs in the peritoneal cavity are lined with a monolayer of epithelial-like mesothelial cells. Tumor cells must first clear through this mesothelial cell layer to invade into the underlying organs. It is still unclear what the precise role of mesothelial cells is during this process. The most common site of metastasis is the peritoneal covering the omentum, a fat pad that drapes over the organs within the abdominal cavity. This mechanism of metastasis

results in multiple tumors, of varying size, in various places within the abdomen making it difficult for surgeons to completely remove (debulk) all peritoneal seeded tumors..

1.1.2 Ovarian cancer genetics

There are multiple subtypes of ovarian cancer: serous carcinoma, mucinous carcinoma, endometrioid carcinoma, clear-cell carcinomas as well as mixes of these subtypes and undifferentiated types. Serous carcinomas are the most common subtype (75-80% of all cases) and can be further classified into high grade and low grade (HGSOC (90%) and LGSOC (10%), respectively). (Kossai et al 2017). HGSOC is likely to be diagnosed at a higher stage and has the highest mortality rate of all the subtypes (Kossai et al 2017). HGSOC is characterized by *TP53* mutations in virtually all cases and a general lack of other common cancer driving mutations.

Genetic mutations lead to cancer initiation. Healthy cells can spontaneously acquire mutations (somatic mutations) that result in altered growth regulation. Or patients can be born with inherited, familial, genomic mutations that predispose them to ovarian, and other, cancer. The most common familial genomic mutations seen in ovarian cancer are BRCA1 and BRCA2 which are observed in about 25% of patients. These mutations often lead to a loss of function of BRCA. BRCA proteins are involved in homologous recombination repairing of DNA breaks so when BRCA loss of function mutations lead to an accumulation of single strand DNA mutations and eventually cell death. Patients with BRCA mutations are diagnosed with cancer at a younger age than patients without BRCA mutations. The average age of diagnosis overall for ovarian cancer patients is 63 years, but for BRCA 1 and 2 patients the median age of diagnosis is closer to 51 years of age (Kostopoulos et al 2018). Patients with BRCA1 or BRCA2 mutations often respond better to platinum agents and after response, the disease-free interval is around 49

months versus 19 months for non BRCA mutated cancer, as well as increased survival. BRCA mutated cancers also have an increase in survival due to their response to both platinum agents and poly-ADP ribose polymerase (PARP) inhibition. PARP inhibitors prevent mechanisms of DNA repair. DNA repair is essential for cell survival so through PARPi treatment in BRCA mutated cancer prevents cells from repairing mutated DNA. Average survival time at around 91 months versus 54 months for non BRCA mutated cancers. But ovarian cancer frequently recurs resistant to platinum and patients eventually succumb to disease (Mylavaraptu et al 2018).

The most common acquired somatic mutation in ovarian cancer is TP53, which is present in over 90% of HGSOC. Many cancer types acquire specific mutations that can potentially respond to newer targeted therapy. In ovarian cancer, however, there is a lack of consistent recurrent mutations (other than TP53 which currently has no targeted therapies). HGSOC can often have additional copy number alterations and gene amplifications. The most frequent type of acquired mutations seen in ovarian cancer are copy number alterations (CNAs). CNAs can affect protein abundance, however, not every gene that has a CNA will experience a dramatic change in protein expression as CNAs can affect expression changes both in *cis,* where the protein level changes based on the CNA of that gene, and in *trans,* where the protein level changes based on a different gene CNA causing altered expression of downstream targets. Additionally, due to signaling and other protein interactions, a single CNA can affect multiple protein expression levels. Due to this, it is difficult to correlate CNA variation to expression level change to predict specific protein drivers of disease despite predicting overall survival (Zhang et al 2016). This is contrary to many other cancers that have specific driver mutations that are predictive of outcomes and can be used to develop targeted therapies. Therefore, to further understand ovarian cancer it is imperative to look at protein expression changes in ovarian cancer

to predict viable therapeutic targets in addition to predicting based on genetic mutations. Therefore, proteomics and protein expression are important factors to consider to better understand ovarian cancer progression. (Zhang et al 2016). HGSOC tumors taken from TCGA and analyzed using proteomics were better able to predict patient outcomes than using genomic information alone due to protein dysregulation impacting signaling pathways and cellular functions (Zhang et al 2016). Because of this, proteomics is an important consideration in studying ovarian cancer and leads to a better understanding of how ovarian cancer functions and to targeted therapies against dysregulated protein expression.

In many cancers, receptor tyrosine kinases (RTKs) have been shown to be highly important. Acquired somatic mutations such as deletions and point mutations in EGFR, HER2 and MET are common driver mutations across many cancers. Point mutation gain of function mutations in RTKs, specifically EGFR, have been identified in uterine and cervical cancer as potential drivers of cancer progression due to dysregulated signaling (Du and Lovly 2018). RTK aberrations in cancer can promote cancer progression to metastases by affecting tumor proliferation, migration, and invasion. All RTKs have similar properties of having an extracellular ligand binding domain, a transmembrane region, and an intracellular kinase domain. Mutations can produce gain of function, amplifications, and inappropriate activation which can lead to a cancerous phenotype. Due to their importance in many cancers, RTK inhibitors have been developed as targeted therapies for certain types of cancer. For example, RTK inhibitors have been used successfully to treat lung cancer, in which EGFR is frequently a driver mutation (Loong et al 2018). EGFR receptors signal to many pro-survival pathways such as PI3k/Akt, RAS/Raf/MEK/Erk and JAK/STAT, and therefore inhibiting EGFR can block many of these cancer promoting pathways (Fodale et al 2011). However, despite success in other cancers, most

RTK inhibitors have not yet been shown to be successful in ovarian cancer treatment. This may be because the impact CNAs have on protein expression have been largely overlooked (Bell et al 2011). Therefore, the identified RTK treatments that are important in other cancers have not been applicable in ovarian cancer. But by looking at altered protein expression, we may be able to identify actionable RTKs to target with more specific inhibitors.

1.2 Ovarian Cancer Treatments

1.2.1 Chemotherapies

The standard primary chemotherapy regiment for (HR competent) ovarian cancer patients is a combination treatment of paclitaxel and carboplatin. Both chemotherapeutic agents interrupt cell division, thereby killing cells that are actively dividing, such as tumor cells.

Platinum based chemotherapies cause DNA damage. Chemotherapeutic agents enter the tumor cell via transmembrane transport proteins such as copper transporter 1 (CTR1) which has been shown to transport cisplatin into cells (Harrach and Ciarimboli 2015). Then the platinum must move into the nucleus to interact with DNA. Platinum acts as a DNA alkylating agent binding to DNA, leading to DNA damage and DNA strand breaks, which result in cells undergoing apoptotic cell death. Cells that are actively dividing are most affected as they need to replicate their genome to divide, which increases the number of platinum-mediated DNA strand breaks.

The other first line chemotherapy is paclitaxel, a taxane-based chemotherapy. Taxane chemotherapies stabilize microtubules within cells. Microtubules are necessary for mitosis as they make up the mitotic spindles. Taxanes block the depolymerization of microtubules by binding to beta-tubulin. This interrupts the dynamic equilibrium in which the microtubules are

assembled and depolymerize at the same rate. Blocking the depolymerization stabilizes the microtubules, preventing them from breaking apart. Without the ability to build and breakdown microtubules, cells arrest in G2/M phase of mitosis and undergo apoptosis.

1.2.2 Targeted therapies

In addition to chemotherapies, there are few targeted therapies available to treat ovarian cancer. The only widely available targeted therapies that are approved to treat ovarian cancer are PARP inhibitors which are used to treat BRCA mutant HR deficient tumors, Bevacizumab (BEV) which is a VEGF-mediated angiogenesis inhibitor, and immune checkpoint inhibitors (Kossai et al 2017).

PARP inhibitors such as Olaparib are frequently used to treat ovarian cancer. Cancer cells are constantly proliferating and when this DNA damage is not repaired, it leads to apoptosis and cell death. There are two major methods of DNA DSB repair. Homologous recombination (HR), which uses a template from the other chromosome to repair the break, and non-homologous end joining (NHEJ), which ligates the strands back together without repairing the section that was damaged. Continued use of NHEJ leads to a buildup in mistakes in the DNA and can lead to cell death as well. Therefore, for a cancer cell to efficiently evade the effects of chemotherapy, it needs to be proficient at HR (Hosoya and Miyagawa 2014). Cells have three main mechanisms of repairing single strand DNA damage. Mismatch repair (MMR) recognizes base mismatches between the two strands. Deficiencies in MMR lead to accumulation of mismatched base mutations which cannot be repaired, leading to cell death. Base excision repair (BER), is utilized to repair single strand DNA damage (ssDNA) through poly(ADP-ribose) polymerase (PARP) action. Homologous recombination (HR) repair is used to mend double strand DNA (dsDNA) breaks. Patients with deficiencies in HR (HRD) from mutations in HR

repair genes cannot repair dsDNA breaks. In combination with chemotherapies that induce DNA damage, PARP inhibitor (PAPRi) treatment in HRD patients leads to increased tumor cell death through synthetic lethality. Patients with mutations in BRCA1 or BRCA2 are considered HRD and thus respond better to treatment with PARP inhibition and lead to increased survival. PARPi treatment is primarily used in combination with frontline chemotherapy in patients that are HRD and as a maintenance therapy. One study showed PARPi treatment in HRD ovarian cancer increased progression free survival from 5.5 months with placebo treatment and 21 months when treated with niraparib, another PARPi. For patients without BRCA genomic mutations, treatment with niraparib increased PFS from 3.8 months to 12.9 months, showing PARPis are more effective in BRCA mutated patients (Miraz et al 2016). Most clinical trials in ovarian cancer for PARP inhibitors only include patients that are sensitive to platinum treatment, thereby limiting the understanding of PARPis in resistant disease. Additionally, less than half of ovarian cancer patients present with HRD disease. (Mirza et al 2020) Therefore, there is a need to create new therapies for ovarian cancer.

Bevacizumab (BEV) is a VEGF inhibitor which functions by binding to VEGF proteins and preventing them from binding to their cell surface receptor (VEGFR2). Angiogenesis, a process in which new blood vessels are formed, is reliant on VEGF to function. Angiogenesis inhibition prevents tumor cells from creating their own blood supply, required to sustain tumor growth, thereby reducing disease. In addition to chemotherapies, BEV is often used in later stage disease. Recent studies have shown that despite BEV treatment increasing progression-free survival, there was no observed difference in overall survival between patients treated with chemotherapy and BEV versus chemotherapy alone (Tewari et al 2019). Additionally, when treatment stops and normal VEGF signaling resumes, angiogenesis is no longer inhibited, and

tumor vasculature can grow back (Hyseni et. Al 2010). Patients with recurrent disease can also become resistant to BEV treatment through acquired mutations in addition to other chemotherapeutic agents.

Another more promising form of targeted therapy that can be used in ovarian cancer are immune checkpoint inhibitors. Immune checkpoints regulate T cell response. Immune checkpoints occur when T-cell receptors bind to receptors on another cell type. This is used to check for cells that are not native to the body so they can undergo apoptosis and programmed cell death. One strategy to treat cancer is to block this checkpoint interaction between the cancer cell and the T-cell, preventing the tumor cells from avoiding apoptosis. Immune checkpoint inhibitors prevent the binding of the cancer cell to the t-cell, preventing the t-cell from recognizing the cancer cell and causing an immune response to kill the tumor cells. One such protein presented on the T-cells is Programmed cell death protein 1 (PD-1). T-cells present PD-1 and determine cells to be healthy by binding to the ligand PD-L1 on the target cell. Tumors may overexpress PD-L1 to evade the immune system response. This immune checkpoint can be prevented pharmacologically to prevent binding of PD-1 to PD-L1. Pembrolizumab is a monoclonal antibody inhibitor of PD-1 that has been approved for use in ovarian cancer patients. Recent studies have shown via meta-analysis that, despite its success in other cancers, PD1 or PDL1 inhibition alone does not increase survival for ovarian cancer patients (Zhu et al 2021). However, PD-1/PD-L1 inhibitors in combination with other chemotherapeutic agents such as platinum, taxanes, and BEV, has shown modest success in ovarian cancer with under a third of patients responded to the combination treatment either partially or fully (Zhu et al 2021). Cancer cells have other mechanisms for avoiding immune detection. Often, cancer cells will present the

correct proteins to prevent an immune response from killing the tumor cells. In this way, cancer cells can go undetected by the immune system and are allowed to continue proliferating.

Given the limited success of currently available treatments for ovarian cancer and lack of ways to overcome disease resistance, there is a need to identify new methods of treatment..

1.2.3 Resistance to Chemotherapy

Resistance to chemotherapy is not fully understood as mechanisms of chemo-resistance can involve diverse processes. Resistance to chemotherapy can be intrinsic to the patient or acquired through mutations in the cancer cells. Intrinsic resistance often is due to genetic mutations in DNA repair pathways in the patient genome rather than acquired mutations. Additionally, differences in chemotherapy mechanism of action lead to different mechanisms of resistance. Molecular mechanisms of chemo-resistance that may come from genetic mutations and adaptations include prevention of chemotherapeutic agents from entering the cell, efflux of chemo before it can damage the DNA, upregulation of DNA damage repair pathways, avoidance of apoptosis, proteins preventing chemo from reaching its target (Pokhriyal et al 2019). Chemo-resistance is multifactorial and any or all of these mechanisms may be at work when a patient develops chemo-resistant disease. One theory is that chemo-resistant tumor cell clones are present initially and treatment kills sensitive clones leading to the outgrowth of chemo-resistant clones (Zahreddine and Borden 2013).

Acquired genetic mutations can lead to resistance. Mutations in MMR pathway can overcome DNA repair deficiencies leading to platinum resistance as cells can repair DNA damage which allows cells to continue proliferating. Upwards of 40% of platinum resistant ovarian cancer have secondary mutations restoring BRCA function (Mylavaraptu et al 2018). For example, the PEO1 cell lines were collected from a patient at initial surgery and then again

(PEO4) when the patient recurred with resistance to platinum agents (Sakai et al 2009). This patient initially presented with a genomic BRCA2 mutation, preventing HR in response to chemotherapeutic damage to the DNA. A gain of function somatic mutation in BRCA2 in this patient's disease led to recovery of the HR pathway allowing DNA damage to be repaired.

Tumor cells can exhibit resistance to chemotherapies through preventing chemo from encountering DNA. Tumor cells can sequester chemotherapeutic agents within the cell to prevent contact with DNA. There are multiple mechanisms in which cells can interact with platinums after they enter the tumor cell, which includes binding and preventing the molecules from entering the nucleus and causing DNA damage. This can also arise from changes to the tumor microenvironment. Changes in the extra-cellular matrix (ECM) structure around tumor cells can change how chemotherapy comes in contact with the cells. Stiffening of the ECM has been shown to prevent chemotherapeutic molecules from entering the cells (Jiang et al 2022). Similarly, there is a mechanism of chemo-resistance in which tumor cells are able to efflux the chemotherapeutic agent before it can damage the DNA. One such mechanism is through a family of transport proteins, ATP binding cassette proteins (ABC proteins). ABCs can efflux substrates out of the cell and into the extracellular matrix (Fodale et al 2011). They use ATP to pump a variety of substrates out of the cell, which, when used against a chemotherapeutic agent can prevent DNA damage and cell death by removing the chemotherapy before it comes into contact with the DNA. It has been shown that ABC proteins can create resistance to a variety of therapeutic agents that have unrelated mechanisms of causing cell death due to their efflux potential (Fodale et al 2011).

Avoidance of apoptosis is another commonly seen mechanism of chemo-resistance. In healthy cells, when DNA damage is not repaired, cells undergo programmed cell death, or

apoptosis. However, in tumor cells, there are multiple mechanisms in which these cells can avoid undergoing apoptosis. Prevention of apoptosis through differential regulation of apoptosis influencing genes can cause cells to survive chemotherapy treatment. Different apoptotic avoidance mechanisms include prevention of DNA damage detection and prevention of apoptotic initiation. These can occur through either somatic mutations or protein dysregulation.

There are certainly more mechanisms that are not well studied and understood, which increases the difficulty of overcoming chemo-resistance.

1.3 Discoidin Domain Receptor 2 (DDR2) overview

1.3.1 DDR2 review

Discoidin Domain Receptor 2 (DDR2) is a receptor tyrosine kinase. It is a transmembrane protein with an extracellular, ligand binding, discoidin domain and an intracellular tyrosine kinase domain. The ligand for DDR2 is collagen, specifically fibrillar collagens (Valiathan et al 2013). Discoidin Domain receptors (DDR1 and DDR2) are unique RTKs in that their ligands are structural proteins (collagens), not growth factors or cytokines. Their activation, determined as tyrosine phosphorylation of the cytoplasmic tail is an unusually slow process, taking hours versus the minutes it takes most other RTKs (Leitinger 2014). It also exists at the cell surface as a preformed, non-covalent homodimer in the absence of ligand (Henriet et al. 2018). After collagen binding, DDR2 auto-phosphorylates and then transduces the cell signal by phosphorylating downstream targets (Valiathan et al 2013). In addition, DDR2 has been shown to have kinase independent functions. Precisely how DDR2 is activated at the cell surface is not completely understood. Collagen is part of the ECM, providing structure for the stroma surrounding epithelial cells. In tumor associated ECM including HGSOC there is increased collagen present. By binding to and interacting with collagens, DDR2 can regulate the

interaction of the tumor cells with their environment (Leitinger 2014). Additionally, DDR2 signals induce expression of metalloproteinases (MMP) 1, 2, 8, and 13 which are all involved in ECM remodeling either building or breaking down structures (Leitinger 2014).

In normal development, the action of DDR2 in chondrocytes functions to regulate bone growth and development (Leitinger 2014). It is involved in ECM remodeling through interactions with its ligand, collagen, as well as migration and invasion through various downstream signaling pathways (figure 3, Henriet et al. 2018). Knockout DDR2 mice are smaller than their littermates with shortened faces due to shorter bones. These mice also have non-germ cell defects in spermatogenesis and ovulation, making them sterile, as well as defects in wound healing (Leitinger 2014). In humans and mice, rare DDR2 mutations can result in skeletal defects (Valiathan et al 2013).

DDR2 has been shown to be upregulated and important in multiple types of cancer (figure 3). It has been linked to many cell biologic functions of cancer such as proliferation, migration, invasion, avoidance of apoptosis, and metastasis in many cancer types (Henriet et al. 2018, Figure 3, 4). DDR2 can promote cancer cell survival through signaling to MAPK and PI3K-AKT. High levels of DDR2 expression have been linked to poor prognosis in colorectal cancer (Sasaki et al 2017). It has also been implicated in lymphomas and leukemias, breast cancer, head and neck cancers, and thyroid cancer as well (Valiathan et al 2013).

In HGSOC ovarian cancer increased DDR2 expression is associated with worse clinical outcomes (survival) (Ramalho et al 2019, Grither et al 2018). Additionally, the EMT factor TWIST1 induces DDR2 expression in ovarian tumor cells, and genetic depletion of DDR2 in ovarian tumor cells promote ovarian cancer metastasis (Grither et al 2018). (Figure 3, Grither et

al 2018). They also showed that stromal DDR2 expression was also predictive of reduced survival and that patients with high DDR2 expression in stroma had worse overall survival than patients with low DDR2 stroma status regardless of tumor DDR2 expression. Therefore, DDR2 is highly important in ovarian cancer metastasis and progression as it has been shown to be involved in many of the hallmarks of cancer, not just in ovarian cancer, but it is unclear how it may lead to worse prognosis and survival (figure 4). It may be that DDR2 is involved in the development of chemo-resistant disease which would lead to lower survival and more aggressive disease, but the link between DDR2 and chemo-resistance has not yet been investigated.

1.3.2 DDR2 in chemo-resistance

It has been shown through whole genome sequencing of matched primary and recurrent disease that there are no specific driver mutations common to chemo-resistant ovarian cancer disease (Patch et al 2015). Therefore, investigators have begun to apply proteomics and examine protein expression changes. Using mass spectrometry of receptor tyrosine kinases to compare protein expression pre- and post-chemotherapy, DDR2 expression was found to be more highly expressed in patients that did not respond to chemotherapy compared to ones that did (unpublished data). This observation raises the possibility that DDR2 could play a role in the development of chemo-resistance in HGSOC. My preliminary data shows that DDR2 is upregulated during experimental *in vivo* evolution of chemo-resistant cell lines. However, the role of DDR2 in chemo-resistance mechanisms is still yet to be determined.

Due to its importance in many cancers, DDR2 stands out as a potential target for developing new targeted therapies. A few general RTK inhibitors are currently approved therapies for other cancers, however none exist that are specific to DDR2. Since many other cancers have gain-of-function mutations in RTKs, RTK inhibitors are often effective. However,

RTK inhibitor treatment of relapsed ovarian cancer does not improve ovarian cancer patient survival (Wei et al 2023). Additionally, despite the variety of RTK inhibitors available as targeted therapies for other cancers, none are specific to DDR2. Dasatinib, for example, is a general RTK inhibitor and has been used in lung cancers that express DDR2 with moderate success (Beuachamp et al 2013). Ovarian cancer patients show no response to dasatinib (Beuachamp et al 2013, Bast R 2011). Therefore, although some of these already developed drugs may show some effect in high DDR2 expressing cancer therapy, they are not ideal for DDR2 inhibition. A more specific DDR2 inhibitor that inhibits both tyrosine kinase dependent and tyrosine kinase independent actions of DDR2 is the ideal drug to be used in high DDR2 expressing cancer such as ovarian cancer. In collaboration with Greg Longmore's lab, the Fuh lab is utilizing a novel, specific, allosteric inhibitor specific to DDR2 called CR13452. It disrupts DDR2's ability to bind to its ligand collagen. CR13452 does not inhibit the kinase independent functions of DDR2 making it useful in deciphering the multiple signaling pathways DDR2 may be involved in and worth further investigation.

1.4 Thesis Rational and Significance

Ovarian cancer is a highly deadly disease which metastasizes easily. Most patients are diagnosed after the cancer has already metastasized making treatment difficult. Additionally, most patients will experience disease relapse and resistance to chemotherapy. There are few approved therapies to treat ovarian cancer, and many of them only moderately increase survival. Therefore, it is essential to further our understanding of the disease to create new therapies and increase patient survival.

The goal of my project is to investigate what changes between chemo-sensitive tumors and their progression to chemo-resistance occur that lead to acquired resistance in ovarian

cancer. We want to identify proteins that are essential to chemo-resistance in ovarian cancer which can then be targeted with novel therapies. I decided to create matched chemo-resistant and chemo-sensitive mouse ovarian cancer cell lines to study this. The aim is to fill a need in the field of ovarian cancer chemo-resistance research by creating this new tool. Additionally, our lab identified DDR2 to be upregulated at the protein level in chemo-resistant ovarian cancer patients compared to chemo-sensitive patients in comparing pre- and post-chemo tumor protein expression. I predict that DDR2 may be essential to the development of chemo-resistance in ovarian cancer.

Chapter 2: Development of Novel, Chemo-resistant mouse ovarian cancer cell lines

2.1 Declarations

All experiments were designed, performed, and analyzed by Alyssa Oplt. Patrick Cannon assisted in mouse sacrifices and maintenance of CHRP cells in culture.

2.2 Introduction

Ovarian cancer has an extremely low 5-year survival rate at under 30%. Additionally, up to 80% of ovarian cancer patients experience recurrence of their disease which is often resistant to treatment and ultimately leads to patient death. This resistance can either be intrinsic to the cancer where the cancer does not respond to chemotherapy within 6 months of initial treatment, or resistance can be acquired over time. Acquired resistance is much more common than intrinsic resistance to chemotherapy, therefore it is important to understand what changes lead to resistance in initially sensitive tumors. There are many potential mechanisms that lead to chemo-resistance, including avoidance of apoptosis, sequestering chemotherapy agents away from DNA, efflux of chemotherapy agents out of the cell before they can cause damage, and recovery of homologous recombination function, all of which are poorly understood. There are a limited number of ovarian cancer cell lines that are considered resistant to specific chemotherapeutic agents. However, all these cell lines are human immortalized cell lines, and most do not have a matched chemo-sensitive cell line. Ideally, studies of acquired resistance would use pre-chemo and post-chemo matched cells to compare what changes in gene and protein expression exist between the two. Currently there is only one matched chemo-sensitive chemo-resistant set of cell

lines PEO1 and PEO4 which are matched cell lines isolated from a patient before and after resistance was acquired. These cells are useful as they uncovered a mechanism of resistance through a mutation in BRCA2 that lead to recovery of homologous recombination in these cells (citation). While useful, these cells do not capture all the potential mechanisms of chemo-resistance, therefore, there is a need for novel matched cell lines to investigate other mechanisms of chemoresistance in ovarian cancer to further our understanding and potentially leading to better treatment options and increased patient survival.

Human cell lines are useful tools in understanding chemo-resistance, but to fully capture the microenvironment and the effects it may have on tumor progression requires *in vivo* data. To perform experiments on human cell lines *in vivo* requires implanting human cell lines into immunocompromised mice. A defective immune system could impact the biological relevance of the data as immune cells have been shown to have a large impact on cancer development and treatment. Additionally, to understand the mechanisms of acquired chemo-resistance would require a matched pair of chemo-sensitive and chemo-resistant cell lines. At present, there are no matched chemo-sensitive and chemo-resistant mouse ovarian cancer cells. In order to identify and understand mechanisms by which ovarian cancer cells develop chemo-resistance, I developed matched chemo-sensitive and chemo-resistant mouse ovarian cancer cell lines from serial *in vivo* passaging. I passaged cells through mice with increasing doses of chemotherapy. Similar models such as this have been used in other cancers and have proven to be useful. In prostate cancer, the cell line LNCaP was derived from a patient and made into an immortalized cell line. This cell line was then injected orthotopically into nude mice and allowed to metastasize. Bone metastases were then used to create a new immortalized cell line. In this way they were able to create a metastatic prostate cancer cell line that is a powerful tool in studying

prostate cancer metastasis mechanisms (Thalmann et al 1994). Taking a similar approach in injecting cells into mice to produce a novel cell line with new characteristics, I was able to create a matched chemo-sensitive and chemo-resistant mouse ovarian cancer cell line to fill the need for a syngeneic model of acquired chemo-resistance.

To study ovarian cancer in the context of the surrounding microenvironment, ID8 cells have proven to be extremely useful because these cells can be injected and grown in immunocompetent mice. ID8 cells are a syngeneic mouse ovarian cancer cell line. These cells are one of the only syngeneic models of ovarian cancer. The original ID8 cells were created by the Terranova lab via isolation from mouse ovarian tumors and grown clonally (Roby et al 2000). To emulate high grade serous ovarian cancer (HGSOC) more closely, the McNeish lab introduced a TP53 null mutation and methylation silencing of BRCA2 to the ID8 cells (Walton et al 2016). These cells were also transfected with GFP and luciferase to label the cells genetically resulting in the cell line ID8 TP53-/- BRCA2-/- GFP LUC (ID8PBGL). However, ID8PBGL cells are not resistant to any forms of chemotherapy, so they are not useful in studying the mechanisms of chemo-resistance. Here I present the characterization and development of novel syngeneic cell lines by passing ID8PBGL cells through C57/BL6 mice which were treated with increasing doses of chemotherapy to create matched chemo-sensitive and chemo-resistant syngeneic cell lines.

2.3 Materials and Methods

2.3.1 Cell culture

ID8 trp53$^{-/-}$ BRCA2$^{-/-}$ GFP LUC cells were a generous gift from Ian McNeish. All cell lines that originated from the ID8 cells were cultured in DMEM (Sigma-Aldrich) 4% FBS 1% insulin-transferrin-selenium, 1% penicillin and 1% streptomycin. All cells were maintained at 37

°C in a 5% CO2 incubator. Cell lines were confirmed Mycoplasma negative with MycoAlert Mycoplasma Detection Kit (Lonza) before experiments. Ascites cells from mice were plated in the same medium as the parental cells. Ascites were collected from mice and plated on tissue culture plates and left to attach overnight. The next day we washed the plates with PBS to remove red blood cells and other non-adherent cell types. Cells were then passaged in culture as described above.

2.3.2 Chemo-Resistance passaging *in vivo*

All animal experiments were done in accordance with the guidelines of the American Association for Accreditation for laboratory Animal Care and the U.S. Public Health Service Policy on Humane Care and Use of Laboratory Animals. Additionally, all studies were approved by the Washington University Institutional Animal Care and Use Committee in accordance with the Animal Welfare Act, the Guide for the Care and Use of Laboratory Animals, and NIH guidelines. Female, 6-week-old, C57BL6 mice (The Jackson Laboratory) were injected with $5*10^6$ ID8 trp53$^{-/-}$ BRCA2$^{-/-}$ GFP LUC cells. After 42 days the mice were treated with 2mg/kg of carboplatin and 2mg/kg paclitaxel twice a week until day 61 when mice were sacrificed and the tumors and ascites were collected. Ascites plated in tissue culture plates and grown in the same media used for the original cells. These cultured cells were propagated and $5*10^6$ were injected into a new set of mice and allowed to grow for 41 days and then were treated with 5mg/kg of chemotherapy twice a week until day 48 at which point the mice were sacrificed and the same tumor and ascites and propagation occurred with slightly higher chemo doses each passage. See table for treatment doses for each passage. After 5 passages through the mice with the highest dose of 10mg/kg of both carboplatin and paclitaxel, cells were established as chemo-resistant and used for the rest of the experiments. Each passage of cells through the mice were collected and

saved and denoted chemoresistance passage N (CHRP-N) so the final passage was named CHRP-5. These cells were then sorted for GFP expression on MoFlo cell sorter so only tumor cells remained in culture.

2.3.3 Western Blot

Performed as described previously (Mullen et al 2021). Briefly, cultured cells were lysed and proteins were quantified by Bradford assay. Lysates were reduced via SDS-PAGE by standard methods and transferred to a nitrocellulose membrane. Each membrane was incubated with primary antibody at 4°C for 1 to 3 nights, washed in TBST, and incubated with corresponding horseradish peroxidase-conjugated secondary antibodies. Antibodies DDR2 (cell signaling) and beta-actin (Sigma) were used. Signal was detected with the Pierce ECL Western Blotting Substrate, and chemiluminescence was measured on a ChemiDoc (Biorad).

2.3.4 MTS survival assays

96-well plates (Techno Plastic Products) were coated in 30uL/well of 1mg/mL rat tail collagen and 1N NaOH and allowed to polymerize for half an hour prior to cell plating. Cells were plated at 1500 cells/well and allowed to attach overnight. Plates were then treated with serial dilutions of carboplatin, diluting by half between each column and starting at 1000uM carboplatin. Cells were incubated for 72 hours and then 20uL/well MTS (3-(4,5-dimethylthiazol-2-yl)-5-(3-carboxymethoxyphenyl)-2-(4-sulfophenyl)-2H-tetrazolium) solution (Promega) was added to the cells, incubated for 2 hours at 37 C, and then the absorbance was measured at 490 nm with a 96-well plate reader (Tecan infinite M200 Pro). Analysis was done using GraphPad Prism 8.

2.3.5 RT qPCR

RNA was isolated from cells or tumors using the Qiagen easy RNA kit. cDNA was made from the RNA. qPCR was run using SYBR green. Primers for DDR2, ABCG2, GPNMB, MUC1. qPCR was analyzed using SYBR green reagents. See table 3 for primer sequences.

2.3.6 Whole exome RNA sequencing

Chemoresistance project: Mice were injected with either ChRP-5 or ChRP-1 GFP+ cells and allowed to grow for 21 days. At day 21 mice began treatment of 5mg/kg of carboplatin twice a week. Day 35 tumors and ascites were collected from the mice and RNA was extracted from snap frozen metastatic uterine tumors which was then sent for sequencing. RNA sequencing data was analyzed with Partek to run DEseq2 comparing chemo-resistant to chemo-sensitive gene expression changes.

2.4 Results

2.4.1 Development of Resistant Cell Lines

To understand the mechanisms of chemoresistance in ovarian cancer, I first developed a syngeneic, chemo-resistant mouse ovarian cancer cell lines. I created acquired resistance to chemotherapy in ID8PBGL cells via injecting cells intraperitoneally into mice, treating the mice with increasing doses of carboplatin and paclitaxel (chemotherapy), collecting and plating ascites that developed in the mice, and then repeating the cycle (figure 1a). This resulted in an ID8 based ovarian cancer cell line that is significantly more resistant to carboplatin and paclitaxel than the parental ID8PBGL cells. I repeated this process five times ending at a dose of 10mg/kg of carboplatin and 10mg/kg of paclitaxel (figure 1b). Cell lines from each passage were labeled chemoresistance passage (CHRP-x-y) with X representing the passage number and Y indicates which mouse the cells were isolated from. For example, from our final passage, passage 5, I

labeled CHRP-5-6 indicating these cells are from passage five and were isolated from mouse 6. Each passage I established cell lines from ascites collected from multiple mice to confirm development of resistance.

For the initial passage, after injecting cells intraperitoneally, I waited 42 days to start chemotherapy treatment. I treated the mice with carboplatin (2mg/kg) and paclitaxel (2mg/kg) for 10 days, then sacrificed the mice to assess tumor burden. After sacrifice, tumors were collected and preserved via flash freezing, FFPE fixing, and OTC freezing. Ascites was collected from the mice and plated in tissue culture to grow. Ascites is made up of a diverse range of cell types so to ensure that only tumor cells were growing and no other cell types from the ascites such as blood cells and immune cells. To do this, I passaged the ascites cells in culture through trypsinization at least 3 times to eliminate cells that are not adherent, such as immune cells, and to allow the tumor cells to overtake any other cell population with their aggressive proliferation. After initial passaging, I sorted the resulting cells for GFP to filter out any remaining non-tumor cells. These cells were then injected back into mice intraperitoneally and allowed to implant and grow, treated with chemotherapy. This process was repeated 5 times with increasing doses of chemotherapy. As a control, I also passaged ID8PBGL cells through mice without treating with chemotherapy. I collected ascites and established a cell line through the same process as before via passaging in culture and sorting for GFP+ and called this line chemo-naïve ascites (CNAS). I used these cells as our baseline control to compare to the subsequent passages..

2.4.2 Characterization of Resistant Cell Lines

With each passage, I observed the cells became more resistant to chemotherapy and more aggressive. The mice were becoming noticeably sick much sooner every passage, therefore, I had to shorten the time between injection and treatment and time to sacrifice as mice would die

before I could collect tumors and ascites. I decided to determine when to start treatment by sacrificing a pilot mouse and assessing tumor burden starting at day 21, or when I noticed ascites or tumor development from visual observation of the mice. I determined the ideal treatment should occur when mice have small tumor nodules but had not developed large tumors or ascites (figure 3e). With each passage, I observed the tumor cells became more aggressive, as the mice were developing disease much faster than the first passage. For the first passage I started treatment on day 42 and sacrificed the mice on day 61. By the final passage, I started treatment on day 25 and sacrificed on day 32 (figure 1b).

By passage 5, the mice looked very diseased at time of sacrifice from visual observation. I noted that despite the shorter time to treatment, time to sacrifice, and increased chemotherapy dosage, visually, the disease burden observed in the mice increased (figure 2). I used multiple approaches to assess the disease burden. Tumor burden was quantified by ascites volume, omentum weight, and number of metastatic sites. The primary site of ovarian cancer metastasis is the omentum, therefore I used omentum weight as an approximation of tumor burden. Overall, the average weight of the omentum did not significantly change between passages (figure 3c). Additionally, I collected any ascites present in the peritoneal cavity at time of sacrifice to measure the volume before plating in cell culture. I observed the volume of ascites does correlate with increasing passages as well as the percentage of mice that had ascites from each passage (figure 3a,b). As the cells became more resistant to chemotherapy, I also found that the average number of organs with visible metastases increased as well (figure 3d).

Each CHRP line was characterized between each passage with to look for changes in gene expression, viability, and resistance to chemotherapy. I used MTS survival assays as well as colony formation assays to determine the difference in resistance to chemotherapy between the

subsequent passages of these cell lines. At final passage, I found that CHRP5 cells were significantly more resistant to chemotherapy (IC50 176uM carboplatin) compared to CNAS cells (IC50 24.8uM carboplatin) (figure 4a). We also compared CHRP1 and CHRP5 survival after multiple passages in culture when treated with carboplatin and saw a significant increase in resistance in CHRP5 (IC50=293.4) compared to CHRP1 (IC50=92.52) (figure 4b). MTS assays were used to determine viability of cancer cells and to confirm a decrease in sensitivity with each passage.

2.4.1 Gene Expression Changes in Resistant vs. Sensitive Cells

I decided to move forward using these cells for investigating the mechanisms of acquired chemo-resistance in ovarian cancer. To look at gene expression changes, I sent total RNA from CHRP5 and ID8PBGL tumors to Nanostring for mRNA sequencing using their Mouse Tumor Signaling 360 panel to look specifically at tumor signaling genes as signaling dysregulation is an important part of tumor progression (table 1). Differential expression analysis (DEseq2) showed multiple genes that were upregulated in chemo-resistant tumors versus chemo-sensitive tumors (figure 5a, b). Multiple genes were identified as significantly overexpressed in our chemo-resistant samples including DDR2, GPNMB, AURKA, HGMA1, RASA1, MUC1 which we attempted to confirm with qPCR but only confirmed these results in a few genes (figure 6a-f). A few notable genes that were found to be overexpressed and confirmed by qPCR are ABCG2, a chemo efflux protein, and GPNMB, a transmembrane glycoprotein previously shown to correlate with reduced survival ovarian cancer. Also, breast cancer resistance protein, ABCG2, is an efflux protein that has been shown to pump chemotherapy agents out of ovarian cancer cells (figure 6a) (Ricci et al 2016). Therefore, I was interested in further investigation of ABCG2 expression between CHRP5 and CNAS as a mechanism of acquired resistance. I verified our RNA-seq

results with RT-qPCR and found CHRP5 cells do overexpress ABCG2 compared to CNAS cells. It would be interesting to see if ABCG2 protein is also overexpressed in CHRP5 in addition to mRNA overexpression. The other interesting gene we identified is Glycoprotein non-metastatic protein B (GPMNB), a transmembrane glycoprotein found clinically correlated with reduced survival in ovarian cancer patients (Ma et al 2018). I verified the overexpression of GPNMB mRNA seen in RNA-seq in CHRP5 versus CNAS via qPCR (figure 6a). A recent study showed that inhibition of GPNMB with miRNA reduced ovarian cancer cell ability to migrate and invade (Tuo et al 2022). The role of GPNMB in chemo-resistance has not yet been explored, however our results suggest that GPNMB may be involved in acquired chemo-resistance and is thus worth further investigation.

To further expand our search for targets of chemo-resistance, I then decided to expand to whole genome RNA sequencing to look for other potential targets. To control for differences in chemotherapy treatment and time to initial treatment, I injected either CHRP1 or CHRP5 cells into mice, treated all mice with 10mg/kg of carboplatin starting on day 21 post-injection. I treated the mice for 14 days and then sacrificed the mice to collect tumors and ascites to extract RNA. We used bulk mRNA whole exome sequencing and results were analyzed using Deseq2 for differential expression using Partek (figure 7, table 2). I confirmed that the genes identified in our Nanostring panel were differentially expressed in this experiment as well. I also identified genes that were not included in the Nanostring panel as being highly differentially expressed between chemo-resistant and chemo-sensitive. I then filtered by p-value of below 0.05 and fold change greater than 2. After filtering I found 27 genes to be significantly upregulated in CHRP5 versus CHRP1 cells and 128 genes that are significantly downregulated (figure 7).

2.5 Discussion

These novel cells line fulfil a need in ovarian cancer chemo-resistance research. The ability to use immune competent mice in cancer studies captures a more biologically relevant tumor microenvironment to study the disease. Additionally, treatments that elicit an immune response can be more easily studied. These cells also function as a powerful tool for understanding the progression of chemo-resistance both *in vitro* and *in vivo*. Having multiple cell lines isolated as resistance develops allows for a much closer lens into the mechanisms of acquired resistance. The change in gene and protein expression can be mapped through the development of resistance which can lead to identifying key genes involved in resistance.

Future experiments could include RNA-seq on each subsequent cell line, CHRPs 1-5, to see which genes are differentially regulated at each time point in the development of chemo-resistance. Also, these cells could be used in mass spectrometry to identify proteomic changes in acquiring resistance to chemotherapy. As these cells were only treated with carboplatin and paclitaxel, another experiment could be treating these cells with other chemotherapeutic agents to determine if the resistance mechanisms found are utilized in resistance to other therapies. Additionally, these cells could be treated with carboplatin and/or paclitaxel and another drug to test for synergy or increased chemo-sensitivity through combination treatment.

There were other genes identified via RNA sequencing that we did not follow up on but are interesting targets for further study. Notable genes identified in our RNA sequencing results that are significantly upregulated in our chemo-resistant cells include MSLN (fold change = 5), and IER3 (fold change = 4.12). Mesothelin (MSLN) is a glycoprotein expressed in mesothelial cells. It has been shown that ovarian cancer patients highly express MSLN and that clinically patients that were resistant to treatment overexpressed MSLN compared to chemo-sensitive

treatment (Hillard 2018). However, these are only correlations and thus would be worth further investigation. Immediate early response 3 (IER3) is involved in regulation of apoptosis which makes it interesting as a potential target of chemo-resistance. Overexpression of IER3 has been linked to poor prognosis in other cancer types and has been correlated to shorter progression free survival in ovarian cancer and resistance (Jordan et al 2020). IER3 is worth further investigation for its involvement in chemo-resistance in ovarian cancer.

Nanostring sequencing also identified gene targets we thought might be worthy of further analysis: GPNMB, ABCG2, MUC1, HGMA1, AURKA, RASA1. RT-qPCR of CHRP5 and CNAS showed HGMA1, RASA1 and AURKA did not mirror the overexpression seen in the sequencing data. GPNMB has been clinically linked to ovarian cancer response to treatment, so it would be interesting to perform genetic knockouts and assess changes in resistance to therapy. Transmembrane glycoprotein mucin 1 (MUC1) could be influential in chemo-resistant ovarian cancer as it has been linked to migration and invasion due to its importance in the extra-cellular space. MUC1 was not as highly overexpressed as GPNMB and ABCG2 so we did not investigate it further here, but it may be worth further study.

2.6 Conclusions

I developed a set of novel chemo-resistant, syngeneic ovarian cancer cell lines. MTS assays showed the progression of resistance to chemotherapy. This matched set of cell lines with increasing levels of resistance to chemotherapy fill a need in the field of ovarian cancer chemo-resistance research to further understand acquired chemoresistance. There are many potential uses for these cells to study ovarian cancer chemo-resistance and metastasis such as genetic screens to investigate gene dysregulation, siRNA screens to look at protein expression, or drug

treatment i*n vivo* models. Additionally, the identified gene targets that resulted from sequencing are worth further investigation to determine their role in ovarian cancer chemoresistance.

2.7 Figures and Tables

A

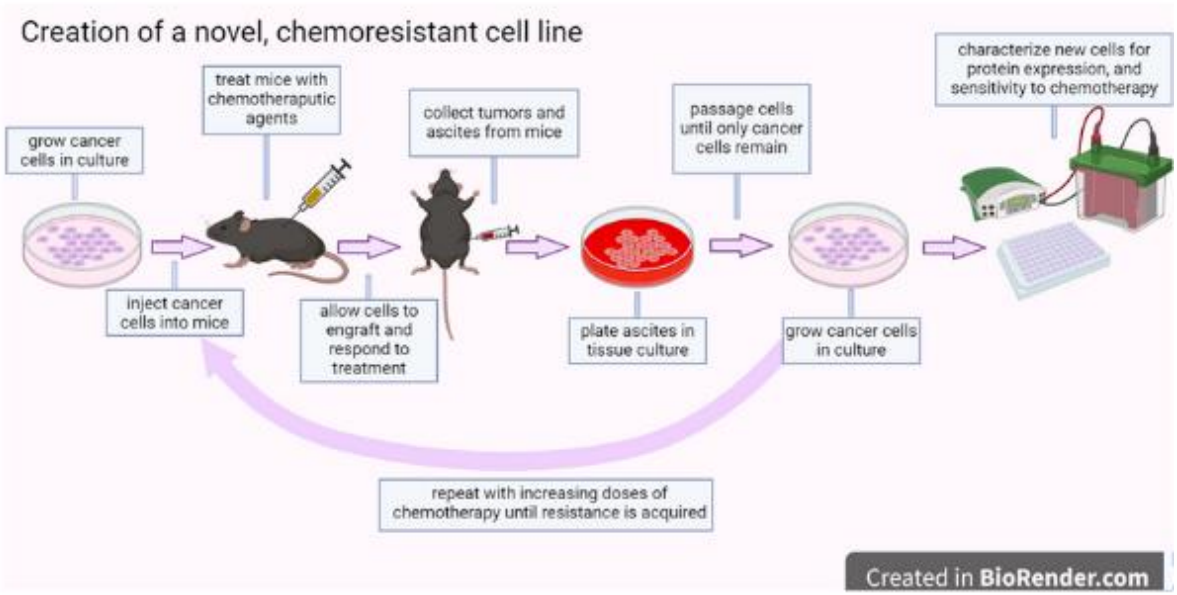

B

Passage	Treatment start day	End point	Carboplatin dose (mg/kg)	Paclitaxel dose (mg/kg)	Cell line created
0	42	61	0	0	CNAS
1	42	61	2	2	CHR-P1
2	41	61	5	5	CHR-P2
3	29	36	5	5	CHR-P3
4	25	32	7	7	CHR-P4
5	21	33	10	10	CHR-P5

Figure 2.1: Process of developing chemo-resistant cells. (A) Schematic showing the process of passaging ID8PBGL cells through mice to create the novel cell lines. (B) Table showing time to treatment, time to endpoint, chemo dosage, and the name of the cell line created by that passage.

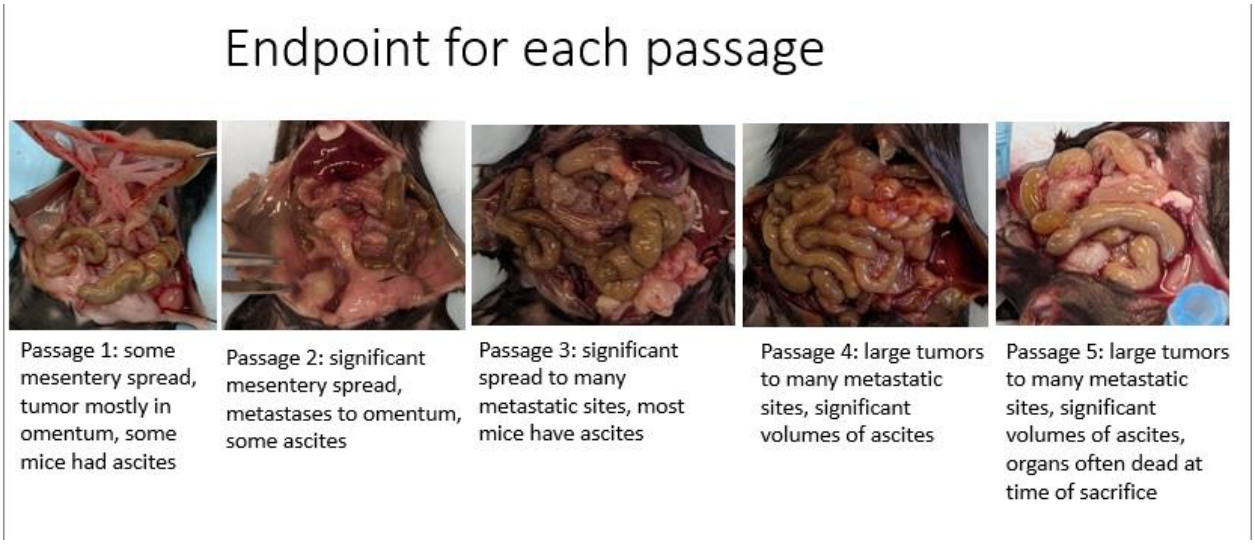

Figure 2.2: CHRP cells caused more tumor burden than the previous passages. Endpoint respresentitive images for each passage.

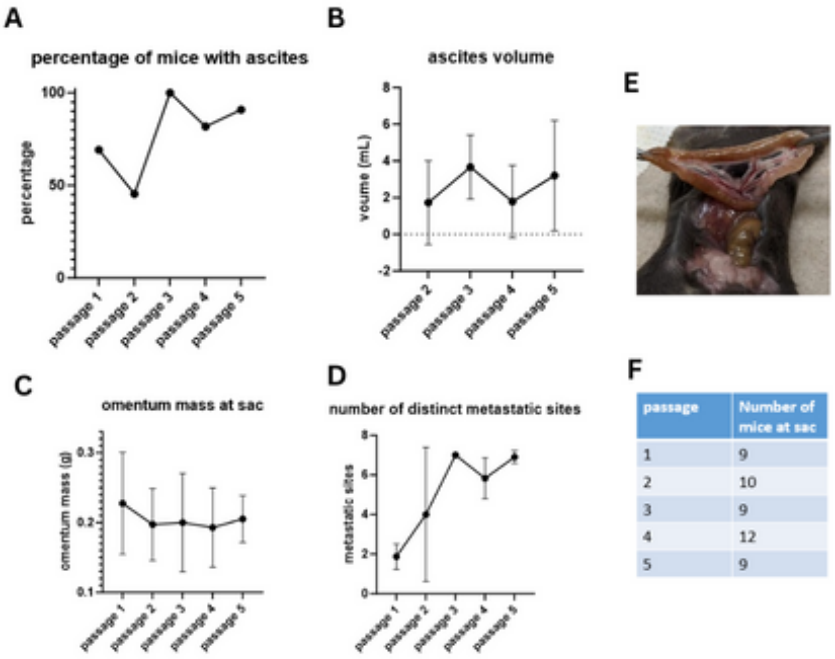

Figure 2.3: Tumor burden increased as resistance developed. Graphs depicting (A) omentum mass, (B) percentage of mice with ascites, (C) number of distinct metastatic sites, and (D) ascites volume for passage endpoint. Table showing the number of mice that survived to sacrifice. Representative image showing tumor burden determining initial treatment timing.

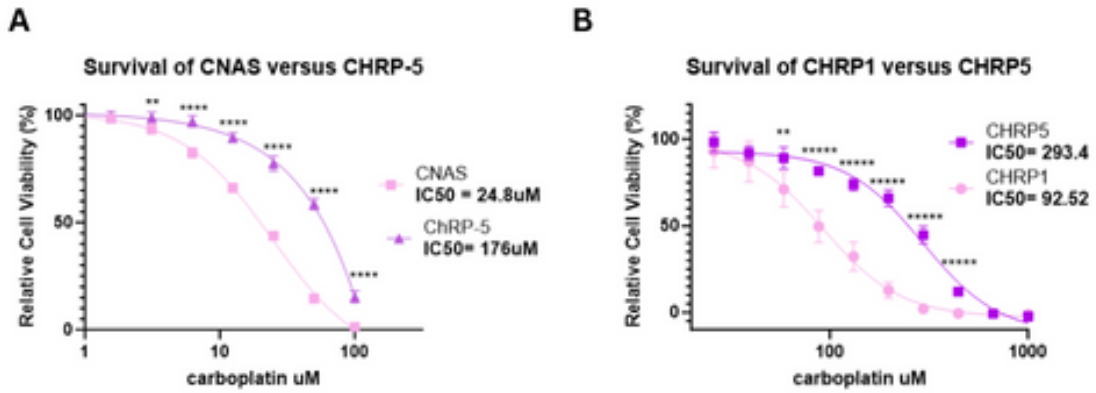

Figure 2.4: Serial passaging of CHRP cells lead to acquired chemo-resistance. (A) Table showing the differences in treatment conditions for each passage. (B) MTS survival curve comparing CNAS (B) or CHRP1 (C) to CHRP5 cells sensitivity to carboplatin.

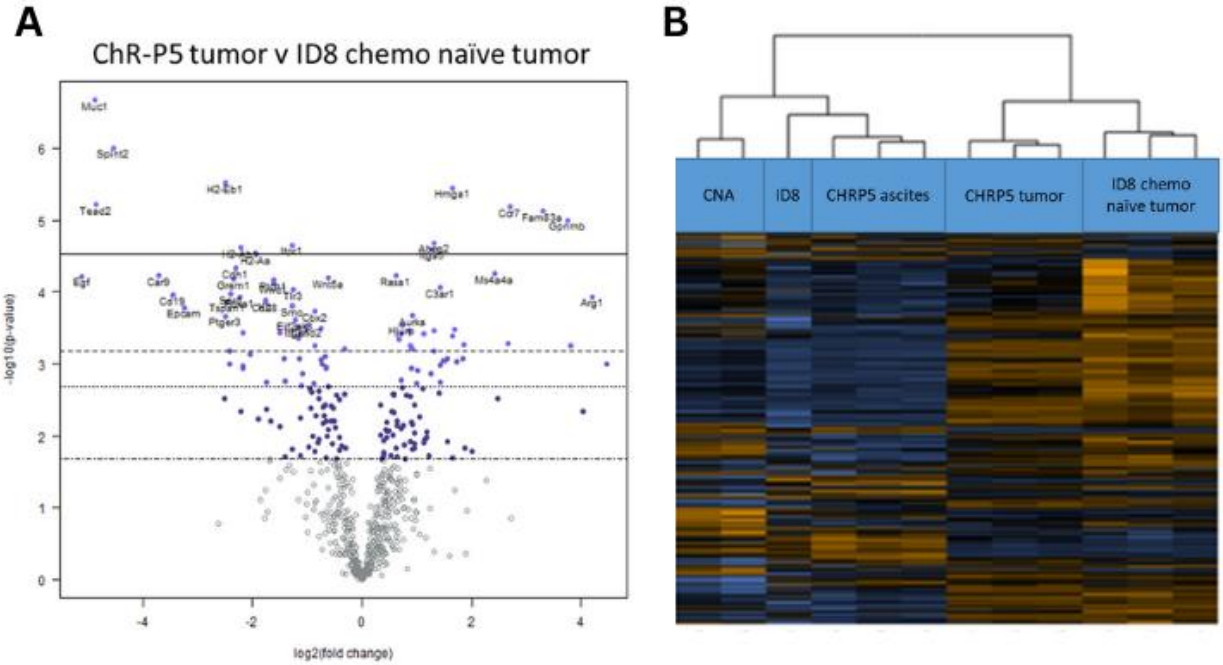

Figure 2.5: Nanostring identified many differentially expressed genes between chemo-sensitive and chemo-resistant. (A) Volcano plot of highly differentially expressed genes via Nanostring sequencing. (B) Heatmap of mRNA expression of Nanostring panel genes.

Table 2.1: Top differentially expressed genes as identified by Nanostring Mouse Tumor signaling 360 gene panel.

Gene name	P-value (R vs. S)	FDR step up (R vs. S)	Ratio (R vs. S)	Fold change (R vs. S)
WNT5A	1.73E-34	4.08E-33	17.22	17.22
COL6A1	2.56E-37	7.13E-36	17.14	17.14
COL6A2	5.11E-20	5.25E-19	15.79	15.79
PGF	2.27E-32	4.92E-31	12.26	12.26
LOX	4.99E-55	4.86E-53	11.79	11.79
CD34	2.46E-51	1.92E-49	10.48	10.48
GLUL	2.19E-28	3.80E-27	10.28	10.28
FLT4	7.85E-40	2.59E-38	9.51	9.51
HSPB1	2.82E-56	3.14E-54	8.77	8.77
FSTL1	6.44E-72	1.68E-69	8.03	8.03
CCNF	1.81E-56	2.35E-54	7.91	7.91
GPT	2.05E-39	6.39E-38	7.74	7.74
CAV1	2.43E-46	1.46E-44	7.44	7.44
SPINT1	5.65E-13	3.58E-12	7.17	7.17
FZD4	7.48E-45	4.17E-43	7.02	7.02
KIF20A	7.96E-40	2.59E-38	6.91	6.91
TNS1	6.15E-31	1.20E-29	6.66	6.66
IDH1	8.55E-42	3.33E-40	6.59	6.59
CCNB2	1.43E-49	1.01E-47	6.23	6.23
KIF2C	9.29E-35	2.34E-33	6.16	6.16
GSTM4	3.06E-19	2.87E-18	5.78	5.78
LMNB1	1.03E-34	2.52E-33	5.53	5.53
KIF23	2.37E-26	3.70E-25	5.53	5.53
AURKB	1.71E-26	2.78E-25	4.97	4.97
PLK1	3.00E-20	3.17E-19	4.95	4.95
VEGFB	8.27E-26	1.26E-24	4.78	4.78
FBLN2	1.13E-18	1.02E-17	4.69	4.69
CCNA2	8.72E-29	1.58E-27	4.62	4.62
SERPINE1	2.87E-15	2.05E-14	4.58	4.58
Pclaf	2.03E-35	5.27E-34	4.55	4.55
RAD54L	1.15E-22	1.40E-21	4.52	4.52
LAMA4	7.54E-11	4.09E-10	4.31	4.31
MCM2	1.29E-31	2.64E-30	4.28	4.28
JUP	2.35E-25	3.46E-24	4.24	4.24

GSR	1.58E-31	3.16E-30	4.11	4.11
PIK3R1	6.25E-23	7.86E-22	4.08	4.08
UBE2C	4.63E-22	5.56E-21	4.01	4.01
SLIT2	2.84E-06	9.85E-06	3.97	3.97
SREBF1	9.48E-20	9.24E-19	3.91	3.91
TGFB3	4.86E-20	5.05E-19	3.90	3.90
RRM2	7.99E-33	1.78E-31	3.86	3.86
LAMB1	1.11E-15	8.43E-15	3.83	3.83
ITGA1	6.95E-05	2.09E-04	3.80	3.80
Fcgr4	3.10E-08	1.26E-07	3.75	3.75
DNMT1	1.43E-15	1.06E-14	3.72	3.72
CDC20	9.37E-24	1.24E-22	3.69	3.69
PKM	1.03E-20	1.11E-19	3.60	3.60
TGM2	7.49E-14	5.03E-13	3.59	3.59
LYN	4.03E-18	3.49E-17	3.56	3.56
CCNB1	3.23E-30	6.15E-29	3.55	3.55
SDC1	5.41E-20	5.41E-19	3.54	3.54
EME1	9.32E-19	8.65E-18	3.54	3.54
ITGB2	8.52E-11	4.58E-10	3.47	3.47
MYBL2	9.67E-19	8.87E-18	3.47	3.47
ELOVL5	3.68E-18	3.22E-17	3.44	3.44
PARVA	2.81E-17	2.29E-16	3.42	3.42
TIMELESS	2.20E-15	1.59E-14	3.40	3.40
ITPR1	6.22E-16	4.80E-15	3.37	3.37
SQLE	1.58E-18	1.41E-17	3.36	3.36
TUBG1	4.87E-21	5.59E-20	3.20	3.20
TOP2A	5.39E-18	4.62E-17	3.20	3.20
AKT1	5.33E-20	5.40E-19	3.18	3.18
PTPN6	7.51E-13	4.72E-12	3.16	3.16
BIRC5	9.42E-21	1.03E-19	3.16	3.16
SIN3A	2.20E-17	1.81E-16	3.15	3.15
AURKA	4.63E-23	5.91E-22	3.10	3.10
FZD1	9.19E-07	3.32E-06	3.10	3.10
CCR7	1.34E-10	7.03E-10	3.09	3.09
GPNMB	1.99E-08	8.26E-08	3.08	3.08
MCM4	1.40E-16	1.10E-15	3.08	3.08
ALDOA	2.35E-19	2.24E-18	3.05	3.05

CXXC5	8.42E-15	5.97E-14	3.04	3.04
NEK2	1.03E-16	8.18E-16	3.04	3.04
G6pdx	4.11E-08	1.66E-07	2.99	2.99
BRIP1	2.09E-17	1.75E-16	2.97	2.97
CDK2	6.63E-22	7.83E-21	2.96	2.96
PARP1	5.38E-10	2.67E-09	2.95	2.95
MAPK3	1.04E-13	6.94E-13	2.88	2.88
GUSB	2.02E-13	1.31E-12	2.85	2.85
TPI1	1.99E-11	1.11E-10	2.85	2.85
CLSPN	4.44E-13	2.84E-12	2.84	2.84
TPX2	1.09E-12	6.73E-12	2.81	2.81
DNA2	1.68E-09	7.84E-09	2.79	2.79
TTK	4.99E-14	3.41E-13	2.79	2.79
TEAD2	7.09E-04	1.82E-03	2.74	2.74
SLC2A1	8.92E-10	4.35E-09	2.70	2.70
GTSE1	7.10E-14	4.82E-13	2.70	2.70
ITGA5	3.42E-10	1.71E-09	2.69	2.69
FANCI	2.30E-14	1.58E-13	2.68	2.68
AMOTL2	1.87E-10	9.56E-10	2.63	2.63
FANCD2	1.78E-12	1.08E-11	2.63	2.63
CTSW	6.33E-04	1.64E-03	2.59	2.59
LIG1	2.62E-09	1.18E-08	2.59	2.59
ITGB5	1.12E-09	5.32E-09	2.57	2.57
ITGB8	1.88E-09	8.69E-09	2.57	2.57
IL3RA	7.85E-09	3.44E-08	2.54	2.54
H2AFX	5.02E-12	2.92E-11	2.53	2.53
FEN1	5.56E-16	4.34E-15	2.52	2.52
BRCA1	6.16E-11	3.36E-10	2.44	2.44
FOXM1	1.10E-09	5.24E-09	2.44	2.44
IL12RB1	3.96E-03	9.14E-03	2.43	2.43
PDGFRA	1.67E-04	4.81E-04	2.37	2.37
CTNNB1	2.66E-11	1.46E-10	2.34	2.34
STK4	2.15E-10	1.09E-09	2.33	2.33
MET	1.57E-10	8.10E-10	2.31	2.31
KEAP1	1.13E-08	4.89E-08	2.23	2.23
EIF4G1	9.67E-08	3.81E-07	2.21	2.21
Sting1	1.50E-08	6.32E-08	2.17	2.17

NUF2	1.08E-11	6.22E-11	2.14	2.14
UCHL5	1.51E-12	9.20E-12	2.14	2.14
CHEK2	1.94E-09	8.92E-09	2.13	2.13
VCP	2.01E-06	7.11E-06	2.10	2.10
ITGB3	1.75E-04	5.00E-04	2.07	2.07
CDC25C	1.58E-07	6.12E-07	2.07	2.07
HJURP	6.52E-09	2.87E-08	2.07	2.07
THBS1	4.08E-04	1.10E-03	2.06	2.06
PTGER4	5.83E-04	1.52E-03	2.06	2.06
EHHADH	9.40E-04	2.40E-03	2.05	2.05
CDCA5	2.45E-09	1.11E-08	2.04	2.04
ERCC3	1.59E-07	6.12E-07	2.02	2.02
FBLIM1	1.45E-05	4.74E-05	2.00	2.00
SPHK2	8.70E-07	3.15E-06	0.50	-2.01
PARD3	6.09E-06	2.06E-05	0.50	-2.01
ASXL2	6.11E-09	2.71E-08	0.50	-2.01
EP300	1.09E-07	4.28E-07	0.49	-2.02
AKT3	4.63E-06	1.58E-05	0.49	-2.03
PSMB7	1.75E-11	9.84E-11	0.49	-2.05
JMJD1C	2.63E-07	9.88E-07	0.49	-2.06
KRT17	1.33E-03	3.32E-03	0.48	-2.06
MCL1	3.44E-12	2.02E-11	0.48	-2.07
ATF4	1.77E-13	1.16E-12	0.48	-2.08
FGFR3	1.02E-03	2.56E-03	0.48	-2.10
H2-Pa	3.29E-03	7.71E-03	0.48	-2.10
EIF4EBP1	2.79E-13	1.80E-12	0.47	-2.12
KMT2D	1.06E-08	4.59E-08	0.47	-2.13
REL	1.93E-07	7.39E-07	0.47	-2.15
KDM5A	1.32E-11	7.49E-11	0.47	-2.15
SPIB	3.71E-03	8.63E-03	0.46	-2.15
INHBA	1.89E-05	6.08E-05	0.45	-2.21
MAML2	7.89E-06	2.64E-05	0.45	-2.21
TNFRSF4	2.23E-04	6.31E-04	0.45	-2.23
TET2	1.42E-07	5.50E-07	0.45	-2.23
ESRP1	3.89E-03	9.00E-03	0.45	-2.23
TSPAN1	2.60E-04	7.21E-04	0.45	-2.25
EGF	1.88E-04	5.34E-04	0.44	-2.25

OSMR	1.02E-10	5.41E-10	0.44	-2.25
TRRAP	1.31E-09	6.20E-09	0.44	-2.28
LCK	2.87E-04	7.92E-04	0.43	-2.31
MGA	2.12E-12	1.27E-11	0.43	-2.33
KRT16	2.06E-03	5.03E-03	0.43	-2.33
CD247	2.68E-03	6.45E-03	0.41	-2.42
H2-M3	3.36E-12	2.00E-11	0.41	-2.46
PDK1	3.29E-09	1.47E-08	0.40	-2.47
KLF5	1.38E-08	5.85E-08	0.40	-2.49
EPCAM	8.21E-04	2.11E-03	0.40	-2.49
KMT2A	1.21E-14	8.39E-14	0.40	-2.52
NF1	1.43E-12	8.77E-12	0.39	-2.55
SFN	3.45E-12	2.02E-11	0.39	-2.56
HUWE1	1.77E-09	8.23E-09	0.39	-2.58
EGLN3	1.17E-15	8.77E-15	0.38	-2.62
BRAF	1.06E-13	7.02E-13	0.38	-2.65
RPA3	9.80E-10	4.75E-09	0.37	-2.67
DOCK2	6.61E-04	1.71E-03	0.37	-2.67
KIT	8.71E-04	2.23E-03	0.37	-2.72
ATXN7	6.33E-12	3.66E-11	0.36	-2.78
KDM6A	9.17E-18	7.77E-17	0.36	-2.78
CSF2RA	8.65E-10	4.24E-09	0.35	-2.88
PRKCB	5.35E-05	1.64E-04	0.35	-2.90
SQSTM1	2.47E-20	2.63E-19	0.34	-2.90
ERN1	5.11E-21	5.77E-20	0.34	-2.90
H2-T23	9.24E-15	6.49E-14	0.34	-2.95
JUN	2.01E-26	3.19E-25	0.33	-3.07
TNFSF13B	2.92E-04	8.02E-04	0.32	-3.09
CREB1	1.24E-25	1.86E-24	0.32	-3.10
CCNT1	5.24E-24	7.17E-23	0.32	-3.13
ATF2	6.44E-17	5.18E-16	0.32	-3.16
NFKB2	1.45E-15	1.07E-14	0.31	-3.19
TLK2	8.46E-23	1.05E-21	0.30	-3.29
RICTOR	1.00E-24	1.42E-23	0.30	-3.29
TAP1	8.57E-13	5.35E-12	0.30	-3.38
ASH1L	5.98E-25	8.64E-24	0.30	-3.38
LAMTOR5	2.26E-18	2.00E-17	0.29	-3.42

LTB	2.63E-06	9.15E-06	0.29	-3.50
PMAIP1	1.16E-03	2.91E-03	0.29	-3.50
H2-DMa	2.44E-11	1.35E-10	0.28	-3.53
SMS	8.30E-21	9.24E-20	0.28	-3.55
TGFB2	2.14E-15	1.56E-14	0.28	-3.62
VWF	4.05E-05	1.26E-04	0.27	-3.69
ICAM1	8.69E-24	1.17E-22	0.27	-3.74
CD47	1.04E-37	2.99E-36	0.25	-3.97
CD274	1.43E-19	1.38E-18	0.25	-4.01
HDC	2.70E-08	1.10E-07	0.24	-4.22
SNAI2	5.53E-27	9.18E-26	0.23	-4.31
IL15RA	4.92E-07	1.83E-06	0.23	-4.31
IL6	1.02E-09	4.91E-09	0.23	-4.37
Trp53	4.58E-43	2.23E-41	0.22	-4.58
Bcl2a1a	1.83E-10	9.39E-10	0.22	-4.64
MYC	3.15E-38	9.46E-37	0.21	-4.82
IL15	2.21E-17	1.81E-16	0.21	-4.86
CXCL10	1.22E-21	1.42E-20	0.20	-4.97
SLC1A5	3.71E-43	1.93E-41	0.20	-4.97
TNFAIP3	6.35E-30	1.18E-28	0.19	-5.23
IRF7	1.43E-27	2.42E-26	0.18	-5.53
Ero1l	3.19E-59	4.97E-57	0.18	-5.64
IL2RG	2.33E-06	8.17E-06	0.18	-5.65
OAS3	6.98E-16	5.34E-15	0.17	-5.87
BIRC3	5.07E-42	2.08E-40	0.17	-5.97
FGFBP1	7.75E-20	7.65E-19	0.16	-6.27
CEACAM1	1.70E-11	9.59E-11	0.16	-6.35
VEGFC	1.08E-35	2.91E-34	0.15	-6.51
VEGFA	4.74E-75	1.85E-72	0.15	-6.68
RELB	2.00E-41	7.42E-40	0.14	-7.01
TNFRSF9	1.14E-23	1.48E-22	0.14	-7.29
Oas1a	9.38E-53	8.13E-51	0.13	-7.50
CDKN1A	9.20E-29	1.63E-27	0.13	-7.56
CCL5	8.67E-41	3.07E-39	0.12	-8.35
TRAF1	1.05E-42	4.83E-41	0.11	-8.89
CXCL11	4.44E-24	6.18E-23	0.10	-10.47
OAS2	3.24E-49	2.11E-47	0.07	-14.78

FAS	3.61E-77	2.82E-74	0.06	-16.01
LCN2	2.69E-32	5.68E-31	0.06	-17.57
PTGS2	3.74E-67	7.30E-65	0.05	-18.28
MX2	1.13E-33	2.59E-32	0.05	-18.94
OSM	4.50E-42	1.95E-40	0.05	-19.05

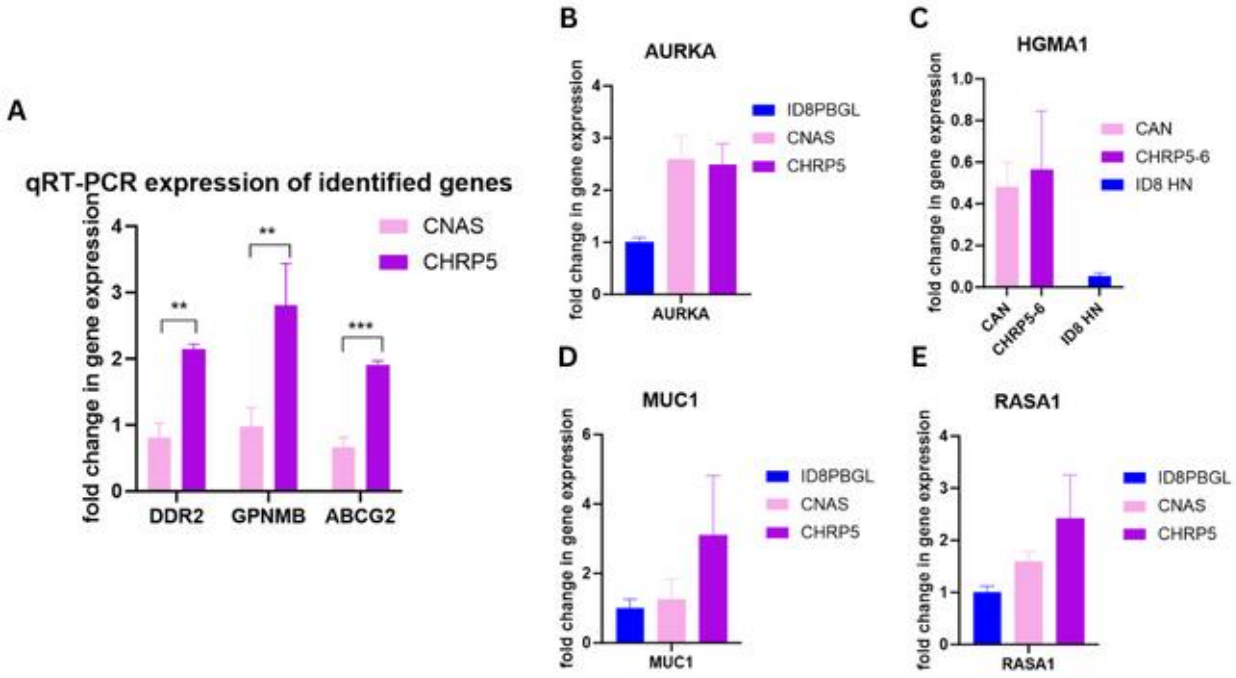

Figure 2.6: Validation of top hits mRNA expression. (A) Quantitative real-time PCR (RT-qPCR) analysis of mRNA expression from top hits identified with Nanostring sequencing (B) Aurora Kinase A (AURKA) (C) High Mobility Group AT-hook (HGMA1) (D) Mucin 1 (MUC1) and (E) RAS P21 Protein Activator 1 (RASA1).

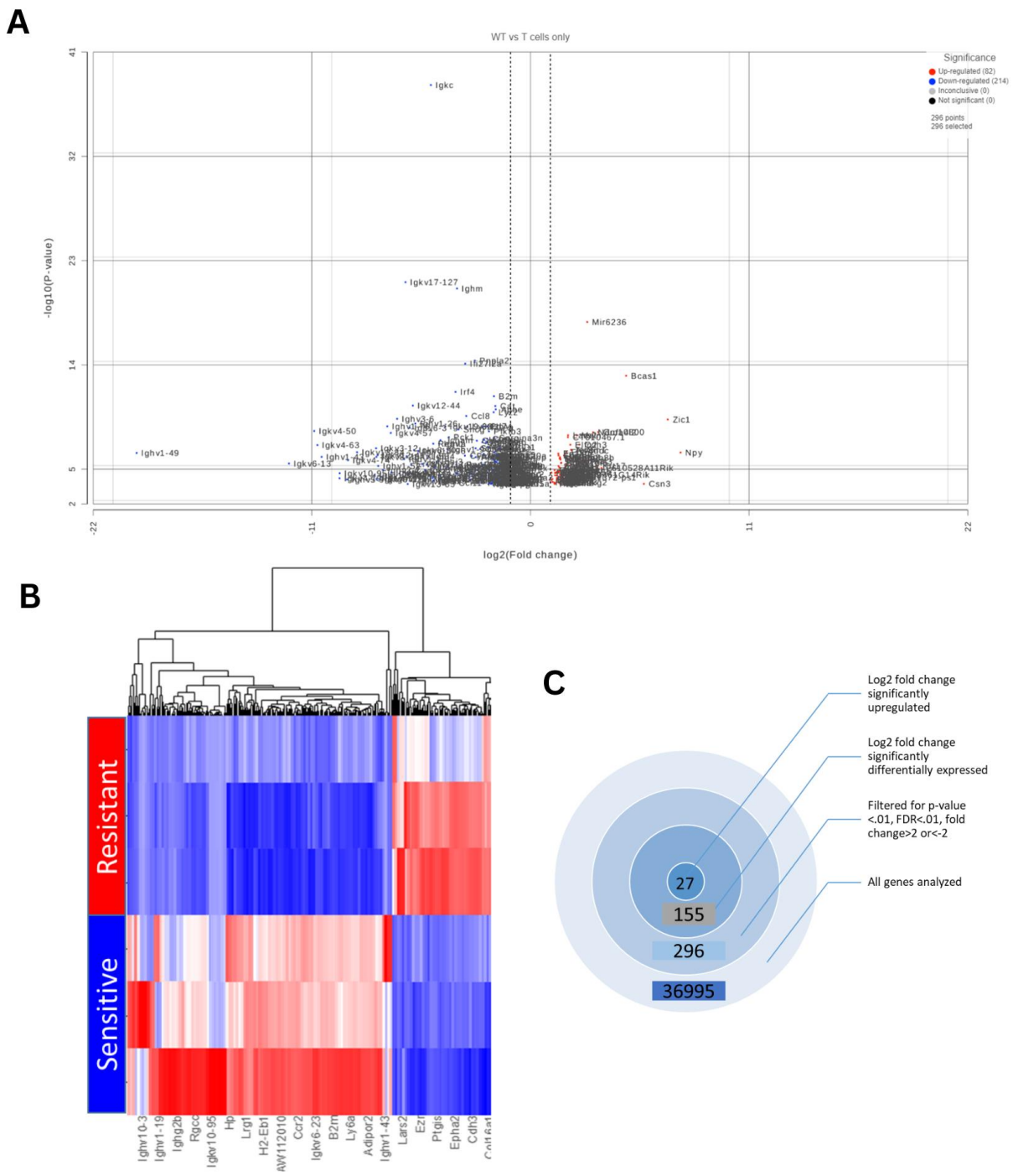

Figure 2.7: Whole exome RNA sequencing identifies differentially expressed genes between chemo-sensitive and chemo-resistant. (A) Heatmap showing mRNA gene expression differential analysis (DEseq2) comparing CHRP5 to CHRP1. (B) Table showing selection criteria for identifying top hits (C) Volcano plot displaying identified top hits fold change in mRNA expression.

Table 2.2 Top differentially expressed genes between CHRP1 and CHRP5 using whole exome RNA sequencing.

Gene symbol	Gene name	P-value (WT vs T cells only)	FDR step up (WT vs T cells only)	Ratio (WT vs T cells only)	Fold change (WT vs T cells only)	LSMean(R) (WT vs T cells only)	LSMean(S) (WT vs T cells only)
Igkc	Igkc	6.96E-39	1.08E-34	3.10E-02	-3.23E+01	5.34E+01	1.72E+03
Igkv17-127	Igkv17-127	7.22E-22	5.58E-18	1.28E-02	-7.82E+01	6.24E-01	4.88E+01
Ighm	Ighm	2.55E-21	1.32E-17	7.70E-02	-1.30E+01	1.20E+02	1.56E+03
Mir6236	Mir6236	2.00E-18	7.74E-15	7.25E+00	7.25E+00	5.39E+02	7.43E+01
Pnpla2	Pnpla2	4.25E-15	1.32E-11	1.43E-01	-6.99E+00	1.45E+02	1.01E+03
Ifi27l2a	Ifi27l2a	7.84E-15	2.02E-11	1.03E-01	-9.75E+00	4.47E+01	4.36E+02
Bcas1	Bcas1	8.71E-14	1.93E-10	2.81E+01	2.81E+01	3.23E+01	1.15E+00
Irf4	Irf4	2.12E-12	4.11E-09	7.33E-02	-1.36E+01	4.72E+00	6.44E+01
B2m	B2m	5.04E-12	8.67E-09	2.79E-01	-3.58E+00	5.25E+02	1.88E+03
Igkv12-44	Igkv12-44	3.25E-11	5.03E-08	1.65E-02	-6.05E+01	9.08E-01	5.49E+01
Cat	Cat	3.58E-11	5.04E-08	2.93E-01	-3.42E+00	1.49E+02	5.09E+02
Apoe	Apoe	6.93E-11	8.94E-08	2.97E-01	-3.36E+00	5.31E+02	1.79E+03
Lyz2	Lyz2	1.22E-10	1.45E-07	2.77E-01	-3.61E+00	1.94E+02	6.99E+02
Ccl8	Ccl8	2.60E-10	2.87E-07	1.06E-01	-9.40E+00	4.52E+00	4.25E+01
Ighv3-6	Ighv3-6	4.57E-10	4.72E-07	9.57E-03	-1.05E+02	2.25E-01	2.36E+01
Zic1	Zic1	5.20E-10	5.03E-07	1.20E+02	1.20E+02	1.13E+01	9.45E-02
Ighv1-26	Ighv1-26	1.15E-09	1.05E-06	1.80E-02	-5.55E+01	3.75E-01	2.08E+01
Cd74	Cd74	1.97E-09	1.43E-06	2.04E-01	-4.90E+00	3.32E+02	1.62E+03
Ighv1-76	Ighv1-76	2.00E-09	1.43E-06	6.77E-03	-1.48E+02	1.75E-01	2.58E+01
Hp	Hp	2.00E-09	1.43E-06	2.21E-01	-4.52E+00	1.32E+02	5.97E+02
Ly6a	Ly6a	2.01E-09	1.43E-06	1.10E-01	-9.07E+00	1.34E+01	1.22E+02
Igkv19-93	Igkv19-93	2.03E-09	1.43E-06	5.09E-02	-1.97E+01	2.51E+00	4.94E+01
H2-Aa	H2-Aa	2.34E-09	1.58E-06	1.85E-01	-5.39E+00	9.79E+01	5.28E+02
Ighv6-3	Ighv6-3	2.72E-09	1.75E-06	1.48E-02	-6.77E+01	1.81E-01	1.23E+01
Sncg	Sncg	3.68E-09	2.28E-06	8.07E-02	-1.24E+01	9.77E+00	1.21E+02
Igkv4-50	Igkv4-50	5.07E-09	3.02E-06	5.30E-04	-1.89E+03	5.42E-03	1.02E+01
Pfkfb3	Pfkfb3	5.39E-09	3.09E-06	2.35E-01	-4.26E+00	7.71E+01	3.29E+02
Gm10800	Gm10800	6.19E-09	3.42E-06	1.06E+01	1.06E+01	7.70E+01	7.28E+00
Ndufa4l2	Ndufa4l2	6.58E-09	3.51E-06	8.88E+00	8.88E+00	1.67E+02	1.88E+01
Igkv4-57	Igkv4-57	7.47E-09	3.85E-06	7.67E-03	-1.30E+02	1.31E-01	1.70E+01
Lars2	Lars2	1.19E-08	5.85E-06	3.71E+00	3.71E+00	6.74E+02	1.82E+02
Msln	Msln	1.21E-08	5.85E-06	5.00E+00	5.00E+00	3.48E+02	6.96E+01
Pck1	Pck1	1.73E-08	7.95E-06	5.79E-02	-1.73E+01	4.18E+01	7.21E+02
CT010467.1	CT010467.1	1.75E-08	7.95E-06	3.68E+00	3.68E+00	1.32E+04	3.60E+03
Serpina3n	Serpina3n	1.99E-08	8.78E-06	2.82E-01	-3.55E+00	4.15E+01	1.47E+02
Crat	Crat	2.41E-08	1.04E-05	2.22E-01	-4.51E+00	3.67E+01	1.65E+02

H2-Eb1	H2-Eb1	2.97E-08	1.24E-05	1.98E-01	-5.05E+00	1.07E+02	5.39E+02
Jchain	Jchain	3.18E-08	1.29E-05	4.32E-02	-2.31E+01	1.56E+01	3.61E+02
Gstz1	Gstz1	3.51E-08	1.39E-05	1.54E-01	-6.49E+00	3.33E+01	2.16E+02
C1qa	C1qa	3.72E-08	1.44E-05	3.02E-01	-3.31E+00	7.59E+01	2.51E+02
Txnip	Txnip	4.71E-08	1.74E-05	3.24E-01	-3.09E+00	2.04E+02	6.28E+02
Dbi	Dbi	4.73E-08	1.74E-05	1.87E-01	-5.35E+00	6.15E+01	3.29E+02
Lpin1	Lpin1	5.04E-08	1.82E-05	2.19E-01	-4.56E+00	4.74E+01	2.16E+02
H2-Ab1	H2-Ab1	5.71E-08	2.01E-05	2.09E-01	-4.79E+00	1.25E+02	5.98E+02
Retnla	Retnla	6.37E-08	2.15E-05	3.36E-02	-2.97E+01	1.65E+00	4.90E+01
Iglv1	Iglv1	6.39E-08	2.15E-05	4.13E-02	-2.42E+01	1.57E+00	3.81E+01
Cdh3	Cdh3	7.70E-08	2.54E-05	5.54E+00	5.54E+00	1.26E+02	2.28E+01
Elfn2	Elfn2	7.90E-08	2.55E-05	4.00E+00	4.00E+00	1.93E+02	4.82E+01
Igkv4-63	Igkv4-63	8.22E-08	2.60E-05	5.92E-04	-1.69E+03	5.42E-03	9.16E+00
H2-D1	H2-D1	1.27E-07	3.92E-05	3.94E-01	-2.54E+00	7.04E+02	1.79E+03
Agpat2	Agpat2	1.29E-07	3.92E-05	1.88E-01	-5.32E+00	6.26E+01	3.33E+02
C4b	C4b	1.32E-07	3.94E-05	2.30E-01	-4.35E+00	1.55E+02	6.74E+02
Tkt	Tkt	1.49E-07	4.36E-05	3.37E-01	-2.97E+00	4.84E+02	1.44E+03
Igkv3-12	Igkv3-12	1.55E-07	4.42E-05	4.59E-03	-2.18E+02	7.35E-02	1.60E+01
Sult1a1	Sult1a1	1.57E-07	4.42E-05	1.48E-01	-6.76E+00	1.21E+01	8.16E+01
Cmklr1	Cmklr1	1.81E-07	4.99E-05	1.73E-01	-5.78E+00	2.40E+01	1.39E+02
Csf1r	Csf1r	1.91E-07	5.09E-05	3.23E-01	-3.10E+00	6.56E+01	2.03E+02
Mknk2	Mknk2	1.94E-07	5.09E-05	3.34E-01	-2.99E+00	1.79E+02	5.35E+02
Ighv1-9	Ighv1-9	1.94E-07	5.09E-05	5.54E-02	-1.80E+01	2.59E+00	4.66E+01
Ier3	Ier3	2.13E-07	5.50E-05	4.12E+00	4.12E+00	2.53E+02	6.14E+01
Ncam1	Ncam1	2.21E-07	5.62E-05	4.23E+00	4.23E+00	1.18E+02	2.80E+01
Igkv8-30	Igkv8-30	2.26E-07	5.63E-05	1.73E-02	-5.80E+01	3.02E-01	1.75E+01
Aldoc	Aldoc	2.49E-07	6.13E-05	5.63E+00	5.63E+00	7.01E+01	1.24E+01
Igkv10-96	Igkv10-96	2.71E-07	6.57E-05	2.01E-02	-4.99E+01	6.51E-01	3.24E+01
Fbln2	Fbln2	3.29E-07	7.83E-05	3.48E+00	3.48E+00	1.60E+03	4.61E+02
Igkv13-84	Igkv13-84	3.44E-07	8.07E-05	2.37E-03	-4.22E+02	1.99E-02	8.43E+00
Sorbs1	Sorbs1	3.57E-07	8.25E-05	2.84E-01	-3.52E+00	5.92E+01	2.08E+02
Npy	Npy	3.65E-07	8.30E-05	1.87E+02	1.87E+02	7.09E+00	3.78E-02
Ighv1-49	Ighv1-49	3.94E-07	8.84E-05	1.08E-06	-9.23E+05	1.00E-04	9.26E+01
Fn1	Fn1	4.43E-07	9.80E-05	2.65E+00	2.65E+00	4.03E+03	1.52E+03
Bscl2	Bscl2	4.79E-07	1.04E-04	1.96E-01	-5.10E+00	3.12E+01	1.59E+02
Mrc1	Mrc1	5.67E-07	1.22E-04	3.06E-01	-3.27E+00	3.73E+01	1.22E+02
Laptm5	Laptm5	5.75E-07	1.22E-04	3.33E-01	-3.00E+00	6.28E+01	1.89E+02
Lrg1	Lrg1	5.98E-07	1.25E-04	1.92E-01	-5.21E+00	3.11E+01	1.62E+02
Igkv12-41	Igkv12-41	6.13E-07	1.26E-04	4.83E-03	-2.07E+02	5.14E-01	1.06E+02
Enc1	Enc1	6.50E-07	1.32E-04	2.66E+00	2.66E+00	3.37E+02	1.27E+02
Lmo7	Lmo7	6.61E-07	1.33E-04	3.21E+00	3.21E+00	1.82E+02	5.67E+01

Cyp2e1	Cyp2e1	6.75E-07	1.34E-04	1.01E-01	-9.87E+00	9.44E+01	9.32E+02
Tmem120a	Tmem120a	6.86E-07	1.34E-04	2.78E-01	-3.60E+00	3.90E+01	1.40E+02
C1qc	C1qc	7.08E-07	1.37E-04	3.23E-01	-3.09E+00	8.04E+01	2.49E+02
Fmo1	Fmo1	7.22E-07	1.38E-04	1.29E-01	-7.76E+00	1.12E+01	8.72E+01
Ighv1-53	Ighv1-53	7.61E-07	1.44E-04	1.33E-02	-7.51E+01	3.12E-01	2.35E+01
Ighj4	Ighj4	7.76E-07	1.45E-04	2.85E-02	-3.51E+01	4.02E-01	1.41E+01
H2-K1	H2-K1	7.96E-07	1.47E-04	4.26E-01	-2.35E+00	5.66E+02	1.33E+03
Lpl	Lpl	8.13E-07	1.47E-04	3.03E-01	-3.30E+00	4.49E+02	1.48E+03
Pdha1	Pdha1	8.17E-07	1.47E-04	2.76E-01	-3.62E+00	6.85E+01	2.48E+02
Ighv1-43	Ighv1-43	8.66E-07	1.54E-04	6.86E-04	-1.46E+03	5.42E-03	7.91E+00
Igkv8-21	Igkv8-21	8.80E-07	1.54E-04	4.65E-03	-2.15E+02	5.02E-02	1.08E+01
Sik2	Sik2	8.87E-07	1.54E-04	2.99E-01	-3.34E+00	6.56E+01	2.19E+02
Apoc1	Apoc1	9.07E-07	1.56E-04	1.48E-01	-6.74E+00	8.29E+00	5.59E+01
Upk3b	Upk3b	9.25E-07	1.57E-04	2.80E+00	2.80E+00	1.19E+03	4.26E+02
Aqp5	Aqp5	9.47E-07	1.58E-04	3.39E+00	3.39E+00	1.09E+02	3.23E+01
Selenop	Selenop	9.50E-07	1.58E-04	4.31E-01	-2.32E+00	2.83E+02	6.57E+02
Ccn2	Ccn2	9.60E-07	1.58E-04	4.45E+00	4.45E+00	2.15E+02	4.83E+01
C1qb	C1qb	9.93E-07	1.62E-04	3.42E-01	-2.93E+00	7.89E+01	2.31E+02
Zbtb8b	Zbtb8b	1.03E-06	1.65E-04	5.55E+00	5.55E+00	8.20E+01	1.48E+01
Mpp2	Mpp2	1.11E-06	1.76E-04	3.94E+00	3.94E+00	1.27E+02	3.23E+01
Mmd	Mmd	1.12E-06	1.76E-04	2.12E-01	-4.71E+00	4.42E+01	2.08E+02
Gsta3	Gsta3	1.15E-06	1.79E-04	2.57E-01	-3.88E+00	2.03E+01	7.89E+01
Flnc	Flnc	1.22E-06	1.89E-04	2.77E+00	2.77E+00	5.65E+02	2.04E+02
Sdc2	Sdc2	1.28E-06	1.96E-04	2.81E+00	2.81E+00	3.18E+02	1.13E+02
Ighv1-15	Ighv1-15	1.38E-06	2.09E-04	1.22E-02	-8.19E+01	1.88E-01	1.54E+01
Sema3c	Sema3c	1.44E-06	2.17E-04	2.84E+00	2.84E+00	5.23E+02	1.84E+02
Glul	Glul	1.48E-06	2.20E-04	2.89E-01	-3.46E+00	2.29E+02	7.91E+02
Acp5	Acp5	1.49E-06	2.20E-04	2.74E-01	-3.65E+00	3.92E+01	1.43E+02
Rasa3	Rasa3	1.62E-06	2.37E-04	3.19E-01	-3.14E+00	5.14E+01	1.61E+02
Igkv4-74	Igkv4-74	1.68E-06	2.44E-04	1.72E-03	-5.80E+02	1.06E-02	6.13E+00
Slc25a1	Slc25a1	1.85E-06	2.65E-04	2.82E-01	-3.54E+00	1.16E+02	4.10E+02
Slc2a1	Slc2a1	2.07E-06	2.94E-04	4.01E+00	4.01E+00	2.17E+02	5.40E+01
Fstl3	Fstl3	2.12E-06	2.99E-04	7.05E+00	7.05E+00	4.40E+01	6.25E+00
Dgat1	Dgat1	2.21E-06	3.08E-04	2.95E-01	-3.38E+00	3.66E+01	1.24E+02
Ighj3	Ighj3	2.23E-06	3.08E-04	3.80E-02	-2.63E+01	5.35E-01	1.41E+01
Vsir	Vsir	2.36E-06	3.23E-04	2.92E-01	-3.42E+00	2.98E+01	1.02E+02
Slc1a5	Slc1a5	2.44E-06	3.32E-04	2.90E-01	-3.45E+00	1.59E+02	5.50E+02
Me1	Me1	2.54E-06	3.42E-04	3.09E-01	-3.23E+00	2.82E+02	9.10E+02
Aldh6a1	Aldh6a1	2.78E-06	3.70E-04	3.38E-01	-2.96E+00	8.45E+01	2.50E+02
S1pr5	S1pr5	2.83E-06	3.70E-04	5.28E+00	5.28E+00	5.10E+01	9.67E+00
Ptgis	Ptgis	2.84E-06	3.70E-04	2.92E+00	2.92E+00	5.45E+02	1.87E+02

Mpeg1	Mpeg1	2.85E-06	3.70E-04	3.94E-01	-2.54E+00	8.30E+01	2.11E+02
Lcp1	Lcp1	2.89E-06	3.73E-04	3.36E-01	-2.97E+00	6.00E+01	1.78E+02
Sdc4	Sdc4	3.02E-06	3.87E-04	2.91E+00	2.91E+00	1.09E+03	3.77E+02
Igkv6-13	Igkv6-13	3.28E-06	4.16E-04	2.20E-04	-4.54E+03	5.42E-03	2.46E+01
Ighv7-1	Ighv7-1	3.58E-06	4.50E-04	2.28E-02	-4.38E+01	3.21E-01	1.41E+01
Erv3	Erv3	3.63E-06	4.53E-04	1.56E-02	-6.40E+01	9.75E-02	6.24E+00
Fras1	Fras1	3.84E-06	4.76E-04	3.45E+00	3.45E+00	8.40E+01	2.43E+01
Ppl	Ppl	3.89E-06	4.77E-04	4.07E+00	4.07E+00	2.60E+02	6.37E+01
Igkv17-121	Igkv17-121	3.94E-06	4.79E-04	7.50E-02	-1.33E+01	4.29E+00	5.72E+01
Rgcc	Rgcc	3.99E-06	4.79E-04	2.02E-01	-4.96E+00	1.84E+01	9.14E+01
Ppp1r1a	Ppp1r1a	4.00E-06	4.79E-04	8.98E-02	-1.11E+01	3.45E+00	3.85E+01
Ighv1-7	Ighv1-7	4.07E-06	4.85E-04	2.69E-02	-3.72E+01	2.29E-01	8.52E+00
Pygl	Pygl	4.12E-06	4.87E-04	1.89E-01	-5.30E+00	3.39E+01	1.79E+02
Aldh1l1	Aldh1l1	4.22E-06	4.95E-04	1.86E-01	-5.36E+00	2.21E+01	1.18E+02
mt-Cytb	mt-Cytb	4.41E-06	5.14E-04	3.73E-01	-2.68E+00	1.30E+03	3.47E+03
mt-Nd4	mt-Nd4	4.70E-06	5.43E-04	3.95E-01	-2.53E+00	5.27E+02	1.33E+03
Lgals3bp	Lgals3bp	5.04E-06	5.78E-04	3.60E-01	-2.78E+00	1.38E+02	3.82E+02
Krt17	Krt17	5.14E-06	5.84E-04	1.05E+01	1.05E+01	2.36E+01	2.25E+00
Ighv1-52	Ighv1-52	5.28E-06	5.93E-04	4.94E-03	-2.02E+02	4.01E-02	8.11E+00
Slc25a10	Slc25a10	5.29E-06	5.93E-04	3.23E-01	-3.09E+00	6.96E+01	2.15E+02
Sulf1	Sulf1	5.41E-06	6.03E-04	2.66E+00	2.66E+00	3.28E+02	1.24E+02
Nr1h3	Nr1h3	5.92E-06	6.54E-04	1.64E-01	-6.11E+00	8.04E+00	4.92E+01
Adhfe1	Adhfe1	6.39E-06	7.01E-04	1.52E-01	-6.57E+00	9.50E+00	6.24E+01
Cd209f	Cd209f	6.94E-06	7.56E-04	8.43E-02	-1.19E+01	2.46E+00	2.92E+01
Col16a1	Col16a1	7.04E-06	7.62E-04	2.74E+00	2.74E+00	2.18E+02	7.95E+01
Unc5b	Unc5b	7.13E-06	7.66E-04	3.31E+00	3.31E+00	2.51E+02	7.58E+01
Igkv6-23	Igkv6-23	7.23E-06	7.72E-04	3.53E-02	-2.83E+01	1.02E+00	2.88E+01
Ly6c2	Ly6c2	7.50E-06	7.95E-04	8.29E-02	-1.21E+01	1.87E+00	2.26E+01
2610528A11Rik	2610528A11Rik	7.92E-06	8.34E-04	1.19E+01	1.19E+01	3.41E+01	2.87E+00
Tmsb4x	Tmsb4x	8.07E-06	8.44E-04	4.65E-01	-2.15E+00	5.08E+02	1.09E+03
Pld4	Pld4	8.44E-06	8.77E-04	2.57E-01	-3.90E+00	1.61E+01	6.28E+01
Igkv4-59	Igkv4-59	8.66E-06	8.93E-04	5.22E-02	-1.91E+01	5.60E-01	1.07E+01
Krt18	Krt18	8.72E-06	8.93E-04	2.81E+00	2.81E+00	5.67E+02	2.02E+02
Aacs	Aacs	8.98E-06	9.15E-04	3.06E-01	-3.27E+00	7.18E+01	2.35E+02
Dlg2	Dlg2	9.34E-06	9.39E-04	4.59E+00	4.59E+00	4.94E+01	1.08E+01
Ighj2	Ighj2	9.34E-06	9.39E-04	5.78E-02	-1.73E+01	7.67E-01	1.33E+01
Irs3	Irs3	9.84E-06	9.83E-04	1.20E-01	-8.36E+00	3.57E+00	2.98E+01
Dock2	Dock2	9.94E-06	9.87E-04	2.59E-01	-3.86E+00	1.79E+01	6.90E+01
Scp2	Scp2	1.09E-05	1.07E-03	3.61E-01	-2.77E+00	1.09E+02	3.02E+02
Cybb	Cybb	1.14E-05	1.12E-03	2.72E-01	-3.68E+00	2.87E+01	1.06E+02
Hmcn1	Hmcn1	1.16E-05	1.13E-03	3.45E+00	3.45E+00	1.37E+02	3.98E+01

Igkj5	Igkj5	1.18E-05	1.14E-03	2.53E-02	-3.96E+01	2.26E-01	8.96E+00
Ighv2-2	Ighv2-2	1.19E-05	1.15E-03	5.82E-03	-1.72E+02	5.88E-02	1.01E+01
Wdfy4	Wdfy4	1.20E-05	1.15E-03	2.36E-01	-4.23E+00	2.01E+01	8.52E+01
C1qtnf7	C1qtnf7	1.22E-05	1.15E-03	4.76E+00	4.76E+00	4.05E+01	8.51E+00
Ddr1	Ddr1	1.22E-05	1.15E-03	2.32E+00	2.32E+00	5.68E+02	2.45E+02
Unc93b1	Unc93b1	1.25E-05	1.17E-03	3.32E-01	-3.01E+00	4.61E+01	1.39E+02
Clec10a	Clec10a	1.28E-05	1.20E-03	1.56E-01	-6.40E+00	4.88E+00	3.13E+01
Pde3b	Pde3b	1.31E-05	1.21E-03	3.07E-01	-3.26E+00	4.55E+01	1.48E+02
Plbd1	Plbd1	1.31E-05	1.21E-03	2.38E-01	-4.21E+00	1.82E+01	7.65E+01
Rxra	Rxra	1.35E-05	1.23E-03	3.32E-01	-3.01E+00	5.76E+01	1.74E+02
H1f0	H1f0	1.42E-05	1.29E-03	2.69E+00	2.69E+00	4.83E+02	1.80E+02
Lama5	Lama5	1.44E-05	1.31E-03	2.81E+00	2.81E+00	1.04E+03	3.69E+02
Ptprc	Ptprc	1.52E-05	1.37E-03	2.77E-01	-3.62E+00	2.67E+01	9.64E+01
Ctss	Ctss	1.62E-05	1.45E-03	3.72E-01	-2.69E+00	8.89E+01	2.39E+02
Crip1	Crip1	1.63E-05	1.45E-03	2.62E+00	2.62E+00	8.37E+02	3.19E+02
Bmp4	Bmp4	1.74E-05	1.53E-03	3.83E+00	3.83E+00	8.65E+01	2.26E+01
Eln	Eln	1.74E-05	1.53E-03	2.52E+00	2.52E+00	3.37E+02	1.34E+02
Igkv6-32	Igkv6-32	1.83E-05	1.60E-03	1.20E-02	-8.33E+01	1.00E-01	8.33E+00
Tmem255a	Tmem255a	1.88E-05	1.63E-03	2.68E+00	2.68E+00	2.09E+02	7.80E+01
Igkv5-43	Igkv5-43	1.91E-05	1.65E-03	7.80E-03	-1.28E+02	4.09E-02	5.24E+00
Lgals1	Lgals1	1.94E-05	1.67E-03	2.49E+00	2.49E+00	4.47E+03	1.79E+03
Pkhd1l1	Pkhd1l1	2.00E-05	1.71E-03	2.08E+00	2.08E+00	5.06E+02	2.43E+02
Chst1	Chst1	2.02E-05	1.72E-03	3.48E-01	-2.87E+00	3.24E+01	9.30E+01
Plac8	Plac8	2.04E-05	1.73E-03	2.26E-01	-4.42E+00	9.93E+00	4.39E+01
P4hb	P4hb	2.07E-05	1.74E-03	2.35E+00	2.35E+00	1.60E+03	6.79E+02
Ighv1-39	Ighv1-39	2.08E-05	1.74E-03	7.40E-02	-1.35E+01	4.00E+00	5.40E+01
Ezr	Ezr	2.14E-05	1.78E-03	2.40E+00	2.40E+00	9.22E+02	3.84E+02
Adig	Adig	2.22E-05	1.84E-03	1.24E-01	-8.08E+00	1.01E+01	8.15E+01
Enpp2	Enpp2	2.24E-05	1.84E-03	3.62E-01	-2.77E+00	1.07E+02	2.96E+02
Igkv10-95	Igkv10-95	2.27E-05	1.86E-03	1.29E-03	-7.76E+02	5.42E-03	4.21E+00
Igkv6-17	Igkv6-17	2.39E-05	1.95E-03	1.03E-02	-9.68E+01	6.88E-02	6.66E+00
Cidec	Cidec	2.40E-05	1.95E-03	7.61E-02	-1.31E+01	7.56E+01	9.94E+02
Igha	Igha	2.45E-05	1.98E-03	1.59E-02	-6.28E+01	1.63E+01	1.03E+03
Acsm3	Acsm3	2.54E-05	2.04E-03	1.29E-01	-7.76E+00	2.94E+00	2.28E+01
Adipor2	Adipor2	2.63E-05	2.10E-03	4.30E-01	-2.32E+00	2.01E+02	4.67E+02
Siglec1	Siglec1	2.64E-05	2.10E-03	3.00E-01	-3.33E+00	2.82E+01	9.41E+01
Aldh3b2	Aldh3b2	2.73E-05	2.15E-03	1.41E-01	-7.09E+00	3.80E+00	2.70E+01
Ighv1-19	Ighv1-19	2.82E-05	2.22E-03	1.44E-02	-6.93E+01	1.89E-01	1.31E+01
Ctsd	Ctsd	2.85E-05	2.23E-03	4.77E-01	-2.09E+00	3.12E+02	6.54E+02
4930461G14Rik	4930461G14Rik	3.02E-05	2.34E-03	4.91E+00	4.91E+00	4.37E+01	8.91E+00
Sema4g	Sema4g	3.03E-05	2.34E-03	2.97E-01	-3.37E+00	2.09E+01	7.05E+01

Pou2af1	Pou2af1	3.04E-05	2.34E-03	8.73E-02	-1.15E+01	1.93E+00	2.21E+01
Krt8	Krt8	3.06E-05	2.34E-03	2.79E+00	2.79E+00	9.64E+02	3.46E+02
Megf6	Megf6	3.07E-05	2.34E-03	3.03E+00	3.03E+00	1.16E+02	3.83E+01
Ighv1-75	Ighv1-75	3.34E-05	2.52E-03	4.32E-03	-2.31E+02	2.84E-01	6.56E+01
Ivd	Ivd	3.34E-05	2.52E-03	3.27E-01	-3.06E+00	5.10E+01	1.56E+02
Adam8	Adam8	3.35E-05	2.52E-03	3.53E+00	3.53E+00	5.97E+01	1.69E+01
Podxl	Podxl	3.43E-05	2.55E-03	2.36E+00	2.36E+00	7.36E+02	3.12E+02
Selplg	Selplg	3.43E-05	2.55E-03	2.54E-01	-3.94E+00	1.21E+01	4.78E+01
Slc44a2	Slc44a2	3.54E-05	2.62E-03	2.53E+00	2.53E+00	3.84E+02	1.51E+02
Dapk1	Dapk1	3.63E-05	2.67E-03	2.15E-01	-4.65E+00	3.04E+01	1.42E+02
Ighj1	Ighj1	3.77E-05	2.76E-03	4.86E-02	-2.06E+01	4.88E-01	1.01E+01
Igkv1-117	Igkv1-117	3.88E-05	2.83E-03	4.24E-02	-2.36E+01	9.97E-01	2.35E+01
Lgi2	Lgi2	4.01E-05	2.92E-03	2.52E-01	-3.96E+00	1.24E+01	4.93E+01
Scel	Scel	4.05E-05	2.93E-03	5.77E+00	5.77E+00	3.41E+01	5.92E+00
Igkv4-80	Igkv4-80	4.18E-05	3.00E-03	5.38E-03	-1.86E+02	3.57E-02	6.64E+00
Csdc2	Csdc2	4.19E-05	3.00E-03	3.03E+00	3.03E+00	2.33E+02	7.69E+01
Ighv4-1	Ighv4-1	4.32E-05	3.08E-03	1.70E-02	-5.87E+01	1.53E-01	8.99E+00
AW112010	AW112010	4.40E-05	3.12E-03	1.82E-01	-5.48E+00	6.07E+00	3.33E+01
mt-Nd2	mt-Nd2	4.71E-05	3.33E-03	3.65E-01	-2.74E+00	4.16E+02	1.14E+03
mt-Nd5	mt-Nd5	4.83E-05	3.40E-03	4.57E-01	-2.19E+00	1.26E+03	2.75E+03
Olfr1372-ps1	Olfr1372-ps1	5.11E-05	3.58E-03	4.88E+00	4.88E+00	4.75E+01	9.73E+00
Ly6e	Ly6e	5.22E-05	3.64E-03	4.49E-01	-2.23E+00	3.83E+02	8.53E+02
Tns1	Tns1	5.27E-05	3.64E-03	3.99E-01	-2.50E+00	2.87E+02	7.18E+02
Lipe	Lipe	5.28E-05	3.64E-03	1.18E-01	-8.45E+00	6.52E+01	5.52E+02
Ralgapa2	Ralgapa2	5.29E-05	3.64E-03	4.48E-01	-2.23E+00	8.13E+01	1.82E+02
Dpep1	Dpep1	5.33E-05	3.65E-03	1.46E-01	-6.85E+00	5.64E+00	3.86E+01
Pdpn	Pdpn	5.36E-05	3.65E-03	2.53E+00	2.53E+00	2.68E+02	1.06E+02
Loxl2	Loxl2	5.51E-05	3.73E-03	2.83E+00	2.83E+00	3.20E+02	1.13E+02
Cdh2	Cdh2	5.52E-05	3.73E-03	3.01E+00	3.01E+00	1.21E+02	4.01E+01
Stbd1	Stbd1	5.71E-05	3.84E-03	3.33E+00	3.33E+00	5.42E+01	1.63E+01
Ighg2b	Ighg2b	5.74E-05	3.85E-03	3.29E-02	-3.04E+01	4.24E+00	1.29E+02
Hspb1	Hspb1	6.01E-05	4.01E-03	2.90E+00	2.90E+00	2.82E+02	9.71E+01
Igkv4-79	Igkv4-79	6.10E-05	4.05E-03	1.28E-03	-7.79E+02	5.42E-03	4.23E+00
Igkv1-110	Igkv1-110	6.15E-05	4.07E-03	3.05E-02	-3.27E+01	3.50E-01	1.15E+01
Art3	Art3	6.34E-05	4.17E-03	1.51E-01	-6.60E+00	9.88E+00	6.52E+01
C3	C3	6.47E-05	4.24E-03	4.60E-01	-2.18E+00	2.86E+03	6.21E+03
Ccr2	Ccr2	6.65E-05	4.34E-03	2.32E-01	-4.31E+00	1.08E+01	4.65E+01
Igkv4-57-1	Igkv4-57-1	6.78E-05	4.40E-03	4.67E-03	-2.14E+02	2.00E-02	4.29E+00
Ighv1-69	Ighv1-69	6.80E-05	4.40E-03	7.33E-03	-1.36E+02	3.88E-02	5.29E+00
Pkm	Pkm	6.92E-05	4.46E-03	2.51E+00	2.51E+00	1.85E+03	7.36E+02
Bsg	Bsg	7.03E-05	4.51E-03	2.15E+00	2.15E+00	8.39E+02	3.89E+02

F13a1	F13a1	7.11E-05	4.55E-03	3.50E-01	-2.86E+00	3.55E+01	1.01E+02
Pgc	Pgc	7.22E-05	4.60E-03	9.61E-02	-1.04E+01	1.93E+00	2.01E+01
Igkv9-120	Igkv9-120	7.29E-05	4.62E-03	5.26E-03	-1.90E+02	4.40E-01	8.37E+01
Cd52	Cd52	7.48E-05	4.73E-03	2.46E-01	-4.06E+00	1.23E+01	4.98E+01
Acta1	Acta1	7.52E-05	4.73E-03	4.33E-02	-2.31E+01	4.70E-01	1.09E+01
Clic5	Clic5	7.72E-05	4.84E-03	2.65E+00	2.65E+00	1.34E+02	5.06E+01
Ccdc80	Ccdc80	7.75E-05	4.84E-03	4.12E-01	-2.42E+00	2.31E+02	5.60E+02
Ighv5-9-1	Ighv5-9-1	7.78E-05	4.84E-03	1.66E-03	-6.01E+02	5.42E-03	3.26E+00
Apol6	Apol6	7.90E-05	4.88E-03	1.25E-01	-8.01E+00	7.13E+00	5.71E+01
Mgst1	Mgst1	7.91E-05	4.88E-03	4.78E-01	-2.09E+00	2.01E+02	4.19E+02
Itih4	Itih4	7.94E-05	4.88E-03	1.77E-01	-5.66E+00	4.90E+00	2.77E+01
Mlxipl	Mlxipl	7.99E-05	4.89E-03	2.60E-01	-3.85E+00	2.22E+01	8.54E+01
Zbp1	Zbp1	8.03E-05	4.89E-03	2.72E-01	-3.67E+00	1.77E+01	6.49E+01
Slit3	Slit3	8.23E-05	5.00E-03	3.77E-01	-2.65E+00	6.09E+01	1.62E+02
Slc9a3r1	Slc9a3r1	8.48E-05	5.13E-03	2.07E+00	2.07E+00	3.97E+02	1.92E+02
Igfbp4	Igfbp4	8.80E-05	5.30E-03	4.46E-01	-2.24E+00	3.08E+02	6.90E+02
Itga3	Itga3	8.94E-05	5.36E-03	2.52E+00	2.52E+00	5.82E+02	2.31E+02
Clec7a	Clec7a	9.06E-05	5.41E-03	2.44E-01	-4.09E+00	1.05E+01	4.31E+01
Igkv14-111	Igkv14-111	9.08E-05	5.41E-03	3.47E-02	-2.88E+01	2.77E-01	7.99E+00
Cluh	Cluh	9.47E-05	5.62E-03	4.54E-01	-2.20E+00	1.42E+02	3.12E+02
Aldh2	Aldh2	9.56E-05	5.65E-03	4.30E-01	-2.33E+00	2.93E+02	6.81E+02
Slc7a10	Slc7a10	9.74E-05	5.73E-03	1.19E-01	-8.38E+00	5.40E+00	4.53E+01
Fry	Fry	9.85E-05	5.78E-03	2.47E-01	-4.05E+00	3.11E+01	1.26E+02
Abhd5	Abhd5	1.00E-04	5.84E-03	3.10E-01	-3.22E+00	2.07E+01	6.67E+01
Igkv15-103	Igkv15-103	1.01E-04	5.90E-03	3.35E-02	-2.98E+01	5.10E-01	1.52E+01
H2-DMa	H2-DMa	1.03E-04	5.95E-03	2.67E-01	-3.74E+00	1.45E+01	5.44E+01
Gpat3	Gpat3	1.03E-04	5.95E-03	2.55E-01	-3.93E+00	1.53E+01	6.02E+01
Ighv10-3	Ighv10-3	1.12E-04	6.43E-03	1.74E-02	-5.76E+01	2.03E-01	1.17E+01
Igfbp2	Igfbp2	1.15E-04	6.62E-03	3.03E+00	3.03E+00	4.62E+02	1.53E+02
Gpt2	Gpt2	1.18E-04	6.72E-03	3.41E-01	-2.93E+00	5.89E+01	1.73E+02
Tpm1	Tpm1	1.26E-04	7.15E-03	2.16E+00	2.16E+00	7.52E+02	3.48E+02
Cadm3	Cadm3	1.27E-04	7.21E-03	3.01E+00	3.01E+00	7.26E+01	2.41E+01
Ptafr	Ptafr	1.31E-04	7.36E-03	2.36E-01	-4.23E+00	7.98E+00	3.38E+01
Hspa5	Hspa5	1.34E-04	7.49E-03	2.01E+00	2.01E+00	1.08E+03	5.37E+02
Htra3	Htra3	1.35E-04	7.56E-03	2.40E-01	-4.17E+00	3.69E+01	1.54E+02
Prkg2	Prkg2	1.40E-04	7.80E-03	5.13E+00	5.13E+00	3.45E+01	6.73E+00
Crip2	Crip2	1.44E-04	7.99E-03	2.29E+00	2.29E+00	2.42E+02	1.06E+02
Acadm	Acadm	1.45E-04	8.04E-03	3.99E-01	-2.50E+00	5.68E+01	1.42E+02
Ccl11	Ccl11	1.50E-04	8.27E-03	6.86E-02	-1.46E+01	1.14E+00	1.66E+01
Epha2	Epha2	1.52E-04	8.27E-03	2.72E+00	2.72E+00	1.58E+02	5.81E+01
Phlda3	Phlda3	1.52E-04	8.27E-03	3.14E-01	-3.19E+00	3.97E+01	1.27E+02

Dram1	Dram1	1.52E-04	8.27E-03	2.61E-01	-3.83E+00	1.93E+01	7.40E+01
Lpgat1	Lpgat1	1.55E-04	8.40E-03	2.94E-01	-3.41E+00	5.58E+01	1.90E+02
Adgre1	Adgre1	1.56E-04	8.40E-03	2.86E-01	-3.50E+00	1.87E+01	6.55E+01
Tmem120b	Tmem120b	1.56E-04	8.40E-03	1.79E-01	-5.59E+00	7.91E+00	4.42E+01
Pacsin2	Pacsin2	1.57E-04	8.45E-03	2.37E+00	2.37E+00	4.45E+02	1.88E+02
Reep6	Reep6	1.67E-04	8.91E-03	2.61E-01	-3.83E+00	9.80E+00	3.75E+01
Slfn5	Slfn5	1.67E-04	8.91E-03	2.43E-01	-4.11E+00	2.40E+01	9.88E+01
Ppp2r5a	Ppp2r5a	1.76E-04	9.34E-03	4.69E-01	-2.13E+00	1.99E+02	4.24E+02
Adgrd1	Adgrd1	1.77E-04	9.38E-03	4.72E-01	-2.12E+00	8.68E+01	1.84E+02
Csn3	Csn3	1.81E-04	9.59E-03	5.21E+01	5.21E+01	5.93E+00	1.14E-01
Klf2	Klf2	1.86E-04	9.80E-03	2.53E-01	-3.95E+00	2.40E+01	9.50E+01
Plec	Plec	1.87E-04	9.82E-03	2.33E+00	2.33E+00	2.36E+03	1.02E+03
Itga4	Itga4	1.88E-04	9.83E-03	2.30E-01	-4.34E+00	1.14E+01	4.93E+01
Igkv13-85	Igkv13-85	1.90E-04	9.90E-03	1.39E-02	-7.21E+01	1.27E-01	9.18E+00

Table 2.3: Primer sequences used in RT-qPCR.

	forward	reverse
mLGR6	CTG TGG CTT TGC GCT GTG	AAG GGC ACC AAA CGA GTG T
mCADM1	TTTGAAGGACAGCAGGTTTCA	AGGACTGTGATGGTGGTGTAACT
galnt13	CTGGCGAGAATAAAGGAAGACAG	TTGAGGGACAGGATACCATCGG
msx2	AAGACGGAGCACCGTGGATACA	CGGTTGGTCTTGTGTTTCCTCAG
hoxd10	TGGCTGAGGTTTCCGTGTCCAG	GCACCTCTTCTTTCTGCCACTC
hoxd11	AGTCCCTGCGCCAAGGCGAC	CTTGGTGTAGGGACAGCGCTTT
DDR2 targeting exon 8	GGGAACCCACTGCTGTCTAC	ATCATCCACGTGTCGGCAAA
GREB1	GCAACACGGTGCCTCCACCA	GAGGCGCCTGCTGGTACTGC
PGR	CTA CTCGCTGTGCCTTACCATG	CTGGCTTTGACTCCTCAGTCCT
DKK2	CGGCATAGAGATCGCAACCATG	GCAGTCTGATGACCGTAGGCAT

Chapter 3: The Role of Tyrosine Kinase Receptor DDR2 in Ovarian Cancer Chemo-Resistance and Metastasis

3.1 Declarations

Experiments were designed, performed, and analyzed by Alyssa Oplt unless otherwise noted. Hollie Noia and Katherine Fuh assisted in experimental design for genetic DDR2 knockdown i*n vivo* experiments. Elizabeth Stock performed the analysis of IHC patient DDR2 expression and survival curves.

3.2 Introduction

Ovarian cancer is a highly deadly disease with 5-year survival around 30%. Up to 80% of ovarian cancer patients will experience relapse and resistance to treatment which leads to patient death. Understanding how chemo-resistance occurs in ovarian cancer is key to creating new therapies and improving patient survival. Acquired resistance to chemotherapy is a poorly understood process requiring further investigation.

One target our lab has identified as a potential key player in acquired chemo-resistance is receptor tyrosine kinase, discoidin domain receptor 2 (DDR2) as it was overexpressed in patients with chemo-resistant tumors analyzed via mass spectrometry. DDR2 has been shown to be involved in cell adhesion, migration, and invasion in many cancer types both clinically and experimentally, in part due to its involvement in the extracellular matrix and collagen (Henriet et al. 2018). Previous work in the lab has shown DDR2 is a regulator of ovarian cancer metastasis via TWIST1 and SNAIL1 regulation (Grither et al 2018). DDR2 has also been linked to aggressiveness and other hallmarks of cancer in multiple other types of cancers. Therefore, we

decided to investigate if DDR2 also plays a role in the development of chemo-resistance in ovarian cancer.

PD-1 inhibition is a targeted therapy treatment option that is an immune checkpoint inhibitor which has not been fully researched for its effectiveness on ovarian cancer. Anti-PD-1 therapy has been shown to increase patient survival in many cancer types and has thus become a frontline therapy for multiple cancer types including lung, melanoma, and Hodgkin lymphoma (Wu et al 2019). Additionally, anti-PD1 treatment effectiveness has been shown to be affected by DDR2 status in other cancers. Specifically, DDR2 depletion in colon cancer, breast cancer, and melanoma among others has been shown to increase the effectiveness of anti-PD1 treatment *in vivo* (Tu et al 2019). Therefore, in addition to determining the role of DDR2 on chemoresistance, we also asked if response to other treatments including anti-PD1 is influenced by DDR2 expression in tumor cells.

3.3 Materials and Methods

3.3.1 Patient tumor collection

Ovarian cancer patient tumor cores were collected from consenting patients at Washington University in Saint Louis and FFPE preserved. The tumor cores were then used for IHC and stained for DDR2. Kaplan-Meijer curves were made using Prism.

3.3.2 Chemo-resistance passaging *in vivo*

I used the same CNAS and CHRP5 cells made in Chapter 2. ID8PBGL cells were used as the initial cells and passaged as specified in Chapter 2.

3.3.3 Immunohistochemistry

Formalin-fixed, paraffin-embedded human and xenograft tumor slides were deparaffinized and IHC performed and scored for DDR2 expression as previously published (Schab et al 2023).

3.3.4 Cell culture

ID8 TRP53-/- BRCA2-/- GFP LUC cells were a generous gift from Ian McNeish. All cell lines that originated from the ID8 cells were cultured in DMEM (Sigma-Aldrich) 4% FBS 1% insulin-transferrin-selenium, 1% penicillin and streptomycin. KPCA cells were a generous gift from Robert Weinberg. KPCA cells and cells generated from the KPCA cell line were cultured in DMEM 4% FBS 1% insulin-transferrin-selenium, 1% EGF, 1% penicillin and streptomycin. All cells were maintained at 37 °C in a 5% CO2 incubator. Cell lines were confirmed Mycoplasma negative with MycoAlert Mycoplasma Detection Kit (Lonza) before experiments.

3.3.5 Lenti-viral transfection

CHRP5 GFP+ cells were transfected using either shSCRM or shDDR2 lentiviral transfection and selected for transfection by sorting for turbo RFP expression on MoFlo cell sorter. CHRP5 shDDR2 UTR, CHRP1 and KPCA cells were transfected with either an empty flag control or flag tagged DDR2 overexpression plasmid and selected with neomycin for 5 days to select for transfected cells.

3.3.6 Western blots

Performed as described preciously (Mullen et al 2022) Briefly, cultured cells were lysed and proteins were quantified by Bradford assay. Lysates were reduced via SDS-PAGE by standard methods and transferred to a nitrocellulose membrane. Each membrane was incubated with primary antibody at 4°C for 1 to 3 nights, washed in TBST, and incubated with corresponding horseradish peroxidase-conjugated secondary antibodies. Signal was detected

with the Pierce ECL Western Blotting Substrate, and chemiluminescence was measured on a ChemiDoc (Biorad).

3.3.7 Clearance Assays

TDT+ Mouse Meso cells either DDR2 WT or DDR2 KO were plated at 500,000 cells/well in a 6-well plate and allowed to attach overnight. GFP+ BPPMN cells, a gift from the lab of Dr. Robert Weinberg were plated 300 cells/well in low adherence round bottom plates to for small spheroids and allowed to congregate overnight. The next day, up to 12 spheroids were added to each well of the mesothelial cells. Cells were imaged every 30min for 24 hours on (Nikon Ti-E). Images were analyzed using Nikon software and mesothelial cell clearance was measured based on dark area present at each time point and normalized to the area of the initial spheroid.

3.3.8 MTS survival assays

96-well plates (Techno Plastic Products) were coated in 30uL/well of 1mg/mL rat tail collagen and 1N NaOH and allowed to polymerize for half an hour prior to cell plating. Cells were plated at 1500 cells/well and allowed to attach overnight. Plates were then treated with serial dilutions of carboplatin, diluting by half each column, and starting at 1000uM carboplatin. Cells were treated for 72 hours and then 20uL/well MTS (3-(4,5-dimethylthiazol-2-yl)-5-(3-carboxymethoxyphenyl)-2-(4-sulfophenyl)-2H-tetrazolium) solution (Promega) was added to the cells, incubated for 2 hours at 37 C, and then the absorbance was measured at 490 nm with a 96-well plate reader (Tecan infinite M200 Pro). Analysis was performed using GraphPad Prism 8.

3.3.9 RT-qPCR

RNA was isolated from cells or tumors using the quiagen easy RNA kit. cDNA was made from the RNA using oligos and reverse transcription. qPCR was run using SYBR green. Primers

for DDR2, ABCG2, GPNMB, PGR, CADM1, MUC1, LGR6, GRB1, GALNT13, DKK2, MSX2. qPCR was analyzed using SYBR green reagents. See table (table 1, chapter 2) for primer sequences.

3.3.10 Whole exome bulk mRNA sequencing

For the chemo-resistance project, mice were injected with either CHRP5 or CHRP1 GFP+ cells and allowed to grow for 21 days. At day 21 mice began treatment of 5mg/kg of carboplatin twice a week. Day 35 tumors and ascites were collected from the mice and RNA was extracted from snap frozen metastatic uterine tumors which was then sent for sequencing. RNA sequencing data was analyzed with Partek to run DEseq2 comparing chemo-resistant to chemo-sensitive gene expression changes.

For our Mesothelial cell project, TDT+ DDR2 CRE mice were injected with tamoxifen to induce the CRE mechanism which knocks out DDR2 by removing a section of exon 8 and then inducing TD tomato expression. Control mice did not have DDR2 knockout but still has TDT expression. Mice were sacrificed and their omentum collected to isolate mesothelial cells from these mice. Cells were then transfected with SV40 to immortalize them and grown in cell culture. RNA was extracted from mesothelial cells for both DDR2 KO and DDR2 WT. Which was then sent for sequencing. RNA sequencing data was analyzed with Partek to perform DEseq2 comparing DDR2 KO to DDR2 WT gene expression changes.

3.4 Results

3.4.1 DDR2 expression correlates with reduced survival in ovarian cancer patients

Previous work in the Fuh lab performed mass spectrometry specifically on receptor tyrosine kinases (RTKs) to identify overexpressed RTKs in patients with reduced survival and sensitivity to chemotherapy. Tumor samples were isolated from ovarian cancer patients before (neo-adjuvant) and after chemotherapy (adjuvant) treatment and labeled chemo-resistant if cancer recurred less than 6 months after initial treatment, or chemo-sensitive if the patients did not experience recurrence within 6 months. Samples were then analyzed via mass spectrometry focused on RTK expression differences between pre- and post- chemotherapy tumors. We found out of our panel of proteins, DDR2 was the only protein that had increased expression in post-chemo tumors specifically in the chemo-resistant samples (figure 1a). For these reasons, we decided to determine whether DDR2 mRNA and protein expression contributed to ovarian cancer treatment resistance. Patients with high DDR2 mRNA expression have significantly shorter survival compared to patients with low DDR2 expression (figure 1b). We wanted to know if this expression change was due to mutations in DDR2. To do so, we then used TCGA data sets of mRNA expression in ovarian cancer and found DDR2 is only mutated in about 2% of cases, meaning mutations are not the cause of the overexpression seen in chemo-resistant patients (TCGA).

We asked if DDR2 performed immunohistochemistry (IHC) to measure DDR2 protein expression in ovarian cancer patient tumor samples. We used 164 patient tumor samples to compare subjective protein expression levels, patient survival, and chemotherapy treatment success. We found patients with high tumor DDR2 protein expression had significantly shorter overall survival (33 months) than patients with low tumor DDR2 protein expression (83 months)

(figures 2a, 2b). We also found that patients with high DDR2 expression had shorter platinum free interval (15 months) compared to patients with low DDR2 expression (28 months) (figure 2c).

3.4.2 Genetic depletion of DDR2 does not impact tumor burden after chemotherapy *in vivo*

To determine if the presence of DDR2 in ovarian tumor cells impacted chemotherapeutic responses in *in vivo* preclinical models we utilized genetic and pharmacologic approaches. I used human A2780 ovarian cancer cells transfected using lenti-virus for either shDDR2 or shSCRM plasmids for this purpose. I injected 19 NCR/NU mice with 1 million A2780 shSCRM (N=9) or shDDR2 (N= 10) cells into the peritoneal cavity of the mice and left them to engraft for 4 days. After engraftment, I treated the mice with carboplatin (20mg/kg) and paclitaxel (10mg/kg) combination or vehicle control every 3 days for 2 weeks. After treatment, we sacrificed the mice and measured the tumor burden for each mouse: total tumor weight, number of large nodules (>1mm), and number of small nodules (<1mm). I found there was a significant decrease in the number of small nodules in mice engrafted with DDR2-deficient cells and treated with chemotherapy compared to control tumor cells with the same treatment (figure 3a-c). However, there was no difference in total tumor burden between the two sets of mice.

We suspected that DDR2 may play a larger impact on chemotherapy treatment response at higher doses. I repeated this experiment with 6 mice per group of shDDR2 cells, shSCRM cells treated with either vehicle or a higher dose of chemotherapy (40mg/kg carbo, 10mg/kg paclitaxel) and injected 1 million cells per mouse intraperitoneally. I allowed the tumors to engraft for 7 days after tumor injection before we began treatment. I treated mice every 3 days with chemotherapy (40mg/kg carboplatin, 10mg/kg paclitaxel) for 2 weeks and then sacrificed the mice to assess tumor burden using the same methods as previously. I again did not see a

significant difference in tumor burden between the mice injected with shSCRM cells and those injected with shDDR2 cells in response to chemotherapy (figure 3d-f). These results indicated DDR2 genetic knockdown did not increase sensitivity or response to chemotherapy *in vivo* this model.

3.4.3 DDR2 status does not change response to PD-1 inhibition *in vivo*

Pembrolizumab is an immune checkpoint PD-1 inhibitor. It has been shown to be an effective treatment for various other cancers. Thus, we decided to determine if DDR2 knockdown would also increase the effectiveness of anti-PD1 therapy in ovarian cancer.

To answer this question, we injected 10 million ID8PBGL shSCRM (N=20) or shDDR2 (N=20) cells intraperitoneally into C57/BL6 mice to assess differences in treatment response based on DDR2 status. Additionally, we wanted to assess if the timing of pembrolizumab treatment initiation would affect treatment. We treated mice with either vehicle (IgG) or pembrolizumab and divided mice into early treatment and late treatment groups (N=5 for all groups; early or late treatment, and shSCRM or shDDR2 cells, and pembrolizumab or vehicle treatment). For the early group we started treatment on day 26 post tumor cell injection and sacrificed on day 40. For the late group we started treatment on day 40 and sacrificed on day 54. For both early and late groups, we treated the mice with 10mg/kg of pembrolizumab for the first dose and then with 5mg/kg for every subsequent treatment. We measured tumor burden via multiple methods including the number of large tumor nodules (>1mm^3), number of small tumor nodules (<1mm^3), tumor mass, tumor volume, and ascites volume. We did not see any significant reduction in tumor burden between any of the treatment groups or treatment timing (figure 4a-c). After this experiment, we realized we were using human pembrolizumab in a syngeneic mouse model which may have decreased the effectiveness of the drug. Thus, the

experiment was repeated a year later with the help of Dr. Michael Toboni and Favour Akinjiyan using mouse specific pembrolizumab. When we treated mice in the same way but using mouse specific pembrolizumab, we saw that DDR2 knockdown cells were much more sensitive to pembrolizumab treatment and had significantly less tumor burden than control mice (figure 4d-f).

3.4.4 Pharmacological inhibition of DDR2 does not increase effectiveness of chemotherapy *in vitro* or *in vivo*

First we attempted to use a novel small molecule inhibitor, specific to DDR2. The Longmore lab identified small molecule inhibitor WRG28 which then was used to create an allosteric inhibitor for DDR2 called CR13452 (CR) (Grither and Longmore 2018, Rotapharm). This inhibitor binds to the extra-cellular region of DDR2, modulating the receptor to prevent the ligand, fibrillar collagen I, from binding properly and signaling to ERK and SNAIL1. We used this inhibitor in addition to chemotherapy to determine if inhibition of DDR2 would increase sensitivity to chemotherapy carboplatin both *in vitro* and *in vivo*.

To study the effects of this drug *in vitro,* we used ID8PBGL cells in MTS survival assays and treated the cells with no treatment, CR alone, chemotherapy alone, or a combination of CR and chemotherapy to compare the survival of the cells in different doses of the drugs. We saw that CR alone does not cause more cell death than no treatment, and that CR in combination with chemotherapy (carboplatin and paclitaxel) does not cause more cell death than chemotherapy alone *in vitro* (figure 5a).

We then asked if CR would affect response to chemotherapy *in vivo.* Next, we injected 28 C57/BL6 mice with either 5x10^6 ID8PBGL shSCRM (N=14) or shDDR2 (N=14), into the peritoneal cavity of the mice and let the cancer cells engraft for 47 days. After engraftment, had three treatment groups: vehicle (every 3 days), chemotherapy (carboplatin 20mg/kg and

paclitaxel 10mg/kg every 3 days), CR (every 12 hours), or combination CR and chemotherapy. Mice were treated for 2 weeks. Then, we sacrificed the mice and measured the tumor burden via total tumor weight, number of large nodules, and number of small nodules. We found that CR treatment alone did not reduce tumor burden in mice compared to mice treated with vehicle. We also found treatment with CR in combination with chemotherapy did not significantly reduce tumor burden in mice compared to chemotherapy alone, regardless of DDR2 status (figure 5b-e). We also observed that treatment with CR13452 the mice became more visibly ill than mice that did not receive CR treatment. Mice were observed to be jaundiced and hunched at sacrifice when treated with CR either alone or in combination.

3.4.5 DDR2 status in mesothelial cells does not change tumor cell clearance

Tumor cells are only one of many cell types present in the tumor microenvironment. During ovarian cancer metastasis, tumor cells must first clear through a monolayer of mesothelial cells to invade into any organ in the peritoneal cavity. These mesothelial cells are the first line of defense against metastasis and thus worthy of further investigation. Angela Schab isolated mesothelial cells from the omentum of DDR2 genetic null mice and from DDR2 wild type (WT) mice (Schab et al 2023). These cells were then grown in culture and confirmed to be mesothelial cells and to be DDR2 wild type or null respectively.

We wanted to determine if DDR2 expression in the mesothelial cells increased metastatic potential of ovarian cancer cells. We used whole exome mRNA sequencing comparing DDR2 null and DDR2 WT mouse mesothelial cells. There is a clear difference in gene expression between the two groups (figure 5a,b). Some notable genes we found to be significantly downregulated in DDR2 null cells compared to WT DDR2 mesothelial cells are progesterone receptor PGR and GREB1, an estrogen receptor, which are both hormone signaling proteins.

Despite confirmation that PGR and GREB1 are differentially expressed at the mRNA level, western blot revealed no change in protein expression between DDR2 null and DDR2 WT for either gene (figure 5c,d). We then performed clearance assays to compare the ability of DDR2 WT and DDR2 null mesothelial cells to be cleared by mouse ovarian tumor organoids. We did not see a significant difference in the clearance of our mesothelial cells by the tumor spheroids based on DDR2 status of the mesothelial cells (figure 5e).

3.4.6 Tumor cell DDR2 depletion does not change sensitivity to chemotherapy *in vivo*

Neither DDR2 inhibition nor genetic knockdown showed a significant improvement in treatment response when combined with other therapies. So, I decided to shift my focus to mechanisms of chemo-resistance in ovarian cancer. Specifically, the role that DDR2 may play in the development of acquired chemo-resistance. Our patient data comparing platinum free interval and DDR2 expression suggests DDR2 could be important in the context of chemo-resistance, if not in ovarian cancer progression in general. We decided to investigate if downregulation or inhibition of DDR2 expression in chemo-resistant ovarian tumors can increase cancer cells response to chemotherapy. I decided to use a syngeneic mouse model which allows for capturing more biologically relevant data on how mice respond to cancer and treatments. We used CHRP5 cells (chemo-resistant cell line) and CNAS (chemo-naïve control cell line) I created (see chapter 2).

We established a genetic knockdown of DDR2 in our cells using lentiviral transfection. We discovered the shDDR2 plasmid we used to transfect the ID8PBGL cells used in previous experiments uses a puromycin selection marker which is already present from previous CRIPSR editing (Walton et al 2016). We had confirmed knockdown in shDDR2 transfected cells for each

experiment we performed before we realized this, but the inability to select cells for plasmid expression made DDR2 expression in these cells inconsistent (figure 6a). Therefore, we needed to find a mouse specific shDDR2 plasmid containing a selection marker that is not already present in this cell line. First, I attempted to clone the shDDR2 plasmid our lab used on other cells and add in neomycin resistance, however, but could not successfully create the new plasmid. When cloning did not work, we tried using CRISPR to knock out DDR2 in my cells. That did not work either, so finally we found a shDDR2 plasmid tagged with turboRFP marker which can be used for selection via cell sorting. After transfecting these cells with 3 unique shDDR2 RFP plasmids and one shSCRM plasmid as a control, we then sorted the cells to select for GFP+ (tumor cell marker) and turboRFP+ (transfected cell marker). After sorting we had cells with DDR2 knockdown or control plasmid. I confirmed these results by western blot and qPCR (figure 6c). The three different knockdown plasmids target different parts of the DDR2 gene. We labeled these shDDR2 plasmids as RFP#5 (UTR targeted), #6 (CDS targeted) and #7 (CDS targeted). When we blotted for DDR2 expression, we saw that shDDR2 #77 plasmid showed the most efficient knockdown, so we proceeded with cells transfected with it.

Between each chemo-resistance passage, we established a cell line that is more resistant than the previously created passage as shown by MTS survival assays (figure 7) (see Chapter 2 for more details). Western blots comparing these passages showed that as chemo-resistance developed, DDR2 expression increased (figure 7c). Next, we decided to test if DDR2 was necessary for chemo-resistance development. MTS survival assays showed that shDDR2 CHRP5 cells were slightly more sensitive to carboplatin than shSCRM CHRP5 cells, meaning DDR2 may have an impact on acquired resistance (figure 7e). However, the change in sensitivity to chemotherapy was not large enough to be worth further investigation at this point in time.

3.5 Discussion

Our patient data shows DDR2 expression correlates with reduced survival and response to chemotherapy. However, we found that tumor DDR2 expression *in vitro* and *in vivo* does not influence ovarian cancer response to chemotherapy or chemo-resistance. Tumor microenvironments are diverse and contain many cell types as well as extracellular structures. Potentially the DDR2 overexpression we see in chemo-resistant patient samples could be from a non-tumor cell type present in patient tumors. DDR2 overexpression seen in patients with reduced survival could result from dysregulation of another pathway in the cancer and, thus, not directly correlated with DDR2 expression. Cancers modify their surrounding microenvironment and ECM structure. Since the ligand for DDR2 is collagen, ECM structure changes not regulated by DDR2 may cause the overexpression of DDR2 seen in patients. Our lab has shown previously that DDR2 expression in tumor cells is critical for metastasis by regulation by TWIST1 and stabilization of SNAIL1 (Grither et al 2018). So, DDR2 overexpression may be from the role of DDR2 in metastasis which in turn leads to patient death rather than its involvement in acquired chemo-resistance.

One limitation of our data was that, though we verified DDR2 expression to be lower in the shDDR2 ID8PBGL cells before each experiment, it would be beneficial to repeat these experiments with a verified, selectable, and efficient DDR2 knockdown in ID8PBGL cells.

Future directions could include further investigation of the top hits identified in CHRP5 and CHRP1 RNA sequencing data to look for key genes in the development of chemo-resistance (see chapter 2 for more details). Additionally, RNA sequencing of the in-between CHRP passages (2,3,4) would be useful to compare gene expression changes as chemo-resistance develops. Ideally, I would continue to passage my CHRP cells to create cells that are resistant to

higher doses of chemotherapy. This could determine if DDR2 knockdown has a bigger impact on resistance when the cells can survive higher doses of chemotherapy.

Mass spectrometry could be performed on the CHRP cell lines to compare protein expression changes in addition to mRNA expression. Specifically, using mass spectrometry specifically looking at the top hits identified in the RNA seq data. Then, we could see if the gene expression changes are also affected at the protein level. Additionally, exploring the protein expression changes that correspond to the development of chemo-resistance may lead to discoveries of genes important to resistance that did not have significant mRNA differential expression.

3.6 Conclusions

This study aimed to determine the role of DDR2 in ovarian cancer. Specifically, I wanted to determine if DDR2 depletion would increase ovarian cancer sensitivity to chemotherapeutic agents such as carboplatin and paclitaxel, and anti-PD1 therapy pembrolizumab. Through many experiments, I have shown that DDR2 expression in ovarian cancer cells *in vitro* does not significantly alter tumor cell sensitivity to chemotherapies. Additionally, I have shown that neither genetic knockdown nor pharmacological inhibition of DDR2 in combination with chemotherapies reduces tumor burden *in vivo*.

3.7 Figures and Tables

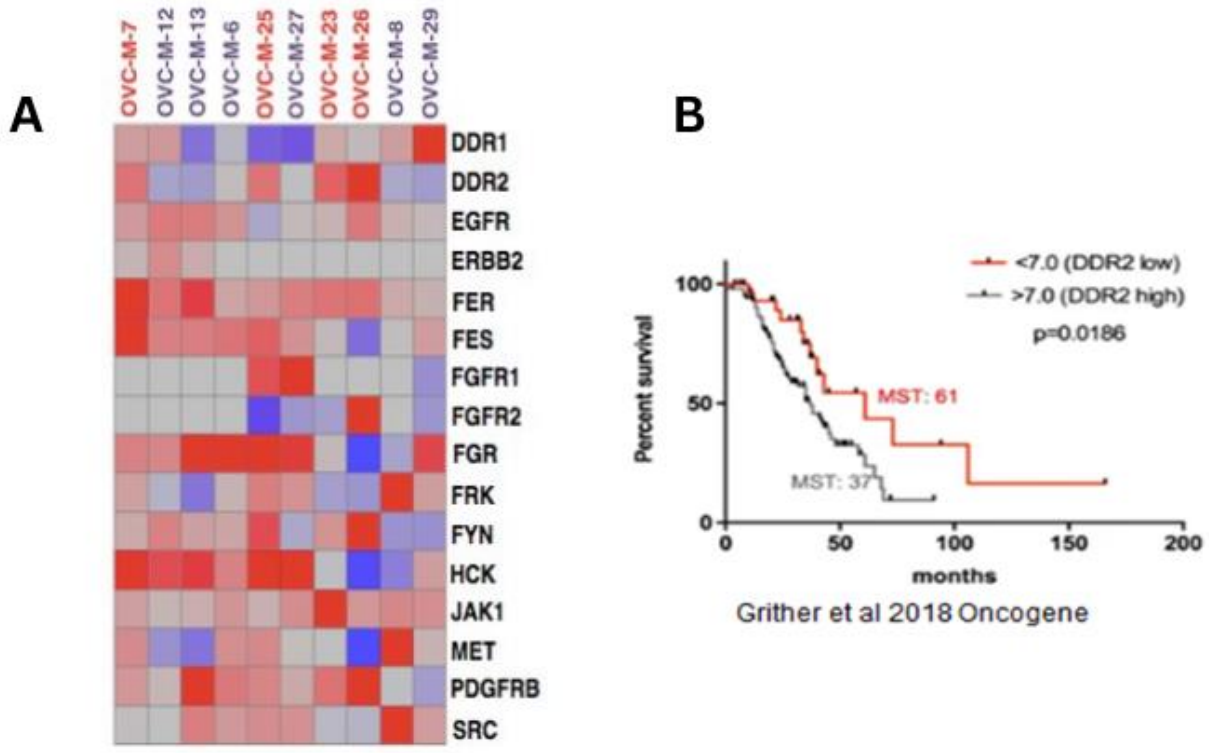

Figure 3.1: DDR2 is identified as potentially important in resistance to chemotherapy. (A) Heat map of mass-spec data. Each column represents a single patient. The heatmap shows the change in protein expression between pre- and post- chemo tumors. Red patient IDs did not respond to chemo and blue patient IDs did. (B) Survival chart comparing patients with high versus low DDR2 mRNA expression (Grither et al 2018).

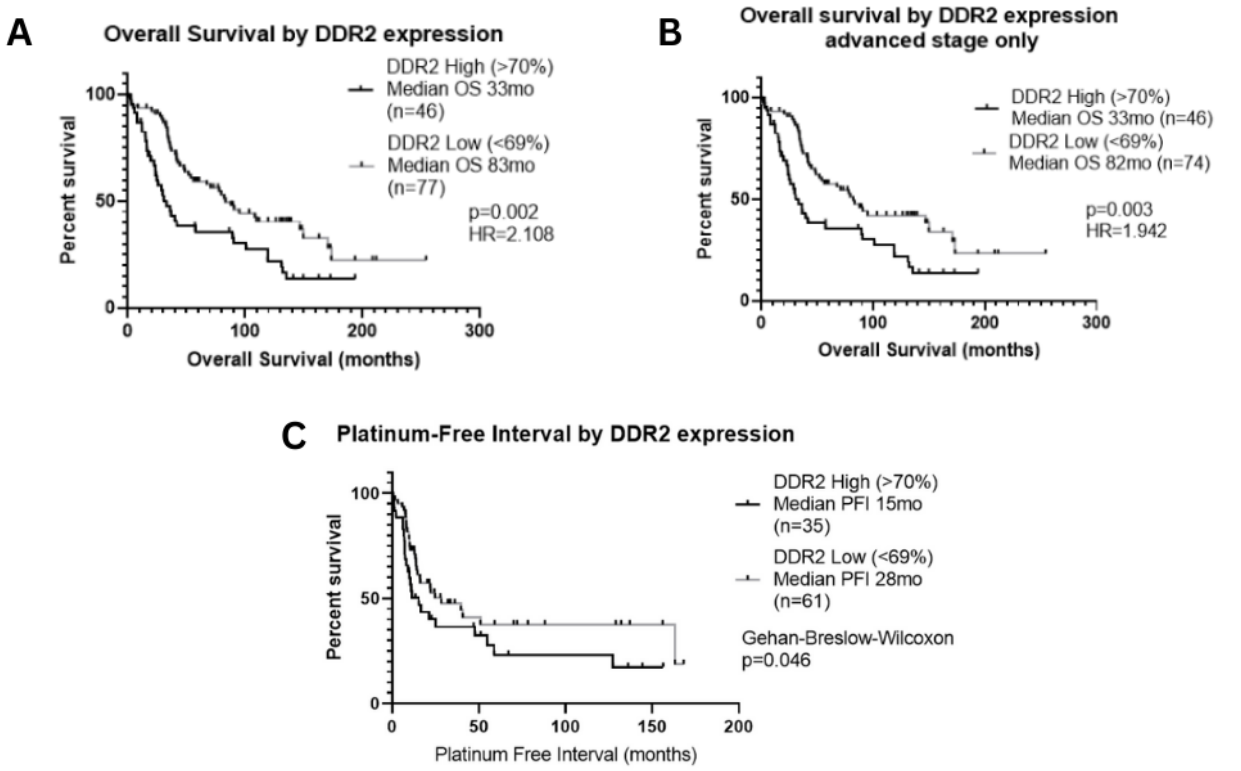

Figure 3.2: Survival curves of patients with high versus low DDR2 expression as quantified by IHC. (A) Overall survival (time from diagnosis to death) for all stages at diagnosis, (B) Overall survival for patients diagnosed with advanced stage disease only, (C) Platinum free interval (time from initial chemotherapy treatment ending and disease recurrence).

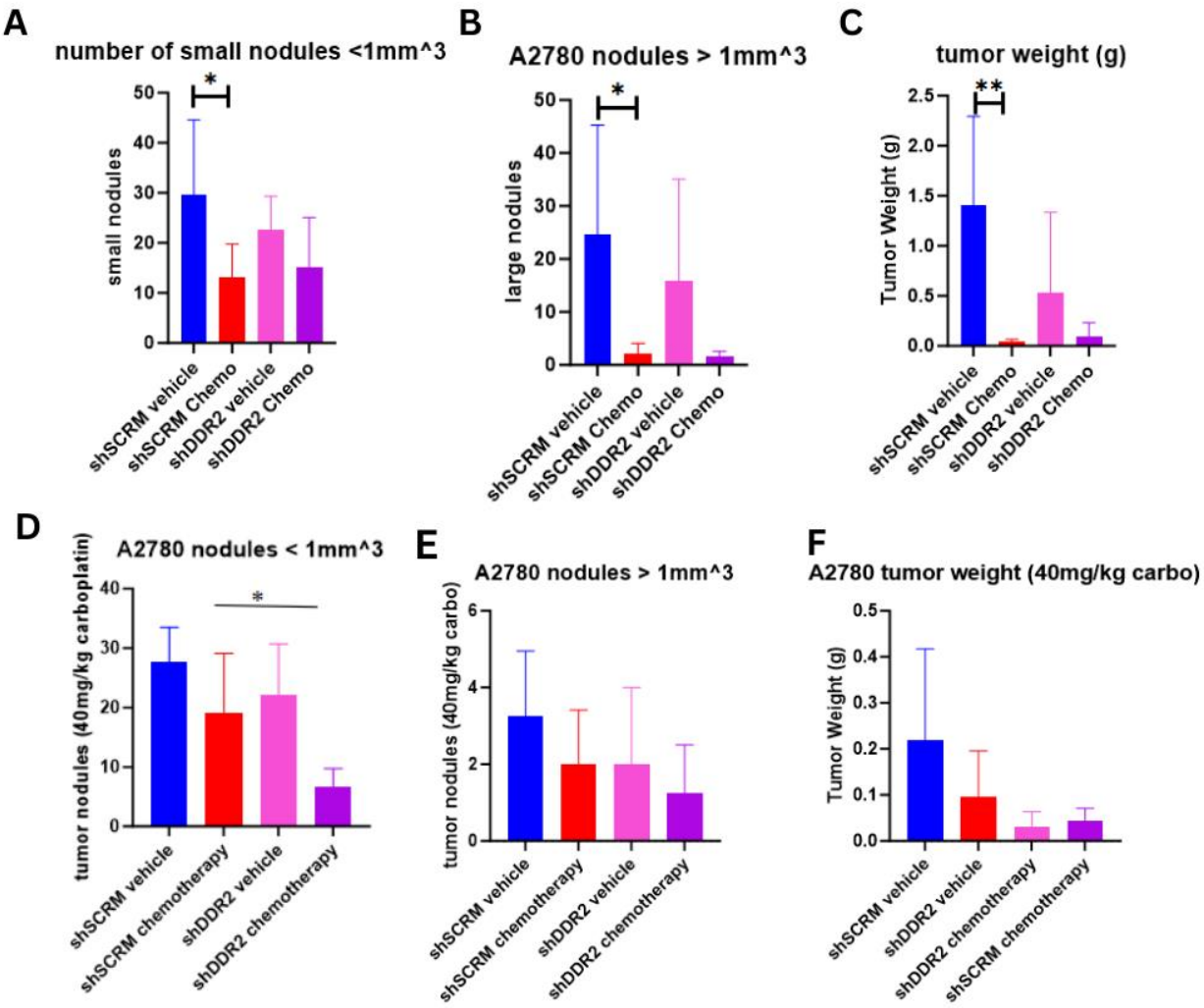

Figure 3.3: Genetic knockdown of DDR2 in A2780 cells *in vivo.* Average (A) number of small nodules, (B) number of large nodules, and (C) toral tumor weight (g) for mice injected with A2780 shSCRM or shDDR2 cells and treated with 20mg/kg of carboplatin and 10mg/kg paclitaxel. (D-E) Same comparisons but mice were treated with 40mg/kg carboplatin and 10mg/kg paclitaxel.

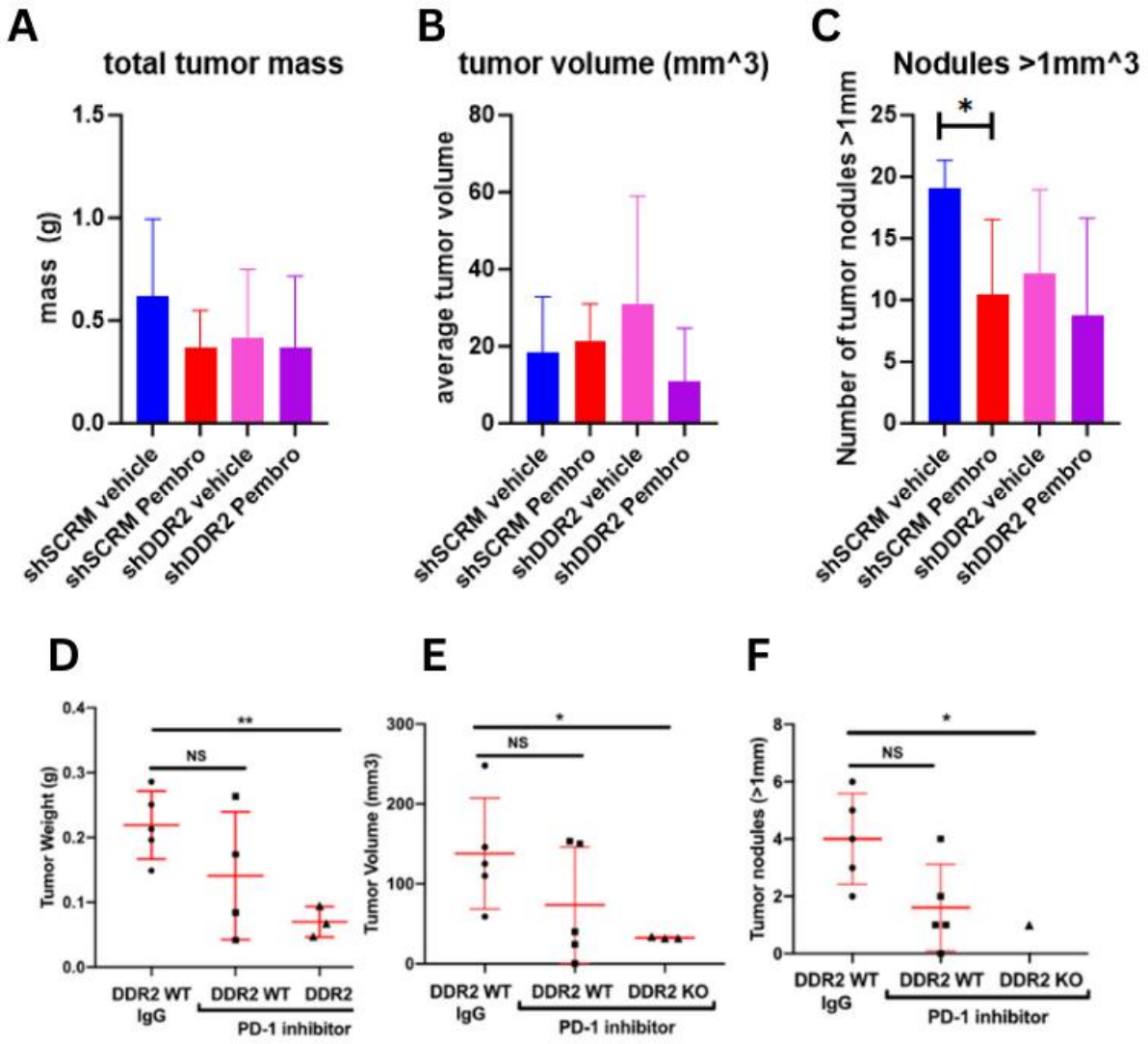

Figure 3.4: Genetic knockdown of DDR2 and anti-PD1 treatment (pembrolizumab). Bar charts showing average (A) total tumor mass (g), (B) tumor volume (mm^3), and (C) number of large nodules when using human specific pembrolizumab. Dot plots showing (A) total tumor mass (g), (B) tumor volume (mm^3), and (C) number of large nodules when using mouse specific pembrolizumab.

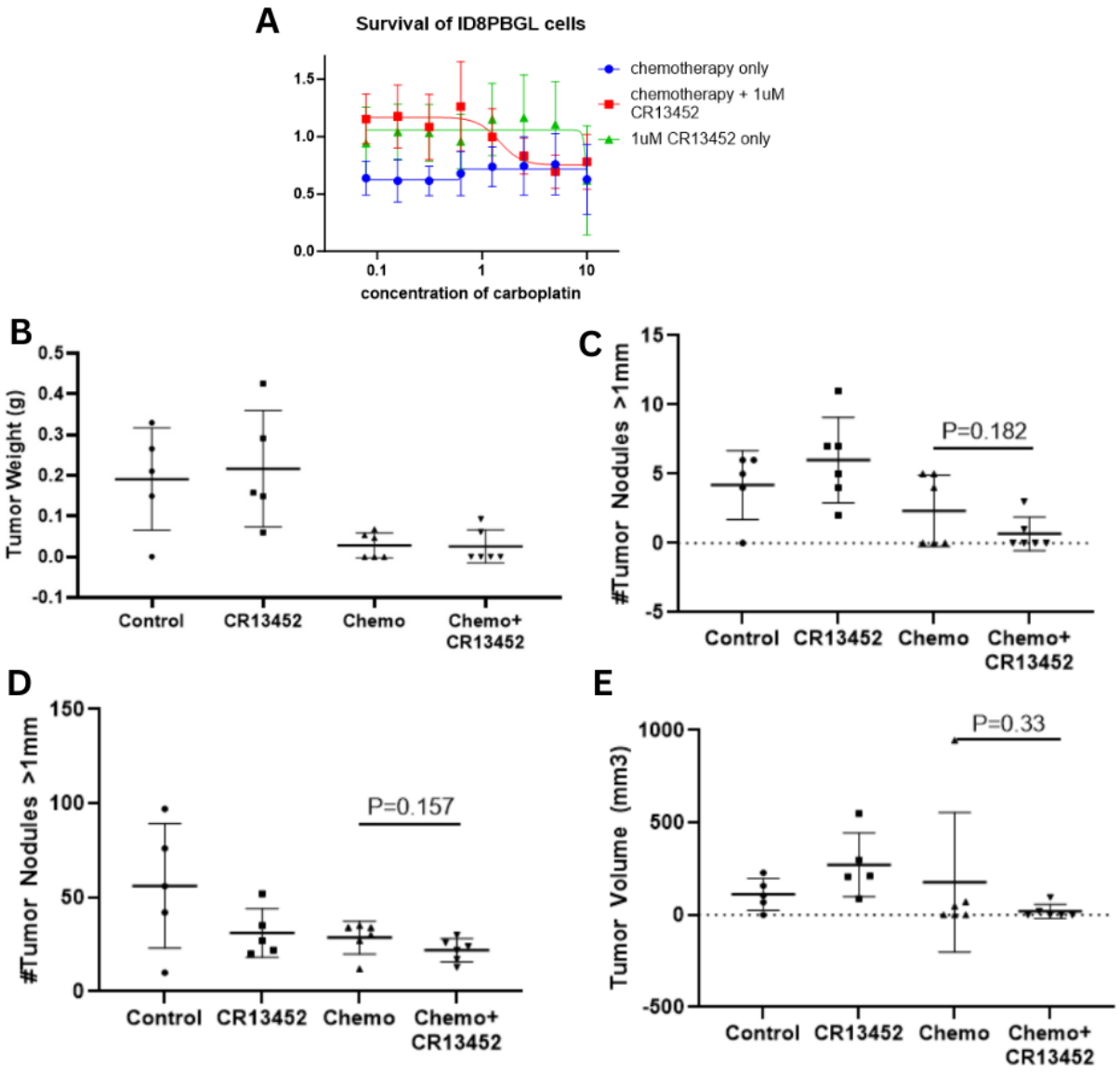

Figure 3.5: Combination CR and chemotherapy treatment does not significantly reduce tumor burden compared to chemotherapy alone. (A) MTS survival curve comparing sensitivity to chemotherapy, CR, or a combination of chemotherapy and CR. Dot plots showing average (B) total tumor weight (g) (C) number of large nodules (D) number of small nodules (E) tumor volume (mm^3) for mice treated with vehicle, chemotherapy (carboplatin 40mg/kg, paclitaxel 10mg/kg), CR13452, or a combination of chemotherapy and CR.

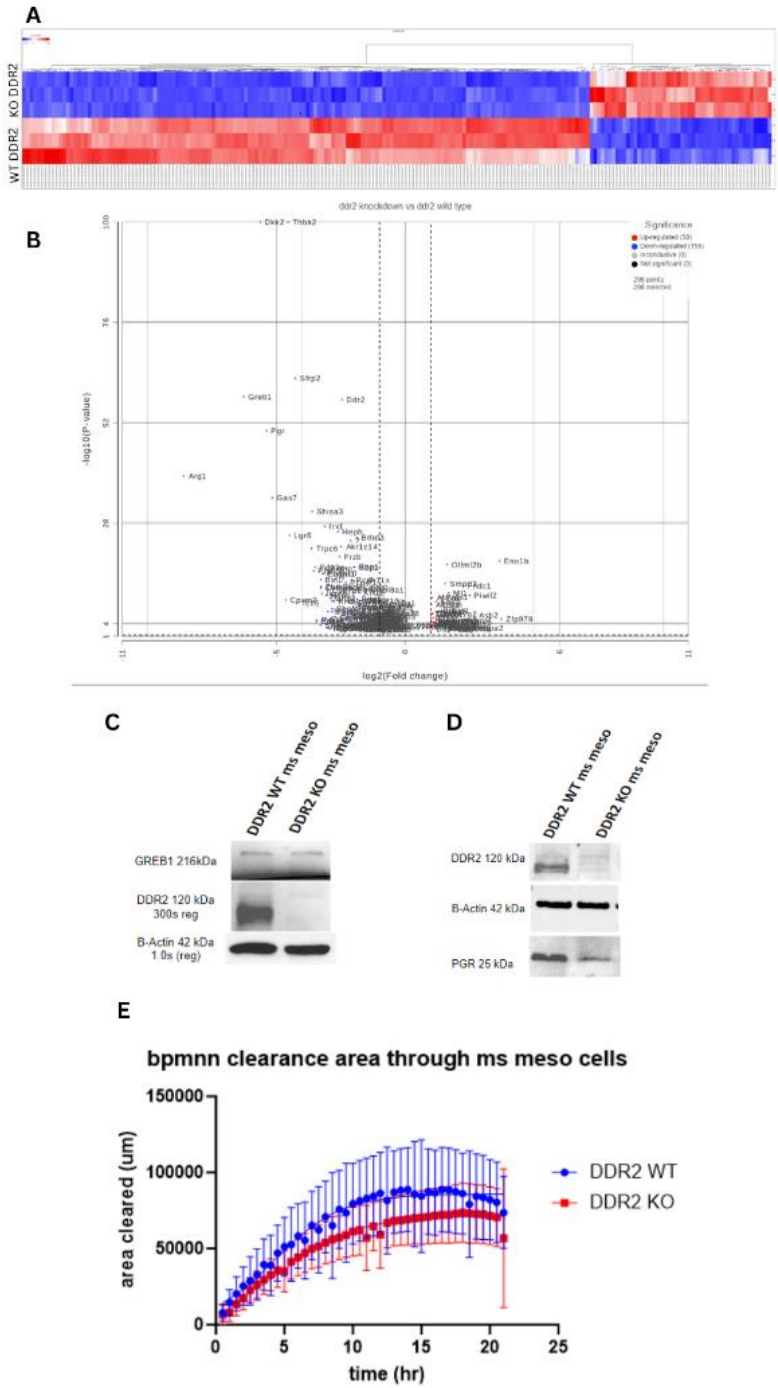

Figure 3.6: DDR2 expression in mouse mesothelial cells also changes expression of other genes. (A) Heatmap of mRNA differential expression between KO DDR2 mouse mesothelial cells and WT DDR2 mouse mesothelial cells. (B) Volcano plot displaying identified “top hits” fold change in mRNA expression. (C) Graph showing the area of mesothelial cells cleared by the tumor cells between WT and KO DDR2 in the mesothelial cells.

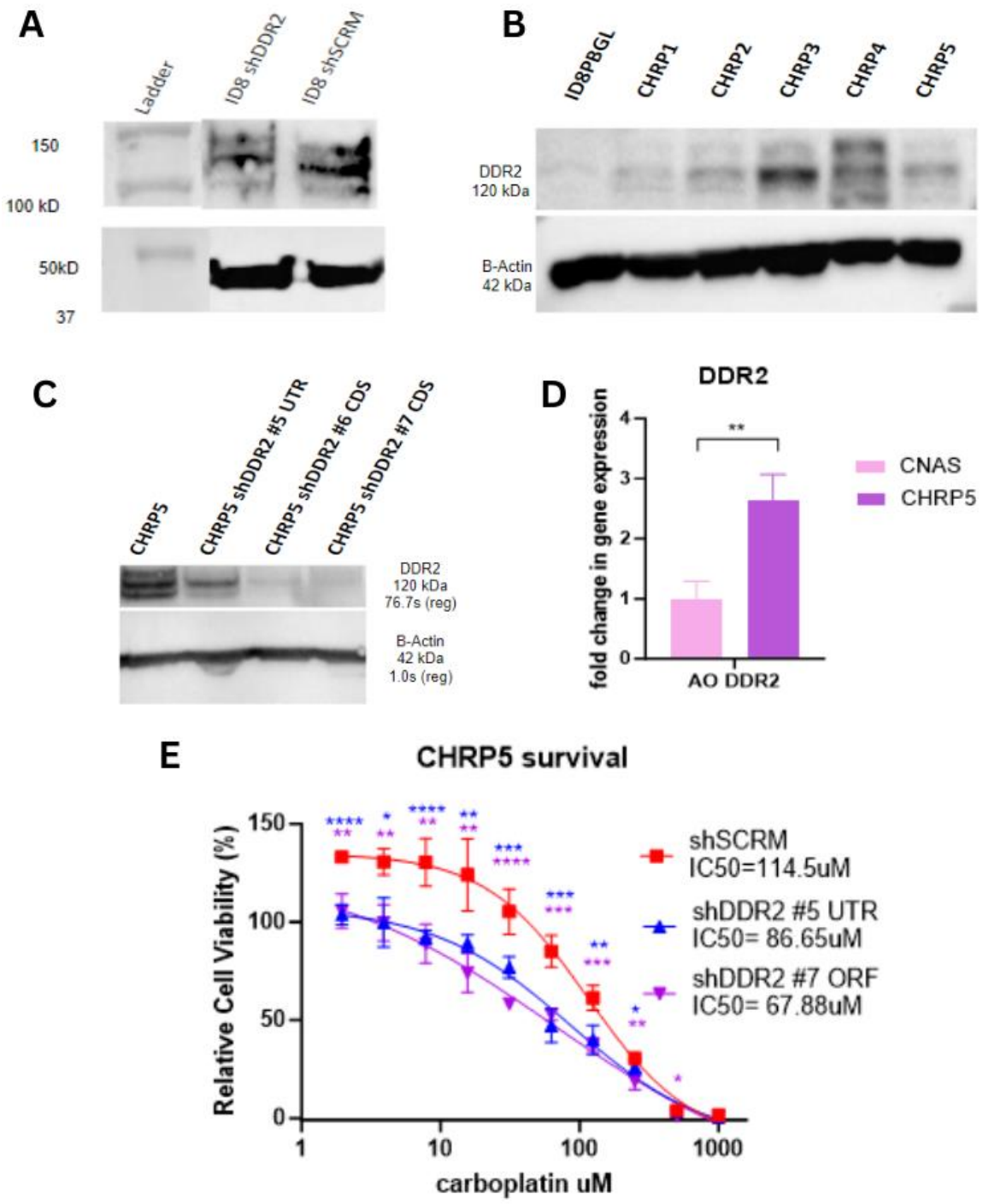

Figure 3.7: DDR2 expression increases with increased resistance to chemotherapy. (A) Western blot comparing ID8PBGL shSCRM and shDDR2 expression of DDR2. (B) Western blot showing DDR2 expression across CHRP cells from parental ID8PBGL to CHRP5. (C) Western blot showing knockdown efficiency of the three shDDR2 plasmids. (D) RT-qPCR analysis of DDR2 mRNA expression between CNAS and CHRP5 cells.

Chapter 4: Small Molecule AXL Inhibitor AVB-500 Increases Response to Treatment in Gynecological Cancers

4.1 Declarations

All ovarian cancer *in vivo* mouse models were performed by Alyssa Oplt and analyzed in collaboration with Maggie Mullen. Mouse models of endometrial cancer were done in collaboration with Shaina Bruce and Michael Toboni. Maggie Mulle, Shaina Bruce, and Michael Toboni designed the experiments for their respective publications that I assisted with.

4.2 Introduction

Over 80% of women with high-grade serous ovarian cancer develop tumor resistance to chemotherapy and die of their disease. There are currently no FDA-approved agents to improve sensitivity to first-line platinum- and taxane-based chemotherapy or to poly (ADP-ribose) polymerase (PARP) inhibitors. One candidate target in ovarian and other cancers is growth arrest-specific 6 (GAS6), which binds to and activates the receptor tyrosine kinases Tyro3, AXL, and Mer (Lew et al 2014). AXL mRNA expression is upregulated in several ovarian cancer cell lines. Data from The Cancer Genome Atlas, as well as other sources, indicate that AXL and GAS6 overexpression are associated with poor prognosis in ovarian cancer (Kanlikilicer et al 2017). Furthermore, Buehler et al. found that epithelial ovarian cancers commonly had high GAS6 mRNA and protein expression, and ovarian cancers from patients with residual disease after primary cytoreductive surgery had higher GAS6 expression than those without residual disease (Buehler et al 2013).

Endometrial cancer is another deadly gynecological malignancy with poor survival and evidence of associations with AXL expression. Seventy-five percent of endometrial cancer patients are diagnosed with disease confined to the uterine corpus, which leads to a greater than 90% 5-year survival (American Cancer Society). However, prognosis for advanced endometrial cancer is poor with a 5-year overall survival of 40–65% for stage III and 15–17% for stage IV disease (Wang et al 2020). A subtype of endometrial cancer, uterine serous cancer (USC) patients are more likely to be diagnosed at advanced stages of disease and often do not respond well to chemotherapy. Initial lines of treatment for endometrial cancer are platinum and taxane treatment and radiation, but there is a need for novel therapies to improve patient survival. Previous work from our lab demonstrated that patients with chemotherapy resistant USC had higher AXL expression than patients with chemotherapy sensitive USC (Divine et al 2016). High-grade endometrial carcinomas, which tend to be more chemotherapy resistant, are also more likely to demonstrate high AXL expression compared to low-grade endometrial carcinomas (Divine et al 2016). In addition, AXL knockdown improved sensitivity to paclitaxel, a chemotherapeutic agent frequently used to treat endometrial cancer (Palisoul et al 2017). This data supports AXL as a potential therapeutic target in endometrial cancer.

One promising GAS6/AXL inhibitor is AVB-S6-500 (AVB-500), a highly selective AXL decoy receptor that binds to GAS6 with high affinity. Given the safety profile in healthy volunteers, AVB-500 was recently granted FDA fast-track designation for potential treatment of platinum-resistant ovarian cancer. Here, our objectives were to determine the utility of AVB-500 in combination with standard of care treatments in ovarian cancer and to determine whether GAS6 could be associated with treatment response.

4.3 Materials and Methods

4.3.1 Ovarian cancer clinical samples

This study was approved by the Washington University in St. Louis Institutional Review Board (#201407156). Patients were included if they had stage III-IV ovarian cancer of serous, endometrioid, or clear cell histology and were planning to undergo neoadjuvant chemotherapy and interval cytoreductive surgery. Patients were excluded if they had previously undergone chemotherapy. Blood and tissue specimens were collected before and after three cycles of neoadjuvant chemotherapy.

Cases were evaluated for response to neoadjuvant chemotherapy according to a modified form of a published pathologic scoring system (Böhm et al 2015). All cases were scored for histological response to neoadjuvant chemotherapy and given a chemotherapy response score (CRS) of 1–3 as previously published. Additionally, they were given a score of 0–3 (0= no response, 3= complete response) for radiologic and surgical response (see Mullen et al 2022 for more details). A score of 0 was assigned if there was persistent large volume disease and ascites, 1 for mild treatment effects but large volume disease, 3 if there was no or minimal residual disease, and 2 for a response not otherwise specified. The sum of each response was subtracted from 10 for a final chemo-response score between 1 and 10. Cases were considered to have a good response if the score was 5 or lower and a poor response if the score was 6 or higher. This cutoff was representative of a moderate response or higher in two of the three categories evaluated. This novel score was utilized due to its comprehensive nature and clinical applicability. Progression-free and overall survival were calculated from the time of interval cytoreductive surgery.

4.3.2 Endometrial cancer clinical samples

See Toboni et al 2021 for more details. A tissue microarray containing specimens from patients with primary and metastatic USC treated at Washington University in St. Louis, MO, was developed with Institutional Review Board approval (#201409005) in accordance with ethical guidelines per the U.S. Common Rule. All specimens were collected at the time of diagnosis neo-adjuvantly. Written informed consent was obtained for tissue banking. Patients were considered to have had a good response to chemotherapy if their disease recurred greater than 6 months after the last chemotherapy regimen. Patients were considered to have a poor response to chemotherapy if their disease recurred within 6 months of the last chemotherapy regimen. Overall survival (OS) was defined as time in months from date of surgery to date of death or last contact. Progression free survival (PFS) was defined as time in months from date of surgery to date of disease progression or death. Kaplan-Meier methods were used to generate time-to-event curves. A Cox-proportional hazard model was used to estimate the hazard of high GAS6 expression.

4.3.3 GAS6 serum testing

Serum was collected from patients before three cycles of neoadjuvant chemotherapy. The concentration of free, unbound GAS6 was measured by an ELISA in which immobilized AVB-500 was used as a capture reagent. Briefly, the plate was coated with 1 μg/mL AVB-500 in PBS and GAS6 was detected on a Bio Tek 2 plate reader with a biotinylated polyclonal anti-human GAS6 antibody (BAF885, R&D Systems) and streptavidin-conjugated to horseradish peroxidase (DY998, R&D systems). The lower and upper limits of detection were 2 ng/mL and 128 ng/mL, respectively. See Mullen et al 2022 for more information.

4.3.4 Immunohistochemistry

Formalin-fixed paraffin-embedded tissue microarray, human, and xenograft tumor slides were deparaffinized with xylene, rehydrated, and stained with anti-GAS6 primary antibody (R&D Systems) or anti-AXL primary antibody (R&D Systems). Two tumor cores per patient were evaluated for GAS6 and AXL expression (see Buehler et al 2013 for more details). Multiple tumors for each treatment condition from the xenograft models were evaluated for AXL and GAS6 expression. For all immunohistochemistry assays, intensity of staining and percentage of positive cells were blindly scored by two reviewers and averaged for a final score.

4.3.5 Cell line culture

Established ovarian cancer cell lines OVCAR5 and OVCAR8 were obtained from the National Cancer Institute. These cell lines were cultured in RPMI plus 10% fetal bovine serum (FBS) and 1% penicillin and streptomycin. Established and previously characterized USC cell line, ARK1, was provided by Shi-Wen Jiang (Mercer University School of Medicine, Savannah, GA). ARK1 cells were cultured in RPMI (Sigma Aldrich) supplemented with 10% heat inactivated fetal bovine serum (FBS) (Sigma Aldrich) and 1% penicillin and streptomycin (Thermo Fisher Scientific). PUC198 are primary cells derived from ascites of a patient with platinum refractory high-grade endometrioid endometrial adenocarcinoma. Cells were obtained with informed consent. PUC198 were cultured in RPMI supplemented with 20% FBS and 1% penicillin and streptomycin. All cells were maintained at 37 °C in a 5% CO2 incubator. Cell line identities were confirmed by short tandem repeat profiling using the CellCheck9-Human test through IDEXX BioAnalaytics. Cell lines were confirmed mycoplasma negative with MycoAlert Mycoplasma Detection Kit (Lonza) before experiments.

4.3.6 Xenograft models *in vivo*

In vivo experiments were conducted according to Institutional Animal Care and Use Committee Policy. All animal studies were also approved and supervised by the Washington University Institutional Animal Care and Use Committee in accordance with the Animal Welfare Act, the Guide for the Care and Use of Laboratory Animals and NIH guidelines (protocol 20–0378).

ARK1 cells (1×107) were injected intraperitoneally (IP) into female (NOD) SCID mice (Jackson Laboratory) aged 6 to 8 weeks. After tumor engraftment, the mice were treated with either vehicle, 30 mg/kg AVB-500, 20 mg/kg paclitaxel, or a combination of AVB-500 and paclitaxel. Chemotherapy was delivered weekly, and AVB-500 was given every 3 days, both by IP injection. After 21 days of treatment, the mice were sacrificed, and aggregate tumor weight, volume, and number of tumor nodules were recorded for each.

PUC198 cells (5×106) were injected IP into female NSG mice (Jackson Laboratory) aged 6 to 8 weeks. After tumor engraftment, the mice were treated with either vehicle, 30 mg/kg AVB-500, 10 mg/kg paclitaxel, or a combination of 30 mg/kg AVB-500 and 10 mg/kg paclitaxel. Chemotherapy was delivered twice weekly, and AVB-500 was given every 3 days, both by IP injection. After 25 days of treatment, all mice in the vehicle and AVB-500 treatment groups were sacrificed, and three mice in each of the paclitaxel and paclitaxel + AVB-500 groups were also sacrificed. Aggregate tumor weight, volume, and number of tumor nodules were recorded for each. The remaining mice in the paclitaxel + AVB-500 group received maintenance therapy every 3 days with 30 mg/kg AVB-500. The remaining paclitaxel only mice received vehicle maintenance. After 42 days of maintenance therapy, the mice were sacrificed, the pattern of tumor progression was assessed, and tumor nodules ≥ 1 mm were quantified.

For OVCAR5 and OVCAR8 xenograft models, six-week-old female nude (nu/nu) mice (Jackson Laboratory) were used. For patient-derived xenograft (PDX) models, seven-week-old female NSG (NOD.Bg-Prkdcscid Il2rgtm1Wjl/SzJ) mice (Jackson Laboratory) were used. To establish subcutaneous cell line tumors, 1.5×106 OVCAR8 cells were implanted subcutaneously into the flank of the mouse, and the mouse was allowed to rest until tumor engraftment and growth were observed. For the subcutaneous PDX models, flash frozen PB1 or ICS051 tumors were thawed and implanted subcutaneously (previously described in Quinn et al 2019). Treatment was started when the PB1 tumor volume reached 300 mm3 and when the ICS051 tumor volume reached 2 cm3. We used different tumor sizes before beginning treatment to determine whether established, larger tumors could also respond to treatment compared to smaller tumors. Intraperitoneal tumor models were established by IP injection of 2.5×106 OVCAR5 or OVCAR8 cells. Treatment was initiated on day 14. After initiating treatment, tumors were measured every three days with calipers, and tumor volume was calculated with the equation $V= l*w*\pi/6$ (l=longest diameter, w=shortest perpendicular diameter). All mice (subcutaneous or intraperitoneal tumor models) were treated as follows: 20 mg/kg paclitaxel intraperitoneal (IP) weekly, 80 mg/kg carboplatin IP weekly, 30 mg/kg AVB-500 IP every 3 days, or 200 μL saline weekly. After 14 days of treatment mice were sacrificed two or four hours after receiving a single IP injection of 30 mg/kg AVB-500. Tumors were weighed, formalin fixed, and embedded in paraffin.

Tumor models for AVB-500 and BEV treatment were established by injecting 1 × 107 ARK1 cells intraperitoneally (IP) into 6- to 8-week-old female (NOD) SCID mice (Jackson Laboratories Bar Harbor, ME, USA). Beginning 6 days after tumor cell injections, mice were intraperitoneally injected every 3 days for 21 days with 5 mg/kg of bevacizumab (Washington

University Pharmacy), 30 mg/kg of AVB-500 (Aravive, Inc. Houston, TX, USA), or Dulbecco's Phosphate Buffered Saline (Gibco Inc. Billings, MT, USA) supplemented with magnesium chloride (MgCl2) and calcium chloride (CaCl2). Mice were sacrificed on day 27. To determine when to begin treatment, a pilot study was conducted for the ARK4 IP orthotopic tumor model. Female 6- to 8-week-old (NOD) SCID mice (n = 5) were injected with 1 × 107 ARK4 cells. The mice were sacrificed at weekly intervals, revealing that visible tumor burden was evident on day 35. Subsequently, 24 mice were injected with the same number of ARK4 cells. After 7 days, treatment began every 3 days, as described above. The mice were sacrificed on day 35. One mouse from the bevacizumab only group died two days before sacrifice (presumably due to tumor burden) and was excluded from statistical analysis.

4.4 Results

4.4.1 AXL expression correlates with reduced patient survival in both ovarian and endometrial cancer

Given the associations between tumor AXL expression and outcomes in cancer patients, we asked whether AXL expression correlated with resistance to neoadjuvant chemotherapy in ovarian cancer patients. To answer this question, we performed immunohistochemistry on matched serum and tumor samples from 38 patients before neoadjuvant paclitaxel and carboplatin. Table 1 shows the characteristics of our study population stratified by response to neoadjuvant chemotherapy on a 1–10 scale in which a score of 5 or lower was considered a good response, and a score of 6 or higher was considered a poor response (see Methods for more details). By this stratification, 24 (63.2%) of the patients had a good response to chemotherapy and 14 (36.8%) had a poor response. We assigned each tumor an AXL expression score between 0% and 100%. Consistent with previous findings, AXL expression was higher in tumors with

poor response to chemotherapy than in those with a good response to chemotherapy (72% vs 60%, P=0.04) (figure 1a).

We next measured the AXL ligand, GAS6, in serum and tumors collected before neoadjuvant chemotherapy from the same patients. In an attempt to stratify patients into high- and low-risk groups based on GAS6 levels, we explored all observed GAS6 values, identified cutoff values that minimized the P-value, and made statistical adjustments to resolve the increased false positive rate. By this method, patients were grouped into high or low serum GAS6 concentrations (>25 ng/mL vs. <15ng/mL) and high or low tumor GAS6 expression (>80% vs. <35%). Patients with high serum GAS6 concentrations had worse response to chemotherapy than those with low serum GAS6 concentrations (mean score of 5.5 vs. 3.4, P=0.023) (figure 1b). Similarly, patients with high tumor GAS6 expression had significantly worse response to chemotherapy than those with low tumor GAS6 expression (mean score of 6.3 vs 2.8, P=0.002) (figure 1b). Additionally, patients with high serum GAS6 concentrations had significantly shorter progression-free survival (7.8 months vs. 29.5 months, P=0.002) and shorter overall survival (P=0.002) than those with low serum GAS6 concentrations. Additionally, patients with high tumor GAS6 expression had shorter progression-free survival (7.8 months vs. 19.3 months, P=0.015) than those with low tumor GAS6 expression (figure 1c). Thus, high GAS6 concentrations in ovarian cancer serum and tumors before neoadjuvant chemotherapy correlated with poor response to chemotherapy, shorter progression-free survival, and shorter overall survival.

We also wanted to determine the relationship between AXL and GAS6 expression and patient survival in another gynecological cancer, endometrial cancer. We used immunohistochemistry on multiple patient tumor samples to compare protein expression. Of the

61 patients in the uterine cancer TMA, 43 (70.5%) had a good response to chemotherapy and 14 (23%) had a poor response to chemotherapy (defined progression of disease greater than or less than six months after final chemotherapy treatment, respectively). Response to chemotherapy was unknown for 4 (66.5%) patients. We found that mean GAS6 and AXL expression were significantly higher among patients with a poor response to chemotherapy than among those with a good response to chemotherapy (GAS6: 40.9% vs. 30.4%, p=0.012; AXL: 60.7% vs. 42.7%, p=0.013) (figure 2a,b, table 2). Median PFS was 33.6 months in patients with low GAS6 expressing tumors and 10.6 months among patients with high GAS6 expressing tumors (P=0.003) (figure 2c). Similarly, median OS was significantly longer in patients with low GAS6 expressing tumors compared to those with high GAS6 expressing tumors (39.5 months vs. 27.7 months, P=0.003) (figure 2d).

4.4.2 Combination AVB-500 and chemotherapy treatment reduces tumor burden in ovarian and endometrial xenograft models *in vivo*

We assessed AVB-500 in combination with chemotherapy *in vivo* first in subcutaneous mouse models. Chemo-resistant, HR-deficient cell line OVCAR8 was used as a xenograft model and chemo-resistant, HR-proficient tumor samples (PB1 or ICS051) were used for patient-derived xenograft (PDX) models. PDX tumors were surgically implanted into the flank of the mice and allowed to engraft. After the PB1 and OVCAR8 tumors reached ~300 mm^3 and the ICS051 tumors reached 2 cm^3, mice were treated with vehicle, carboplatin plus paclitaxel (chemotherapy), AVB-500 alone, or chemotherapy plus AVB-500 for 12 days. In mice that received combination treatment, tumors grew more slowly and reached lower volume and weight than mice that received chemotherapy alone (figure 3a,b,c).

To further assess the effectiveness of AVB-500 plus chemotherapy, we intraperitoneally implanted the chemo-resistant cell lines OVCAR8 or OVCAR5 into mice. After letting tumors engraft for 14 days, we treated the mice with either vehicle, carboplatin and paclitaxel (chemotherapy), AVB-500, or chemotherapy plus AVB-500 for 14 days and then assessed tumor burden. Mice that received chemotherapy plus AVB-500 had significantly fewer tumor nodules and smaller tumor mass than mice that received chemotherapy alone (figure 3d).

Both *in vivo* ovarian cancer models suggest that chemotherapy plus AVB-500 was more effective at reducing ovarian tumor cell growth than chemotherapy alone in both HR-proficient and HR-deficient cells in ovarian cancer.

We next sought to determine whether AVB-500 would improve endometrial cancer response to chemotherapy *in vivo*. To better emulate a platinum-resistant endometrial cancer clinical scenario, we treated the mice with just paclitaxel rather than carboplatin and paclitaxel. We intraperitoneally injected mice with chemo-resistant endometrial cancer cell line ARK1, allowed tumors to engraft for 7 days, then treated mice with either vehicle, AVB-500, paclitaxel, or AVB-500 and paclitaxel. We observed significantly lower tumor weight (0.025 g vs. 0.079 g, $P<0.001$), fewer tumor nodules (6.3 vs. 13.0, $P=0.007$), and smaller tumor volume (16.8 mm3 vs. 72.3 mm3, $P=0.002$) in mice treated with the combination treatment than in mice treated with paclitaxel alone (figure 4a,b,c).

We then repeated this experiment with endometrioid adenocarcinoma cell line PUC198. We injected cells intraperitoneally, allowed tumors to engraft, then treated mice with either vehicle, AVB-500, paclitaxel, or AVB-500 and paclitaxel. We observed significantly lower tumor weight and fewer tumor nodules ($\geq$ 1mm) in mice treated with AVB-500 + paclitaxel

compared to those treated with paclitaxel alone (figure 4d,e). Visually, we also observed fewer peritoneal and mesenteric small nodules (< 1mm) in the combination treated mice compared to paclitaxel alone, however there were too many nodules to quantify.

4.4.3 Combination AVB-500 and VEGF-A inhibition treatment reduces tumor burden in ovarian and endometrial xenograft models *in vivo*

Given the success in combining AVB-500 with chemotherapies *in vivo* at reducing tumor burden, we next wanted to determine if AXL inhibition can increase effectiveness to other approved treatments for gynecological cancers.

We intraperitoneally injected mice with the chemo-resistant uterine serous cancer cell lines ARK1 or ARK4. We allowed the tumors to engraft for 7 days and then treated the mice with AVB-500, bevacizumab, or a combination of both drugs. In the ARK1 model, mice treated with bevacizumab plus AVB-500 had significantly fewer tumor nodules (>1 mm) than mice treated with AVB-500 alone or bevacizumab alone (4.7 vs. 8.4, $p = 0.0245$; 4.7 vs. 9.0, $p < 0.0001$, figure 5a). Additionally, mice treated with both drugs had a smaller tumor mass (58.03 mg vs. 216.50 mg, $p = 0.0257$; 58.03 mg vs. 171.60, $p = 0.0002$, figure 5b) and a smaller tumor volume (75.1 mm3 vs. 396.6 mm3, $p = 0.0467$; 75.14 mm3 vs. 156.0 mm3, $p = 0.0080$, figure 5c). For mice injected with ARK4 cells, bevacizumab plus AVB-500 had significantly fewer tumor nodules (>1mm) than mice treated with AVB-500 alone or bevacizumab alone (4.25 vs. 12.40, $p = 0.0004$; 4.24 vs. 7.40, $p = 0.0009$, figure 5d). Additionally, mice treated with both drugs had fewer small nodules (< 1 mm) (18.25 vs. 66.80, $p < 0.0001$; 18.25 vs. 42.40, $p = 0.0003$, figure 5e), smaller tumor mass (75.93 mg vs. 424.90 mg, $p < 0.0001$; 75.93 mg vs. 182.70 mg, $p = 0.0007$, figure 5f), and smaller tumor volume than either treatment alone (47.5 mm3 vs. 338.2 mm3, $p = 0.0002$; 47.50 mm3 vs. 176.4 mm3, $p = 0.0009$, figure 5g).

We also observed that mice injected with ARK4 cells developed ascites and diaphragmatic metastases during our pilot experiment. So, we asked whether AVB-500 plus bevacizumab affected these observations. Mice treated with combination treatment were significantly less likely to develop ascites and developed smaller volumes of ascites than those treated with either drug alone (figure 5h). Likewise, mice treated with both drugs were significantly less likely to develop diaphragmatic metastases than those treated with either drug alone (figure 5h). Together, these data indicate that the combination of AVB-500 plus bevacizumab alone is more effective in reducing endometrial tumor growth *in vivo* than either drug alone.

4.5 Discussion

We observed that AXL inhibition in ovarian and endometrial cancer can improve the effectiveness of combination therapies and reduce tumor burden *in vivo.* Using this data and other data from the lab, we were able to start a clinical trial for AVB-500 in ovarian cancer patients in combination with chemotherapies in the recurrent setting. Phase 1b of AVB-500 clinical trial showed patients tolerated treatment with AVB-500 well (Fuh et al 2021). Additionally, AVB-500 treatment in addition to paclitaxel in ovarian cancer patients with platinum-resistant recurrent disease increased patient response to treatment. It was noted that patients who had not received bevacizumab before enrolling in the clinical trial had better response to the combination treatment. AVB-500 was then cleared for a phase 3 clinical trial where, despite promising results from phase 1b, there was no observed difference in survival for ovarian cancer patients treated with AVB-500 (Batiraxcept, Aravive) plus paclitaxel versus paclitaxel alone (NCT04729608). Therefore, AVB-500 is not a good target to improve patient

response to chemotherapy in ovarian cancer. AVB-500 is being investigated as a treatment in other cancer types to improve patient outcomes with much more promising results.

All of the models used to test AVB-500 effectiveness in addition to chemotherapy that we performed used xenograft mouse models, which necessitated using immunocompromised mice. Therefore, the effect of the immune system on AVB-500 treatment was not present. This may have been why we saw promising pre-clinical results but not results in patients. Had we repeated these experiments using a syngeneic model, we may have found that AVB-500 treatment did not improve response.

4.6 Conclusions

In these studies, we performed preclinical models of ovarian cancer treatment. Our goal was to increase tumor cell sensitivity to chemotherapy by the use of a small molecule inhibitor of AXL. We saw promising pre-clinical data showing AVB-500 in combination with chemotherapy and or bevacizumab reduced tumor burden in mice. This led to clinical trials which, although initially hopeful, showed that AVB-500 did not clinically improve outcomes for ovarian cancer patients. Despite this, AVB-500 may improve patient outcomes in other types of cancers and thus is worth further study.

4.7 Figures and Tables

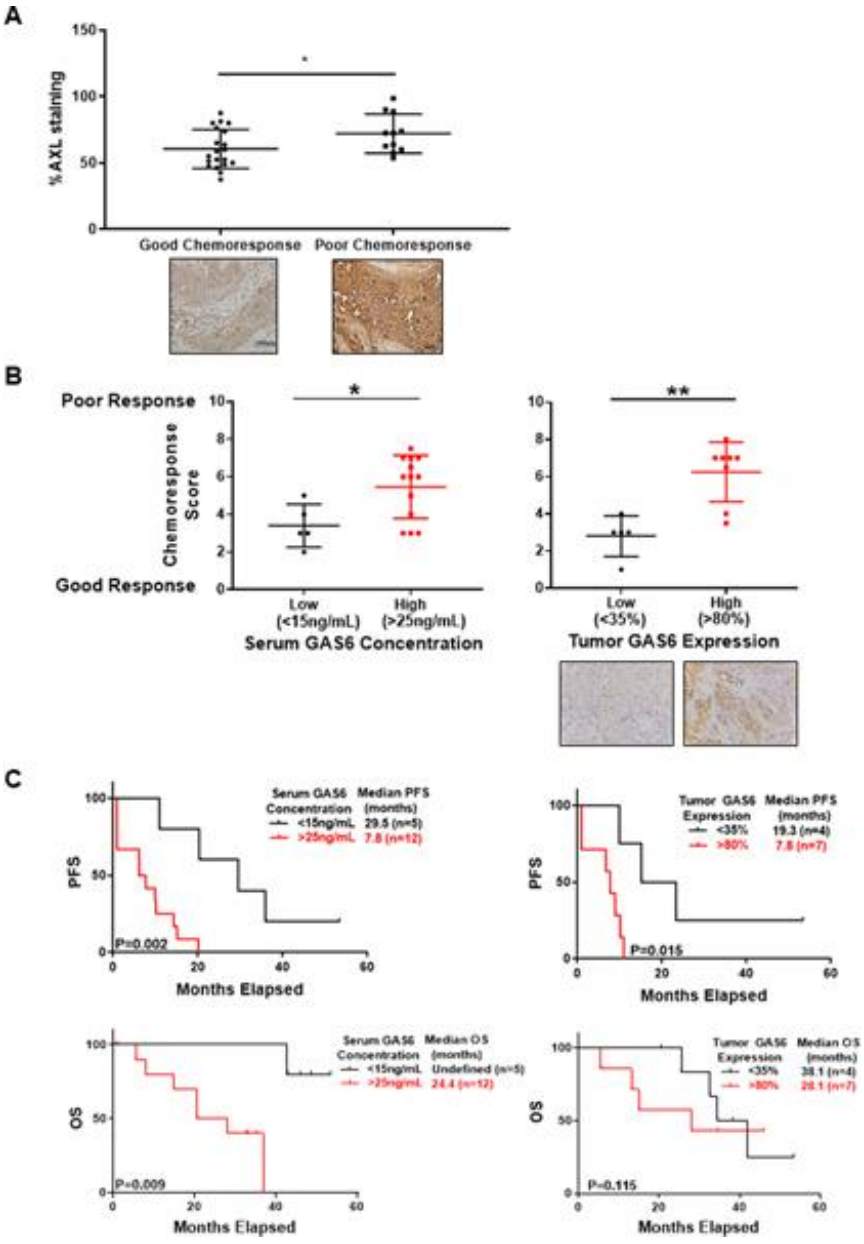

Figure 4.1: High AXL and GAS6 protein expression in patient tumors correlates with reduced survival. (A) Percent of AXL staining in tumor samples with good and poor chemo-response after neoadjuvant chemotherapy. Representative images of AXL staining in tumors before neoadjuvant chemotherapy and at time of interval cytoreductive surgery at 20X magnification. Horizontal lines indicate mean and inter-quartile range. *, $P<0.05$. (B) Mean chemo-response scores for patients with high and low serum and tumor GAS6 concentration. Chemo-response score was a composite of radiologic, surgical, and pathologic response at time of interval cytoreductive surgery. Representative images of GAS6 staining in tumors before neoadjuvant chemotherapy at 40X magnification. (C) Kaplan Meier curve evaluating progression-free

survival (PFS, top) and overall survival (OS, bottom) in patients stratified by serum (left) or tumor (right) GAS6 concentration.

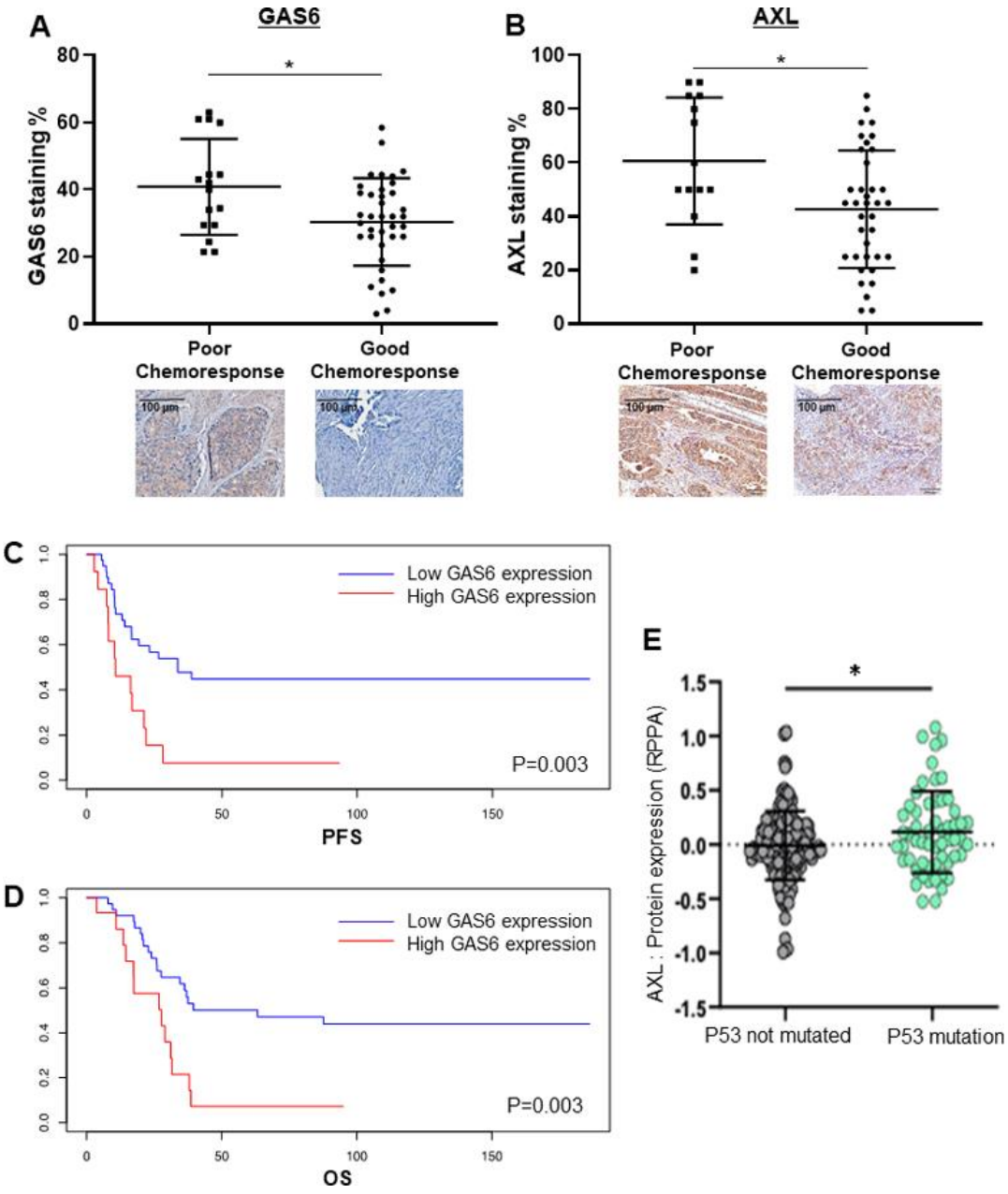

Figure 4.2: High GAS6 and AXL expression in uterine serous tumors is associated with poor response to chemotherapy. (A) Uterine serous tumors with poor response to chemotherapy are associated with higher GAS6 (40.9% vs. 30.4%, p=0.012) and (B) AXL expression (60.7% vs. 42.7%, p=0.013) than uterine serous tumors with a good response to chemotherapy by immunohistochemistry. (C, D) Low GAS6 expression (<42%) is associated with significantly improved PFS and OS compared to high GAS6 expression (≥ 42%).

Figure 3

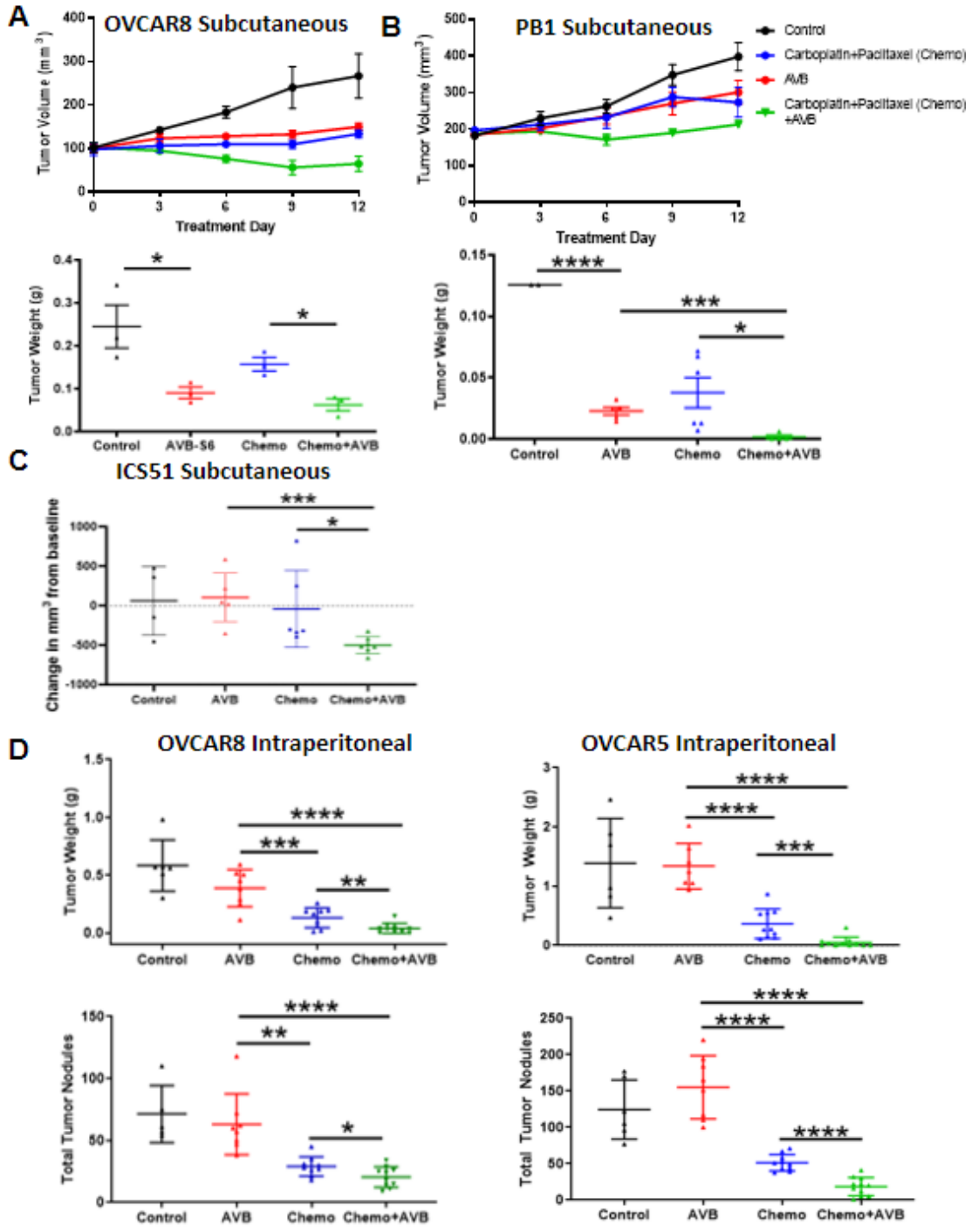

Figure 4.3: Chemotherapy and AVB-500 treatment in combination reduces xenograft mouse model tumor burden. (A) Volume of tumors over 12 days of treatment in mice engrafted subcutaneously with OVCAR8 or PB1 cells and treated with vehicle, 80mg/kg IP weekly carboplatin + 20mg/kg paclitaxel IP weekly paclitaxel (CT), 30mg/kg AVB-500, or chemotherapy and AVB-500 (CT+A). (C) Volume of tumors over 12 days of treatment in mice engrafted with IC051 tumors subcutaneously and treated with vehicle, 80mg/kg IP weekly

carboplatin + 20mg/kg paclitaxel IP weekly paclitaxel (CT), 30mg/kg AVB-500, or chemotherapy and AVB-500 (CT+A). (D) Tumor burden of mice bearing OVCAR8 or OVCAR5 tumors injected intraperitoneally as quantified by tumor weight and number of tumor nodules after treatment with vehicle, CT, AVB-500, or CT+A.

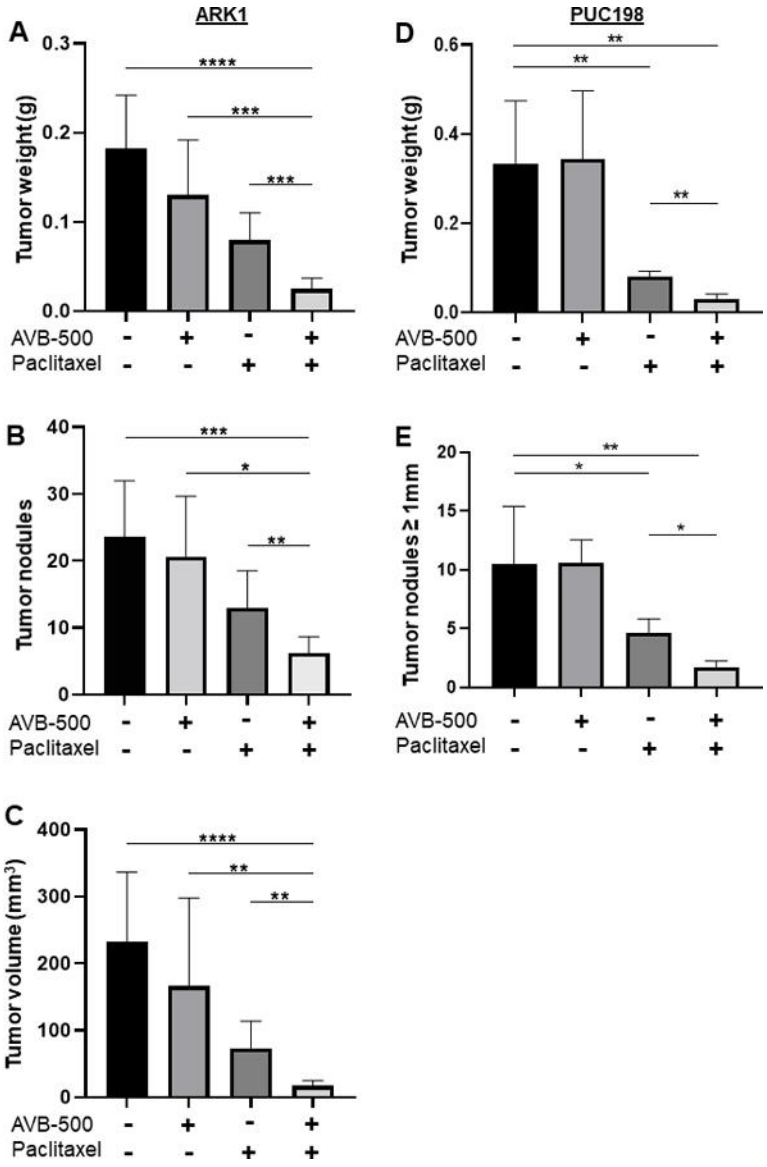

Figure 4.4: GAS6/AXL inhibition improves chemotherapy response of ARK1 and PUC198 intra-peritoneal xenograft tumors *in vivo*. (A) ARK1 total tumor weight, (B) ARK1 tumor nodules, (C) ARK1 tumor volume. (D) PUC198 total tumor weight, (E) PUC 198 tumor nodules ≥ 1mm

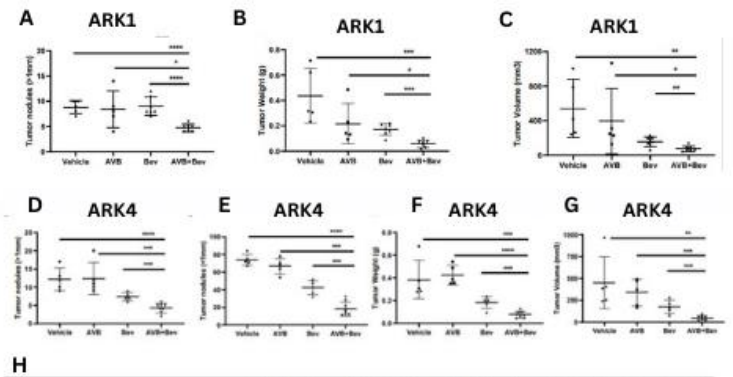

H

	Vehicle (n = 5)	AVB (n = 5)	Bev (n = 5)	AVB + Bev (n = 8)
Diaphragmatic metastases (%)	100	100	60	12.5 ***
Ascites (%)	100	100	40	12.5 ***
Mean volume ascites (μL)	620	340	24	0.625 ^^^

Figure 4.5: Inhibition of AXL and VEGF-A *in vivo*, demonstrates decreased tumor burden. Bev treatment in a USC cell line, ARK1 shows decreases in (A) tumor weight (B) tumor volume and (C) tumor nodules measured to be over 1mm in the AVB + Bev group in ARK1 injected mice. The bars indicate comparisons between each treatment condition and the AVB + Bev combination group. * $p < 0.05$, ** $p < 0.01$, *** $p < 0.001$, **** $p < 0.0001$. Dot plots showing decreases in (D) tumor weight, (E) tumor volume, (F) tumor nodules measured to be over 1 mm, and (G) tumor nodules measured to be under 1 mm in the AVB + Bev group in ARK4 injected mice. The bars indicate comparisons between each treatment condition and the AVB + Bev combination group. ** $p < 0.01$, *** $p < 0.001$, **** $p < 0.0001$. (**F**) Representative images from the *in vivo* experiment. Red circles indicate tumor burden visualized intraperitoneally. AVB + Bev mouse has tumor limited to the pelvis with no upper abdominal disease visualized. (H) Table showing the volume of ascites and diaphragmatic metastases. *** Indicates $p < 0.001$ when comparing AVB + Bev to AVB or vehicle; ^^^ Indicates $p < 0.01$ when comparing AVB + Bev to vehicle and $p < 0.05$ when comparing AVB + Bev to AVB

Table 4.1: Disease characteristics of ovarian cancer patients receiving neoadjuvant chemotherapy and undergoing interval cytoreductive surgery stratified by chemo-response. Data presented as mean and standard deviation or number (percent) (see Mullen et all 2022 for more information).

	All patients (n= 38)	Good Responders (n=24)	Poor Responders (n=14)	*P*-value*
Age (years)	64 ± 10.17	65 ± 1.6	62 ± 13.4	0.550
Primary Site				0.393
Ovary	29 (76.3)	20 (83.3)	9 (64.3)	
Fallopian Tube	5 (13.2)	2 (8.3)	3 (21.4)	
Peritoneum	4 (10.5)	2 (8.3)	2 (14.3)	
FIGO Stage				0.741
IIIB	1 (2.6)	1 (4.2)	0	
IIIC	29 (76.3)	18 (75)	11 (78.6)	
IV	8 (21.1)	4 (20.8)	3 (21.4)	
Histology				0.692
High Grade Serous	36 (94.6)	23 (95.8)	13 (92.9)	
Mixed**	2 (5.3)	1 (4.2)	1 (7.1)	
IP Chemotherapy				0.622
Yes	1 (2.6)	1 (4.2)	0	
No	37 (97.4)	23 (95.8)	14 (100)	
BRCA Mutation				0.183
No	25 (65.8)	15 (62.5)	10 (71.4)	
BRCA1	5 (13.2)	5 (20.8)	0 (0)	
BRCA2	1 (2.6)	0 (0)	1 (7.1)	
No genetic testing	7 (18.4)	4 (16.7)	3 (21.4)	
Chemoresponse Score	4.7 ± 2.4	3.6 ± 1.1	7.9 ± 1.4	<0.01
Median Follow-up*** (Months)	33 ± 14.8 (1.13-53.4)	36.1 ± 11.0 (8.0-53.4)	12.2 ± 12.6 (0-43.2)	<0.01

**P*-values compare good responders to poor responders. Except where noted, data are presented as n (%) or mean ± SD (range)
**High Grade Serous and Endometrioid Adenocarcinoma
***Calculated from time of interval cytoreductive surgery

Table 4.2: Uterine serous carcinoma tissue microarray clinical characteristics, AXL and GAS6 expression by immunohistochemistry. (A) Patient demographic, diagnosis, and treatment information. (B) Mean AXL and GAS6 expression as percentage of positive cells on immunohistochemistry stratified by chemo-response

A

Characteristics	**N(%) (n=61)**
Age, mean (SD)	64.2 (13.2)
Race n(%)	
White	41 (67.2)
Black	19 (31.1)
Hispanic	0 (0)
Asian	0 (0)
Other	1 (1.7)
FIGO stage, n(%)	
I	19 (31.1)
II	3 (4.9)
III	18 (29.5)
IV	21 (34.4)
Chemotherapy received, n(%)	
carboplatin + paclitaxel	56 (91.8)
other	5 (8.2)
Chemo-response, n(%)	
Good	43 (70.5)
Poor	14 (23.0)
Unknown	4 (6.6)
Adjuvant radiation n(%)	14 (23.0)

B

	Good chemo-response (n=43)	**Poor chemo-response (n=14)**
IHC AXL expression (%), mean (SD)	42.7 (21.9)	60.7 (23.7)
IHC GAS6 expression (%), mean	30.4 (13.1)	40.9 (14.3)

Chapter 5: Conclusions and Future Directions

My initial goal in this dissertation work was to understand the role of DDR2 in ovarian cancer and then more specifically to the role of DDR2 in acquired chemo-resistance. I hypothesized that DDR2 would play a crucial role in the development of resistance to chemotherapy. I also created a novel cell line that fills a need in the ovarian cancer chemo-resistance research body of knowledge.

In Chapter 2, I created a set of novel, syngeneic cell lines with increasing levels of resistance to chemotherapy (carboplatin and paclitaxel). I aimed to create a final cell line derived from mouse ovarian cancer cells that is significantly more resistant to chemotherapy than the parental ID8PBGL cells. The creation of these cells was performed with serial passaging of cells through mice and treating with increasing doses of chemotherapy. I successfully created 5 cell lines from chemo-naïve cells derived from ascites of ID8PBGL injected mice (CNAS) to CHRP5 cells that were more resistant to chemotherapy. I characterized these cell lines for their sensitivity to chemotherapy and the changes in gene expression between CHRP1 (first passage treated with chemotherapy) and CHRP5 (final, chemo-resistant cells). These cells fill a need in the field of chemo-resistance research in ovarian cancer of matched chemo-sensitive and chemo-resistant mouse ovarian cancer cells.

Given more time, I would have liked to continue to passage these cells with increasing doses until the maximum 40mg/kg of carboplatin and 10mg/kg paclitaxel which is our standard chemotherapy dose used in other mouse models. Using whole exome RNA sequencing, I

discovered many genes that are significantly differentially expressed between matched chemo-sensitive and chemo-resistant tumors. Further investigation of gene targets identified in RNA sequencing may give insight into pathways that are being dysregulated as cells gain resistance. Additionally, sequencing of the other, less resistant lines CHRP1,2,3, and 4 would give insight into more specifically when genes are upregulated in the process of acquired chemoresistance. Ideally, it would be useful to use a CRISPR knockout screen to investigate all the top overexpressed genes in the CHRP5 cells using either colony formation assays or MTS survival assays treating cells with chemotherapy. This would allow us to quickly identify genes where upregulation is contributing to cancer cell sensitivity to chemotherapy. I would then take any genes that were identified in the screen and use protein expression assays such as ELISA or western blots to confirm that overexpression of mRNA correlates with overexpression of the corresponding proteins. This process would help us identify genes that are regulators of resistance in ovarian cancer and can be further investigated as a potential target for novel therapies.

As one of the goals of this study was to further our understanding of acquired chemo-resistance, it would also be interesting to investigate resistance to other therapy agents. I would treat the CHRP cells with other agents such as BEV, PARP inhibitors, or PD-1 inhibitors to determine if CHPR5 cells are also more resistant to other therapies than our CNAS cells. This could give insight into mechanisms of chemoresistance that can protect against multiple forms of therapies. This may lead to treatments that can overcome multi-drug resistance. Following this logic, it would also be interesting to repeat the process of creating resistant cell lines using different therapies. Then similar methods of characterizing cells and investigating differential expression could be used to identify key genes in resistance to multiple therapies.

Through many experiments in Chapter 3, we have shown that DDR2 expression in ovarian cancer tumor cells does not influence resistance to chemotherapy. We have shown that DDR2 expression *in vitro* does not significantly alter sensitivity to chemotherapies via MTS assays for knockdown DDR2 and wild type DDR2 CHRP5 cells. Additionally, we have shown that neither genetic knockdown nor pharmacological inhibition of DDR2 reduces tumor burden *in vivo* using a number of different ovarian cancer cell lines both human and mouse.

This study did have some limitations. Our initial knockdown of DDR2 in the ID8 cells was not very efficient and did not have a selectable marker to sort cells for plasmid expression. The experiments done with these cells, such as the *in vivo* CR13452 experiment could be repeated on ID8PBGL cells that have a true DDR2 knockdown.

As we have learned that DDR2 does not influence chemo-resistance, future experiments could investigate why we see patient overexpression of DDR2 is correlated with reduced sensitivity to chemotherapies. This could be an artifact of dysregulation of another pathway upstream of DDR2 leading to expression changes. The ECM and collagen play a large role in the tumor microenvironment, so in a chemo-resistant setting, it could be that ECM remodeling due to other mechanisms could be signaling to increase DDR2 expression in response to collagen dysregulation and not because DDR2 is regulating chemo-resistance. by DDR2 may cause the overexpression of DDR2 seen in patients. Previous work in the lab showed that DDR2 expression in tumor cells is critical for metastasis by regulation by TWIST1 and stabilization of SNAIL1 (Grither et al 2018). So, DDR2 overexpression may be from the role of DDR2 in metastasis which in turn leads to patient death rather than its involvement in acquired chemo-resistance. Additionally, others in the lab have found that DDR2 expression in stromal cells such as cancer-associated fibroblasts and mesothelial cells is more predictive of reduced survival than

DDR2 tumor expression (Schab et al 2023). Therefore, it would be interesting to knockdown DDR2 in stromal cells and co-culture with wild type CHRP5 or CNAS cells to perform survival assays. Following that logic, it would also be beneficial to perform co-culture experiments with knockdown DDR2 in both stromal and tumor cells and compare to knockdown of DDR2 in one or neither of the cell types. This could show us if stromal DDR2 expression is involved in resistance to chemotherapy.

In Chapter 4 our goal was to use pre-clinical models to test the effectiveness of small molecule inhibitor AVB-500 at increasing tumor response to chemotherapy. AVB-500 inhibits receptor tyrosine kinase AXL by preferentially binding to the ligand of AXL, GAS6, preventing it from binding to the AXL receptor. We determined that AVB-500 treatment in addition to chemotherapies resulted in less tumor burden than chemotherapy alone using ovarian cancer xenograft and PDX ovarian cancer in preclinical mouse models. Additionally, we saw that AVB-500 in addition to bevacizumab treatment reduced disease burden in mice injected with ARK1 and ARK4 uterine serous cancer cells.

We saw promising pre-clinical data showing AVB-500 in combination with chemotherapy and or bevacizumab reduced tumor burden in mice. This led to clinical trials which, although initially hopeful, showed that AVB-500 did not clinically improve outcomes for ovarian cancer patients. Despite this, AVB-500 has been shown to be clinically successful in other cancer types. (Kanlikilicer et al 2017).

A potential limitation is all the models used above were human xenograft models using immunocompromised mice. Immune cells can express AXL and AXL has been shown to be a regulator of the innate immune system (Engelsen et al 2022). Therefore, by using only xenograft

mouse models, we missed the impact of immune cells on AXL expression, which may be why AVB-500 did not show significant increase of patient survival in clinical trials.

Therefore, I would use the same experimental design as above but using the CNAS and CHRP5 cells I developed earlier in C57/BL6 mice. Then, we could observe the effects of combination chemotherapy and AVB-500 treatment with an intact immune system. This may have shown us pre-clinically that AVB may not increase patient survival. As beneficial as mouse models are, they do not perfectly replicate the tumor microenvironment and thus are not always predictive of clinical success.

Overall, this work contributes to the understanding of chemo-resistance in ovarian cancer by removing DDR2 from the list of genes involved in acquired chemo-resistance in ovarian cancer and identifying novel targets for further study. Additionally, the novel cell lines are a valuable tool for further understanding of acquired chemo-resistance as they are matched chemo-sensitive to chemo-resistant and can be used syngeneically. Lastly, despite promising results observed in pre-clinical mouse models, we saw that AVB-500 did not extend ovarian cancer patient survival.

References

Integrated genomic analyses of ovarian carcinoma. (2011). *Nature, 474*(7353), 609-615. doi:10.1038/nature10166

Acerbi, I., Cassereau, L., Dean, I., Shi, Q., Au, A., Park, C., . . . Weaver, V. M. (2015). Human breast cancer invasion and aggression correlates with ECM stiffening and immune cell infiltration. *Integr Biol (Camb), 7*(10), 1120-1134. doi:10.1039/c5ib00040h

Ai, L., Chen, J., Yan, H., He, Q., Luo, P. A.-O., Xu, Z. A.-O. X., & Yang, X. Research Status and Outlook of PD-1/PD-L1 Inhibitors for Cancer Therapy. (1177-8881 (Electronic)).

Alatise, K. L., Gardner, S., & Alexander-Bryant, A. Mechanisms of Drug Resistance in Ovarian Cancer and Associated Gene Targets. LID - 10.3390/cancers14246246 [doi] LID - 6246. (2072-6694 (Print)).

Ali, B. R., Xu, H., Akawi, N. A., John, A., Karuvantevida, N. S., Langer, R., . . . Leitinger, B. (2010). Trafficking defects and loss of ligand binding are the underlying causes of all reported DDR2 missense mutations found in SMED-SL patients. *Human Molecular Genetics, 19*(11), 2239-2250. doi:10.1093/hmg/ddq103

Antoniou, A., Pharoah, P. D. P., Narod, S., Risch, H. A., Eyfjord, J. E., Hopper, J. L., . . . Easton, D. F. (2003). Average risks of breast and ovarian cancer associated with BRCA1 or BRCA2 mutations detected in case Series unselected for family history: a combined analysis of 22 studies. *American journal of human genetics, 72*(5), 1117-1130. doi:10.1086/375033

Ashour, M., & Ezzat Shafik, H. (2019). Frequency of germline mutations in BRCA1 and BRCA2 in ovarian cancer patients and their effect on treatment outcome. *Cancer Manag Res, 11*, 6275-6284. doi:10.2147/CMAR.S206817

Au-Yeung, G., Lang, F., Azar, W. J., Mitchell, C., Jarman, K. E., Lackovic, K., . . . Bowtell, D. D. (2017). Selective Targeting of Cyclin E1-Amplified High-Grade Serous Ovarian Cancer by Cyclin-Dependent Kinase 2 and AKT Inhibition. *Clin Cancer Res, 23*(7), 1862-1874. doi:10.1158/1078-0432.CCR-16-0620

Bayer, S. V., Grither, W. R., Brenot, A., Hwang, P. Y., Barcus, C. E., Ernst, M., . . . Longmore, G. D. (2019). DDR2 controls breast tumor stiffness and metastasis by regulating integrin mediated mechanotransduction in CAFs. *eLife, 8*. doi:10.7554/eLife.45508

Bayer, S. V. H., Grither, W. R., Brenot, A., Hwang, P. Y., Barcus, C. E., Ernst, M., . . . Longmore, G. D. (2019). DDR2 controls breast tumor stiffness and metastasis by regulating integrin mediated mechanotransduction in CAFs. *eLife, 8*. doi:10.7554/eLife.45508

Beauchamp, E. M., Woods, B. A., Dulak, A. M., Tan, L., Xu, C., Gray, N. S., . . . Hammerman, P. S. (2014). Acquired resistance to dasatinib in lung cancer cell lines conferred by DDR2 gatekeeper mutation and NF1 loss. *Mol Cancer Ther, 13*(2), 475-482. doi:10.1158/1535-7163.MCT-13-0817

Beaufort, C. M., Helmijr, J. C., Piskorz, A. M., Hoogstraat, M., Ruigrok-Ritstier, K., Besselink, N., . . . Helleman, J. (2014). Ovarian cancer cell line panel (OCCP): clinical importance of in vitro morphological subtypes. *Plos One, 9*(9), e103988. doi:10.1371/journal.pone.0103988

Bodelon, C., Killian, J. K., Sampson, J. N., Anderson, W. F., Matsuno, R., Brinton, L. A., . . . Wentzensen, N. (2019). Molecular Classification of Epithelial Ovarian Cancer Based on Methylation Profiling: Evidence for Survival Heterogeneity. *Clin Cancer Res, 25*(19), 5937-5946. doi:10.1158/1078-0432.CCR-18-3720

Böhm, S., Faruqi, A., Said, I., Lockley, M., Brockbank, E., Jeyarajah, A., . . . Singh, N. Chemotherapy Response Score: Development and Validation of a System to Quantify Histopathologic Response to Neoadjuvant Chemotherapy in Tubo-Ovarian High-Grade Serous Carcinoma. (1527-7755 (Electronic)).

Boraschi-Diaz, I., Wang, J., Mort, J. S., & Komarova, S. V. (2017). Collagen Type I as a Ligand for Receptor-Mediated Signaling. *Frontiers in Physics, 5*. doi:10.3389/fphy.2017.00012

Buehler, M., Tse B Fau - Leboucq, A., Leboucq A Fau - Jacob, F., Jacob F Fau - Caduff, R., Caduff R Fau - Fink, D., Fink D Fau - Goldstein, D. R., . . . Heinzelmann-Schwarz, V. Meta-analysis of microarray data identifies GAS6 expression as an independent predictor of poor survival in ovarian cancer. (2314-6141 (Electronic)).

Cai, S.-Y., Yang, T., Chen, Y., Wang, J.-W., Li, L., & Xu, M.-J. (2015). Gene expression profiling of ovarian carcinomas and prognostic analysis of outcome. *Journal of Ovarian Research, 8*(1). doi:10.1186/s13048-015-0176-9

Cancer Genome Atlas Research, N., Kandoth, C., Schultz, N., Cherniack, A. D., Akbani, R., Liu, Y., . . . Levine, D. A. (2013). Integrated genomic characterization of endometrial carcinoma. *Nature, 497*(7447), 67-73. doi:10.1038/nature12113

Chalmers, Z. R., Connelly, C. F., Fabrizio, D., Gay, L., Ali, S. M., Ennis, R., . . . Frampton, G. M. (2017). Analysis of 100,000 human cancer genomes reveals the landscape of tumor mutational burden. *Genome Medicine, 9*(1). doi:10.1186/s13073-017-0424-2

Chen, W., Zhang, Z., Zhang, S., Zhu, P., Ko, J. K., & Yung, K. K. MUC1: Structure, Function, and Clinic Application in Epithelial Cancers. LID - 10.3390/ijms22126567 [doi] LID - 6567. (1422-0067 (Electronic)).

Cho, K. R., & Shih, I.-M. (2009). Ovarian Cancer. *Annual Review of Pathology: Mechanisms of Disease, 4*(1), 287-313. doi:10.1146/annurev.pathol.4.110807.092246

Ciriello, G., Miller, M. L., Aksoy, B. A., Senbabaoglu, Y., Schultz, N., & Sander, C. (2013). Emerging landscape of oncogenic signatures across human cancers. *Nature Genetics, 45*(10), 1127-1133. doi:10.1038/ng.2762

Cole, A. J., Dwight, T., Gill, A. J., Dickson, K. A., Zhu, Y., Clarkson, A., . . . Marsh, D. J. (2016). Assessing mutant p53 in primary high-grade serous ovarian cancer using immunohistochemistry and massively parallel sequencing. *Sci Rep, 6*, 26191. doi:10.1038/srep26191

Cooke, S. L., Ng, C. K. Y., Melnyk, N., Garcia, M. J., Hardcastle, T., Temple, J., . . . Brenton, J. D. (2010). Genomic analysis of genetic heterogeneity and evolution in high-grade serous ovarian carcinoma. *Oncogene, 29*(35), 4905-4913. doi:10.1038/onc.2010.245

Corsa, Callie A. S., Brenot, A., Grither, Whitney R., Van Hove, S., Loza, Andrew J., Zhang, K., . . . Longmore, Gregory D. (2016). The Action of Discoidin Domain Receptor 2 in Basal Tumor Cells and Stromal Cancer-Associated Fibroblasts Is Critical for Breast Cancer Metastasis. *Cell Reports, 15*(11), 2510-2523. doi:10.1016/j.celrep.2016.05.033

Damia, G., & Broggini, M. A.-O. Platinum Resistance in Ovarian Cancer: Role of DNA Repair. LID - 10.3390/cancers11010119 [doi] LID - 119. (2072-6694 (Print)).

Divine, L. M., Nguyen, M. R., Meller, E., Desai, R. A., Arif, B., Rankin, E. B., . . . Fuh, K. C. AXL modulates extracellular matrix protein expression and is essential for invasion and metastasis in endometrial cancer. (1949-2553 (Electronic)).

Dizon, D. S. (2017). PARP inhibitors for targeted treatment in ovarian cancer. *The Lancet, 390*(10106), 1929-1930. doi:10.1016/s0140-6736(17)32418-2

Domcke, S., Sinha, R., Levine, D. A., Sander, C., & Schultz, N. (2013). Evaluating cell lines as tumour models by comparison of genomic profiles. *Nat Commun, 4*, 2126. doi:10.1038/ncomms3126

Du, Z., & Lovly, C. M. (2018). Mechanisms of receptor tyrosine kinase activation in cancer. *Molecular Cancer, 17*(1). doi:10.1186/s12943-018-0782-4

Elias, K. M., Emori, M. M., Papp, E., MacDuffie, E., Konecny, G. E., Velculescu, V. E., & Drapkin, R. (2015). Beyond genomics: Critical evaluation of cell line utility for ovarian cancer research. *Gynecologic Oncology, 139*(1), 97-103. doi:10.1016/j.ygyno.2015.08.017

Englesen, A. S. T., Lotsberg, M. L., Khouzam, R. A., Thierym J., Lorens J. B., Chouaib S., Terry S. (2022). Dissecting the Role of AXL in Cancer Immune Escape and Resistance to Immmune Checkpoint Inhibnition. *Front Immunol*. 2022 Apr 27;13:869676. doi: 10.3389/fimmu.2022.869676. PMID: 35572601; PMCID: PMC9092944.

England, C. G., Ehlerding, E. B., Hernandez, R., Rekoske, B. T., Graves, S. A., Sun, H., . . . Cai, W. (2017). Preclinical Pharmacokinetics and Biodistribution Studies of 89Zr-Labeled Pembrolizumab. *Journal of Nuclear Medicine, 58*(1), 162-168. doi:10.2967/jnumed.116.177857

Fan, Y., Xu, Z., Fan, J., Huang, L., Ye, M., Shi, K., . . . Li, Q. (2016). Prognostic significance of discoidin domain receptor 2 (DDR2) expression in ovarian cancer. *American journal of translational research, 8*(6), 2845-2850.

Figueroa-Gonzalez, G., & Perez-Plasencia, C. (2017). Strategies for the evaluation of DNA damage and repair mechanisms in cancer. *Oncol Lett, 13*(6), 3982-3988. doi:10.3892/ol.2017.6002

Fodale, V., Pierobon, M., Liotta, L., & Petricoin, E. (2011). Mechanism of cell adaptation: when and how do cancer cells develop chemoresistance? *Cancer J, 17*(2), 89-95. doi:10.1097/PPO.0b013e318212dd3d

Fuh, K. C., Bookman, M. A., Liu, J. F., Coleman, R. L., Herzog, T. J., Thaker, P. H., . . . Moore, K. N. Phase 1b study of AVB-500 in combination with paclitaxel or pegylated liposomal doxorubicin platinum-resistant recurrent ovarian cancer. (1095-6859 (Electronic)).

Fuh, K et al. Batiraxcept (AVB-S6-500)/Placebo in Combination With Paclitaxel in Patients With Platinum-Resistant Recurrent Ovarian Cancer (AXLerate-OC). ClincalTrials.gov identifier: NCT04729608. Updated 10-30-2023. Accessed 3-12-2024. https://clinicaltrials.gov/study/NCT04729608

Fuller, E. S., & Howell, V. M. (2014). Culture models to define key mediators of cancer matrix remodeling. *Front Oncol, 4*, 57. doi:10.3389/fonc.2014.00057

Galli, A., Harter, P., Hauke, J., Heitz, F., Reuss, A., Kommoss, S., . . . Schmutzler, R. (2017). Prevalence of deleterious germline variants in risk genes including BRCA1/2 in consecutive ovarian cancer patients (AGO-TR-1). *Plos One, 12*(10). doi:10.1371/journal.pone.0186043

Garziera, M., Roncato, R., Montico, M., De Mattia, E., Gagno, S., Poletto, E., . . . Toffoli, G. (2019). New Challenges in Tumor Mutation Heterogeneity in Advanced Ovarian Cancer

by a Targeted Next-Generation Sequencing (NGS) Approach. *Cells, 8*(6). doi:10.3390/cells8060584
George, E., Kim, H., Krepler, C., Wenz, B., Makvandi, M., Tanyi, J. L., . . . Simpkins, F. (2017). A patient-derived-xenograft platform to study BRCA-deficient ovarian cancers. *JCI Insight, 2*(1). doi:10.1172/jci.insight.89760
Goltsev, Y., Samusik, N., Kennedy-Darling, J., Bhate, S., Hale, M., Vazquez, G., . . . Nolan, G. P. (2018). Deep Profiling of Mouse Splenic Architecture with CODEX Multiplexed Imaging. *Cell, 174*(4), 968-981.e915. doi:10.1016/j.cell.2018.07.010
Gonzalez, M. E., Martin, E. E., Anwar, T., Arellano-Garcia, C., Medhora, N., Lama, A., . . . Kleer, C. G. (2017). Mesenchymal Stem Cell-Induced DDR2 Mediates Stromal-Breast Cancer Interactions and Metastasis Growth. *Cell Rep, 18*(5), 1215-1228. doi:10.1016/j.celrep.2016.12.079
Gorringe, K. L., & Campbell, I. G. (2009). Large-scale genomic analysis of ovarian carcinomas. *Molecular Oncology, 3*(2), 157-164. doi:10.1016/j.molonc.2008.12.005
Grither, W. R., & Longmore, G. D. (2018). Inhibition of tumor–microenvironment interaction and tumor invasion by small-molecule allosteric inhibitor of DDR2 extracellular domain. *Proceedings of the National Academy of Sciences, 115*(33), E7786-E7794. doi:10.1073/pnas.1805020115
Haley, J., Tomar, S., Pulliam, N., Xiong, S., Perkins, S. M., Karpf, A. R., . . . Mitra, A. K. (2016). Functional characterization of a panel of high-grade serous ovarian cancer cell lines as representative experimental models of the disease. *Oncotarget, 7*(22), 32810-32820. doi:10.18632/oncotarget.9053
Hanahan, D., & Weinberg, Robert A. (2011). Hallmarks of Cancer: The Next Generation. *Cell, 144*(5), 646-674. doi:10.1016/j.cell.2011.02.013
Harrach, S., & Ciarimboli, G. Role of transporters in the distribution of platinum-based drugs. (1663-9812 (Print)).
Hasan, S., Taha, R., & Omri, H. E. (2018). Current Opinions on Chemoresistance: An Overview. *Bioinformation, 14*(2), 80-85. doi:10.6026/97320630014080
Henriet, E., Sala, M., Abou Hammoud, A., Tuariihionoa, A., Di Martino, J., Ros, M., & Saltel, F. (2018). Multitasking discoidin domain receptors are involved in several and specific hallmarks of cancer. *Cell Adhesion & Migration*, 1-15. doi:10.1080/19336918.2018.1465156
Heo, E. J., Cho, Y. J., Cho, W. C., Hong, J. E., Jeon, H.-K., Oh, D.-Y., . . . Lee, J.-W. (2017). Patient-Derived Xenograft Models of Epithelial Ovarian Cancer for Preclinical Studies. *Cancer research and treatment : official journal of Korean Cancer Association, 49*(4), 915-926. doi:10.4143/crt.2016.322
Hilliard, T. S. The Impact of Mesothelin in the Ovarian Cancer Tumor Microenvironment. LID - 10.3390/cancers10090277 [doi] LID - 277. (2072-6694 (Print)).
Hillman, R. T., Chisholm, G. B., Lu, K. H., & Futreal, P. A. (2018). Genomic Rearrangement Signatures and Clinical Outcomes in High-Grade Serous Ovarian Cancer. *J Natl Cancer Inst, 110*(3). doi:10.1093/jnci/djx176
Ho, S. M. Estrogen, progesterone and epithelial ovarian cancer. (1477-7827 (Electronic)).
Hosoya, N., & Miyagawa, K. (2014). Targeting DNA damage response in cancer therapy. *Cancer Science, 105*(4), 370-388. doi:10.1111/cas.12366
Hou, D., Xu, G., Zhang, C., Li, B., Qin, J., Hao, X., . . . Shao, C. (2017). Berberine induces oxidative DNA damage and impairs homologous recombination repair in ovarian cancer

cells to confer increased sensitivity to PARP inhibition. *Cell Death Dis, 8*(10), e3070. doi:10.1038/cddis.2017.471
Hu, X., Meng, Y., Xu, L., Qiu, L., Wei, M., Su, D., . . . Han, J. (2019). Cul4 E3 ubiquitin ligase regulates ovarian cancer drug resistance by targeting the antiapoptotic protein BIRC3. *Cell Death Dis, 10*(2), 104. doi:10.1038/s41419-018-1200-y
Jiang, Y. A.-O., Zhang, H., Wang, J., Liu, Y., Luo, T., & Hua, H. Targeting extracellular matrix stiffness and mechanotransducers to improve cancer therapy. (1756-8722 (Electronic)).
Jordan, K. R., Sikora, M. A.-O., Slansky, J. A.-O., Minic, A., Richer, J. K., Moroney, M. R., . . . Bitler, B. A.-O. The Capacity of the Ovarian Cancer Tumor Microenvironment to Integrate Inflammation Signaling Conveys a Shorter Disease-free Interval. (1557-3265 (Electronic)).
Kampan, N. C., Madondo, M. T., McNally, O. M., Quinn, M., & Plebanski, M. Paclitaxel and Its Evolving Role in the Management of Ovarian Cancer. (2314-6141 (Electronic)).
Kanchi, K. L., Johnson, K. J., Lu, C., McLellan, M. D., Leiserson, M. D., Wendl, M. C., . . . Ding, L. (2014). Integrated analysis of germline and somatic variants in ovarian cancer. *Nat Commun, 5*, 3156. doi:10.1038/ncomms4156
Kanlikilicer, P., Ozpolat, B., Aslan, B., Bayraktar, R., Gurbuz, N., Rodriguez-Aguayo, C., . . . Lopez-Berestein, G. Therapeutic Targeting of AXL Receptor Tyrosine Kinase Inhibits Tumor Growth and Intraperitoneal Metastasis in Ovarian Cancer Models. (2162-2531 (Print)).
Kim, H., George, E., Ragland, R. L., Rafail, S., Zhang, R., Krepler, C., . . . Simpkins, F. (2017). Targeting the ATR/CHK1 Axis with PARP Inhibition Results in Tumor Regression in BRCA-Mutant Ovarian Cancer Models. *Clinical Cancer Research, 23*(12), 3097-3108. doi:10.1158/1078-0432.Ccr-16-2273
Kotsopoulos, J., Gronwald, J., Karlan, B., Rosen, B., Huzarski, T., Moller, P., . . . Narod, S. A. (2018). Age-specific ovarian cancer risks among women with a BRCA1 or BRCA2 mutation. *Gynecologic Oncology, 150*(1), 85-91. doi:https://doi.org/10.1016/j.ygyno.2018.05.011
Kroeger, P. T., Jr., & Drapkin, R. (2017). Pathogenesis and heterogeneity of ovarian cancer. *Curr Opin Obstet Gynecol, 29*(1), 26-34. doi:10.1097/GCO.0000000000000340
Kumar, A., Dutta Choudhury, M., Ghosh, P., & Palit, P. (2019). Discoidin domain receptor 2: An emerging pharmacological drug target for prospective therapy against osteoarthritis. *Pharmacol Rep, 71*(3), 399-408. doi:10.1016/j.pharep.2019.01.007
Kurnit, K. C., Fleming Gf Fau - Lengyel, E., & Lengyel, E. Updates and New Options in Advanced Epithelial Ovarian Cancer Treatment. (1873-233X (Electronic)).
Labidi-Galy, S. I., Papp, E., Hallberg, D., Niknafs, N., Adleff, V., Noe, M., . . . Velculescu, V. E. (2017). High grade serous ovarian carcinomas originate in the fallopian tube. *Nat Commun, 8*(1), 1093. doi:10.1038/s41467-017-00962-1
Leitinger, B. (2014). Discoidin domain receptor functions in physiological and pathological conditions. *Int Rev Cell Mol Biol, 310*, 39-87. doi:10.1016/B978-0-12-800180-6.00002-5
Lengyel, E. (2010). Ovarian Cancer Development and Metastasis. *The American Journal of Pathology, 177*(3), 1053-1064. doi:10.2353/ajpath.2010.100105
Lew, E. D., Oh, J., Burrola, P. G., Lax, I., Zagórska, A., Través, P. A.-O., . . . Lemke, G. Differential TAM receptor-ligand-phospholipid interactions delimit differential TAM bioactivities. LID - 10.7554/eLife.03385 [doi] LID - e03385. (2050-084X (Electronic)).

Liu, J. F., Palakurthi, S., Zeng, Q., Zhou, S., Ivanova, E., Huang, W., . . . Drapkin, R. (2017). Establishment of Patient-Derived Tumor Xenograft Models of Epithelial Ovarian Cancer for Preclinical Evaluation of Novel Therapeutics. *Clin Cancer Res, 23*(5), 1263-1273. doi:10.1158/1078-0432.CCR-16-1237

Lu, P., Takai, K., Weaver, V. M., & Werb, Z. (2011). Extracellular matrix degradation and remodeling in development and disease. *Cold Spring Harb Perspect Biol, 3*(12). doi:10.1101/cshperspect.a005058

Ma, R.-q., Tang, Z.-j., Ye, X., Cheng, H.-y., Sun, K.-k., Chang, X.-h., & Cui, H. (2018). Overexpression of GPNMB predicts an unfavorable outcome of epithelial ovarian cancer. *Archives of Gynecology and Obstetrics, 297*(5), 1235-1244. doi:10.1007/s00404-018-4699-3

Ma, Y., Vassetzky, Y., & Dokudovskaya, S. (2018). mTORC1 pathway in DNA damage response. *Biochim Biophys Acta Mol Cell Res, 1865*(9), 1293-1311. doi:10.1016/j.bbamcr.2018.06.011

Macintyre, G., Goranova, T. E., De Silva, D., Ennis, D., Piskorz, A. M., Eldridge, M., . . . Brenton, J. D. (2018). Copy number signatures and mutational processes in ovarian carcinoma. *Nature Genetics, 50*(9), 1262-1270. doi:10.1038/s41588-018-0179-8

Marth, C. A.-O., Abreu, M. H., Andersen, K. K., Aro, K. M., de Lurdes Batarda, M., Boll, D., . . . Schnack, T. H. Real-life data on treatment and outcomes in advanced ovarian cancer: An observational, multinational cohort study (RESPONSE trial). (1097-0142 (Electronic)).

Martin, L. P., Hamilton Tc Fau - Schilder, R. J., & Schilder, R. J. Platinum resistance: the role of DNA repair pathways. (1078-0432 (Print)).

McLaughlin, J. R., Rosen, B., Moody, J., Pal, T., Fan, I., Shaw, P. A., . . . Narod, S. A. (2013). Long-Term Ovarian Cancer Survival Associated With Mutation in BRCA1 or BRCA2. *JNCI: Journal of the National Cancer Institute, 105*(2), 141-148. doi:10.1093/jnci/djs494

Menghi, F., Barthel, F. P., Yadav, V., Tang, M., Ji, B., Tang, Z., . . . Liu, E. T. (2018). The Tandem Duplicator Phenotype Is a Prevalent Genome-Wide Cancer Configuration Driven by Distinct Gene Mutations. *Cancer Cell, 34*(2), 197-210 e195. doi:10.1016/j.ccell.2018.06.008

Mirza, M. R., Monk, B. J., Herrstedt, J., Oza, A. M., Mahner, S., Redondo, A., . . . Matulonis, U. A. Niraparib Maintenance Therapy in Platinum-Sensitive, Recurrent Ovarian Cancer. (1533-4406 (Electronic)).

Mitra, A. K., Davis, D. A., Tomar, S., Roy, L., Gurler, H., Xie, J., . . . Burdette, J. E. (2015). In vivo tumor growth of high-grade serous ovarian cancer cell lines. *Gynecologic Oncology, 138*(2), 372-377. doi:10.1016/j.ygyno.2015.05.040

Mylavarapu, S., Das, A., & Roy, M. Role of BRCA Mutations in the Modulation of Response to Platinum Therapy. (2234-943X (Print)).

Palisoul, M. L., Quinn, J. M., Schepers, E., Hagemann, I. S., Guo, L., Reger, K., . . . Fuh, K. C. Inhibition of the Receptor Tyrosine Kinase AXL Restores Paclitaxel Chemosensitivity in Uterine Serous Cancer. (1538-8514 (Electronic)).

Paragh, G., Kumar, S. M., Rakosy, Z., Choi, S. C., Xu, X., & Acs, G. (2009). RNA interference-mediated inhibition of erythropoietin receptor expression suppresses tumor growth and invasiveness in A2780 human ovarian carcinoma cells. *Am J Pathol, 174*(4), 1504-1514. doi:10.2353/ajpath.2009.080592

Pokhriyal, R., Hariprasad, R., Kumar, L., & Hariprasad, G. (2019). Chemotherapy Resistance in Advanced Ovarian Cancer Patients. *Biomarkers in Cancer, 11*. doi:10.1177/1179299x19860815

Prendergast, E., Green, M., Zakhour, M., Lester, J., Li, A., Walsh, C., . . . Karlan, B. (2015). Surveillance and health outcomes for BRCA mutation carriers following risk-reducing salpingo-oophorectomy (RRSO). *Gynecologic Oncology, 139*(1), 188-189. doi:10.1016/j.ygyno.2015.07.046

Priestley, P., Baber, J., Lolkema, M. P., Steeghs, N., de Bruijn, E., Shale, C., . . . Cuppen, E. (2019). Pan-cancer whole-genome analyses of metastatic solid tumours. *Nature, 575*(7781), 210-216. doi:10.1038/s41586-019-1689-y

Pulliam, N., Fang, F., Ozes, A. R., Tang, J., Adewuyi, A., Keer, H., . . . Nephew, K. P. (2018). An Effective Epigenetic-PARP Inhibitor Combination Therapy for Breast and Ovarian Cancers Independent of BRCA Mutations. *Clin Cancer Res, 24*(13), 3163-3175. doi:10.1158/1078-0432.CCR-18-0204

Ramalho, S., Andrade, L. A. A., Filho, C. C., Natal, R. A., Pavanello, M., Ferracini, A. C., . . . Derchain, S. (2019). Role of discoidin domain receptor 2 (DDR2) and microRNA-182 in survival of women with high-grade serous ovarian cancer. *Tumour Biol, 41*(1), 1010428318823988. doi:10.1177/1010428318823988

Ricci, J. W., Lovato, D. M., Severns, V., Sklar, L. A., & Larson, R. S. Novel ABCG2 Antagonists Reverse Topotecan-Mediated Chemotherapeutic Resistance in Ovarian Carcinoma Xenografts. (1538-8514 (Electronic)).

Rossi, L., Verrico, M., Zaccarelli, E., Papa, A., Colonna, M., Strudel, M., . . . Tomao, F. (2017). Bevacizumab in ovarian cancer: A critical review of phase III studies. *Oncotarget, 8*(7), 12389-12405. doi:10.18632/oncotarget.13310

Roy, R., Chun, J., & Powell, S. N. (2011). BRCA1 and BRCA2: different roles in a common pathway of genome protection. *Nat Rev Cancer, 12*(1), 68-78. doi:10.1038/nrc3181

Ruiz, P. A., & Jarai, G. (2011). Collagen I induces discoidin domain receptor (DDR) 1 expression through DDR2 and a JAK2-ERK1/2-mediated mechanism in primary human lung fibroblasts. *J Biol Chem, 286*(15), 12912-12923. doi:10.1074/jbc.M110.143693

Sakai, W., Swisher, E. M., Jacquemont, C., Chandramohan, K. V., Couch, F. J., Langdon, S. P., . . . Taniguchi, T. (2009). Functional restoration of BRCA2 protein by secondary BRCA2 mutations in BRCA2-mutated ovarian carcinoma. *Cancer Res, 69*(16), 6381-6386. doi:10.1158/0008-5472.CAN-09-1178

Salk, J. J., Loubet-Senear, K., Maritschnegg, E., Valentine, C. C., Williams, L. N., Higgins, J. E., . . . Risques, R. A. (2019). Ultra-Sensitive TP53 Sequencing for Cancer Detection Reveals Progressive Clonal Selection in Normal Tissue over a Century of Human Lifespan. *Cell Rep, 28*(1), 132-144 e133. doi:10.1016/j.celrep.2019.05.109

Society, A. C. Key tatistics for Endometrial Cancer. In.

Squatrito, M., & Holland, E. C. (2011). DNA damage response and growth factor signaling pathways in gliomagenesis and therapeutic resistance. *Cancer Res, 71*(18), 5945-5949. doi:10.1158/0008-5472.CAN-11-1245

Staunton, J. R., Doss, B. L., Lindsay, S., & Ros, R. (2016). Correlating confocal microscopy and atomic force indentation reveals metastatic cancer cells stiffen during invasion into collagen I matrices. *Scientific Reports, 6*(1). doi:10.1038/srep19686

Steding, C. E. (2016). Creating chemotherapeutic-resistant breast cancer cell lines: advances and future perspectives. *Future oncology (London, England), 12*(12), 1517-1527. doi:10.2217/fon-2016-0059

Strange, A. P., Aguayo, S., Ahmed, T., Mordan, N., Stratton, R., Porter, S. R., . . . Bozec, L. (2017). Quantitative nanohistological investigation of scleroderma: an atomic force microscopy-based approach to disease characterization. *International Journal of Nanomedicine, Volume 12*, 411-420. doi:10.2147/ijn.S118690

Taki, M., Abiko, K., Baba, T., Hamanishi, J., Yamaguchi, K., Murakami, R., . . . Matsumura, N. (2018). Snail promotes ovarian cancer progression by recruiting myeloid-derived suppressor cells via CXCR2 ligand upregulation. *Nature Communications, 9*(1). doi:10.1038/s41467-018-03966-7

Testa, U., Petrucci, E., Pasquini, L., Castelli, G., & Pelosi, E. (2018). Ovarian Cancers: Genetic Abnormalities, Tumor Heterogeneity and Progression, Clonal Evolution and Cancer Stem Cells. *Medicines (Basel), 5*(1). doi:10.3390/medicines5010016

Tewari, K. S., Burger, R. A., Enserro, D., Norquist, B. M., Swisher, E. M., Brady, M. F., . . . Monk, B. J. Final Overall Survival of a Randomized Trial of Bevacizumab for Primary Treatment of Ovarian Cancer. (1527-7755 (Electronic)).

Thalmann, G. N., Anezinis Pe Fau - Chang, S. M., Chang Sm Fau - Zhau, H. E., Zhau He Fau - Kim, E. E., Kim Ee Fau - Hopwood, V. L., Hopwood Vl Fau - Pathak, S., . . . Chung, L. W. Androgen-independent cancer progression and bone metastasis in the LNCaP model of human prostate cancer. (0008-5472 (Print)).

Tu, M., Lee, F., Jones, R., Kimball, A., Saravia, E., Graziano, R., . . . Theodorescu, D. (2019). Targeting DDR2 enhances tumor response to anti–PD-1 immunotherapy. *Science Advances, 5*, eaav2437. doi:10.1126/sciadv.aav2437

Tuo, X., Zhou, Y., Yang, X., Ma, S., Liu, D., Zhang, X., . . . Zhao, L. miR-532-3p suppresses proliferation and invasion of ovarian cancer cells via GPNMB/HIF-1α/HK2 axis. (1618-0631 (Electronic)).

Valiathan, R. R., Marco, M., Leitinger, B., Kleer, C. G., & Fridman, R. (2012). Discoidin domain receptor tyrosine kinases: new players in cancer progression. *Cancer and Metastasis Reviews, 31*(1-2), 295-321. doi:10.1007/s10555-012-9346-z

Vickovic, S., Eraslan, G., Salmen, F., Klughammer, J., Stenbeck, L., Schapiro, D., . . . Stahl, P. L. (2019). High-definition spatial transcriptomics for in situ tissue profiling. *Nat Methods, 16*(10), 987-990. doi:10.1038/s41592-019-0548-y

Vidal, A., Munoz, C., Guillen, M. J., Moreto, J., Puertas, S., Martinez-Iniesta, M., . . . Villanueva, A. (2012). Lurbinectedin (PM01183), a New DNA Minor Groove Binder, Inhibits Growth of Orthotopic Primary Graft of Cisplatin-Resistant Epithelial Ovarian Cancer. *Clinical Cancer Research, 18*(19), 5399-5411. doi:10.1158/1078-0432.Ccr-12-1513

Walton, J., Blagih, J., Ennis, D., Leung, E., Dowson, S., Farquharson, M., . . . McNeish, I. A. (2016). CRISPR/Cas9-Mediated Trp53 and Brca2 Knockout to Generate Improved Murine Models of Ovarian High-Grade Serous Carcinoma. *Cancer Res, 76*(20), 6118-6129. doi:10.1158/0008-5472.CAN-16-1272

Walton, J. B., Farquharson, M., Mason, S., Port, J., Kruspig, B., Dowson, S., . . . McNeish, I. A. (2017). CRISPR/Cas9-derived models of ovarian high grade serous carcinoma targeting Brca1, Pten and Nf1, and correlation with platinum sensitivity. *Sci Rep, 7*(1), 16827. doi:10.1038/s41598-017-17119-1

Wang, M., Yao, L. C., Cheng, M., Cai, D., Martinek, J., Pan, C. X., . . . Keck, J. G. (2018). Humanized mice in studying efficacy and mechanisms of PD-1-targeted cancer immunotherapy. *FASEB J, 32*(3), 1537-1549. doi:10.1096/fj.201700740R

Wang, Q., Peng, H., Qi, X., Wu, M., & Zhao, X. Targeted therapies in gynecological cancers: a comprehensive review of clinical evidence. (2059-3635 (Electronic)).

Wei, F., Yan, J., & Tang, D. (2011). Extracellular signal-regulated kinases modulate DNA damage response - a contributing factor to using MEK inhibitors in cancer therapy. *Current medicinal chemistry, 18*(35), 5476-5482. doi:10.2174/092986711798194388

Wei, Y., Erfani, S., Schweer, D., de Gouvea, R., Qadir, J., Shi, J., . . . Yang, X. H. Targeting receptor tyrosine kinases in ovarian cancer: Genomic dysregulation, clinical evaluation of inhibitors, and potential for combinatorial therapies. (2372-7705 (Print)).

Wiedemeyer, W. R., Beach, J. A., & Karlan, B. Y. (2014). Reversing Platinum Resistance in High-Grade Serous Ovarian Carcinoma: Targeting BRCA and the Homologous Recombination System. *Front Oncol, 4*, 34. doi:10.3389/fonc.2014.00034

Wu, X., Gu, Z., Chen, Y., Chen, B., Chen, W., Weng, L., & Liu, X. Application of PD-1 Blockade in Cancer Immunotherapy. (2001-0370 (Print)).

Yaginuma, Y., & Westphal, H. (1992). Abnormal structure and expression of the p53 gene in human ovarian carcinoma cell lines. *Cancer research, 52*(15), 4196-4199.

Zahreddine, H., & Borden, K. L. B. (2013). Mechanisms and insights into drug resistance in cancer. *Frontiers in Pharmacology, 4*. doi:10.3389/fphar.2013.00028

Zhang, C., Xu, C., Gao, X., & Yao, Q. Platinum-based drugs for cancer therapy and anti-tumor strategies. (1838-7640 (Electronic)).

Zhang, H., Liu, T., Zhang, Z., Payne, S. H., Zhang, B., McDermott, J. E., . . . Townsend, R. R. (2016). Integrated Proteogenomic Characterization of Human High-Grade Serous Ovarian Cancer. *Cell, 166*(3), 755-765. doi:10.1016/j.cell.2016.05.069

Zheng, G., Yu, H., Kanerva, A., Försti, A., Sundquist, K., & Hemminki, K. (2018). Familial Ovarian Cancer Clusters with Other Cancers. *Scientific Reports, 8*(1). doi:10.1038/s41598-018-29888-4

Zhu, J., Yan, L., & Wang, Q. (2021). Efficacy of PD-1/PD-L1 inhibitors in ovarian cancer: a single-arm meta-analysis. *Journal of Ovarian Research, 14*(1), 112. doi:10.1186/s13048-021-00862-5